Which Is More Rewarding in Managing Sea Level Rise and Hurricane Storm Surge Flooding: Mitigation or Response?

This study aims to extend the existing climate-change-induced flood mitigation research. We introduce an at-risk network to evaluate optimal cost-benefit strategies for creating dikes and levees to mitigate flood hazard over multiple years. Our proposed model includes the expected flood costs, estimated using possible climate-change-induced sea level states throughout the planning horizon, and the investment costs for developing dikes and levees via land elevations across the at-risk network. Further, given the limitations on infrastructure investment, our model incorporates a budget constraint. The problem is modeled as a multi-stage stochastic program with recourse that minimizes overall expected costs over the planning horizon. Exploiting open-source and freely accessible data sets, the flood risk mitigation model elaborated here can be applied to most urban coastal situations due to its general nature. Using Boston as a case study, our proposed method resulted in a cost reduction of as much as 92.2%, with an average of 63.2%, compared to a "do nothing" strategy in a simulation-based experiment. Under a high sea level rise scenario, the average cost savings observed by implementing the solution suggested by our model could be even 15% higher. This proposed approach offers decision-makers a tool to frequently assess the costs and risks faced by their cities enabling them to effectively mitigate the potential flooding risks.

Key words: Climate change adaptation; Coastal flooding; Decision-making under risk; Mitigation; Network optimization.

1 Introduction

Flooding accounts for nearly half of all natural disasters globally (Sodhi and Tang 2014). Economic losses from floods between 2009 and 2018 are estimated to exceed \$356 trillion, according to The International Disaster Database (EM-DAT 2020). This positions flooding as one of the most catastrophic forms of natural disasters, on par with earthquakes. Making matters worse, projections show a worsening flood hazard trend caused by climate change effects. For instance, by 2050, Boston is projected to experience an annual occurrence of what is currently a one in 10-year winter storm flood, across all emissions scenarios (Douglas and Kirshen 2022). Furthermore, others report that by 2100, the equivalent of today's one in 100-year flood event will probably become an annual disaster in Boston (Baranes et al. 2020, Thompson et al. 2019).

Higher groundwater elevations significantly affect flooding conditions, especially in coastal areas as sea level rises (Douglas and Kirshen 2022). There are many low-lying islands and coastal regions around the world, housing millions of people, that face increased flooding and potential inundation

year-round due to rising sea levels (Martyr-Koller et al. 2021, Nicholls et al. 2007). Thus, it is unsurprising that the total estimated value of potential flooding damages from sea level rise (SLR) is in the trillions of dollars (Abadie 2018). The recurring theme for SLR-related coastal flooding is the lack of existing infrastructure to protect coastal areas that can significantly mitigate the hazard (Chakravarty 2018). Considering the efficacy of storm barricades in mitigating coastal flooding risks, our goal is to create a decision support system for optimizing investments in constructing a flood protection system in the form of dikes and levees.

This study is motivated by a pressing concern for Boston, a coastal city facing the potential risk of increased flooding due to its rapid SLR. In the last two decades, the city has undergone an average SLR rate of 5.4 mm/yr, significantly outpacing the global average and twice the rate of Boston's SLR during the previous century (Douglas and Kirshen 2022). Projections for SLR in Boston Harbor vary based on potential future emissions. As highlighted by multiple sources, when compared to the year 2000's baseline, SLR by 2100 ranges from 35 to 78 cm in the most optimistic scenario, while it could surpass two meters in the worst-case scenario (Oppenheimer 2019, Douglas and Kirshen 2022). This SLR underscores a substantial risk of flooding in coastal areas (Sweet et al. 2017). Even without anticipated sea level rise, Boston has more than 3,000 properties facing substantial damage from flooding, so it can expect flood costs over $35M each year (Abel 2021).

The city's management focuses on eleven strategic initiatives to address the expanded effects of climate change (Boston 2016). Among these are five flood-related strategies: monitoring up-to-date climate change projections, creating a coastal flood protection system, updating zoning and building regulations, retrofitting existing buildings, and insuring buildings against flood damage. Striving to keep momentum, as part of the recommended actions in Boston (2016), this coastal protection strategy called for the city to launch a harbor-wide feasibility study within two years. The subsequent 2018 Boston Harbor barrier feasibility report recommended forgoing a barrier system while implementing incremental steps and continued monitoring to see how the SLR situation unfolds (Kirshen et al. 2018b). The findings recommend using other multi-layer adaptation strategies (i.e., protection, accommodation, and retreat), at least for the next few decades, while monitoring actual SLR to better understand the uncertainty of the city's risks.

It is a positive sign that cities like Boston are working to overcome this inertia of inaction, but the latest Boston report still takes a wait-and-see approach (see Kirshen et al. (2018b)). Unfortunately, cities face challenges requiring unprecedented foresight, complex coordination, and heightened urgency. While facing these challenges, multiple stakeholders are clamoring for attention, such as state and federal agencies, developers, landowners, and non-profit organizations (Wissman-Weber and Levy 2021). In light of these challenges, there are opportunities to improve acknowledging the risks of SLR-related flooding and develop methods that evaluate differential benefits and costs of

public and policymaker (in)action (Mechler et al. 2014, Wissman-Weber and Levy 2021). In the face of rising seas, policymakers need new decision support tools to better assess potential flood risks and investment costs that their communities face.

This article proposes a cost-benefit analysis model to optimize investment decisions over time for alleviating flood hazards. To conduct a more granular analysis, we focus on flooding caused by sea level rise and hurricane storm surges along the sea coast. Our research centers on development of a flood protection infrastructure in the form of dikes and levees through modifications to coastal land elevations. We propose a generalized modeling approach to minimize a cost function composed of two components: (1) the estimated cost of constructing an infrastructure of dikes and levees, and (2) the potential SLR-related flood cost. We formulate a multi-stage stochastic program with recourse to determine the least cost option, considering both permanent and temporary flood damages and flood protection investment costs. This integrated approach offers valuable managerial insights into associated costs for coastal areas, highlighting the advantages of proactive decision-making in preventing damages compared to the alternative of waiting for damages to transpire and subsequently managing the aftermath. We also present a network-based framework for modeling complex flood movement dynamics on land to identify at-risk regions. Our model is more generalized than existing cost-benefit analyses, which are limited to starting from a pre-existing infrastructure and enhancing that infrastructure over time. Developing a cost-benefit analysis that simultaneously assesses flood damage costs and flood protection construction expenses while integrating evolving SLR projections empowers policymakers to adhere to the periodic monitoring advised by experts. Another objective of this study is to showcase the feasibility of conducting this complex cost analysis solely with open-source data (USGSA 2009), thereby expanding the applicability of our approach. To this end and to demonstrate the performance of our proposed model, we discuss a case study of Boston. We consider a grid network representing Boston using open-source land elevation, tax appraisals, tidal gauge data, and published sea level rise elevations for possible climate change scenarios. We also use Google street view visualization to fill in gaps in the open-source tax data.

Using a simulation-based approach in our Boston case study, we demonstrate that, in comparison to a "do nothing strategy" (DNS), our proposed method results in a cost reduction of up to 92.2% (on $338.4M in damages for DNS), with average cost reductions of 63.2% (on $182.7M in average damages for DNS). Moreover, our model demonstrates similar cost savings in four different scenario-based experiments compared to a DNS. Besides the Boston case study, we replicated the experiments with 50 random networks, demonstrating the generalizability of the methodology and insights beyond the Boston case. Finally, across all experiments, we present an extensive parameter sensitivity analysis, allowing decision-makers to compare the outcomes by incorporating the latest financial data or economic values.

We identify a few key takeaways from a policymaker's perspective. The first is that a modest investment at a fraction of the cost of expected damages under the "do nothing" strategy results in a meaningful reduction in flood-related and overall costs. Sea level rise is a real threat, so inaction and relying on chance will inevitably position a coastal area for considerably greater expenses throughout the assessed time horizon. Even under a scenario with no sea level rise featuring only expected annual storm flooding, the model suggests making investments when the build costs of levees are in the low to moderate range. Our model is also a powerful tool that can provide meaningful estimations for the optimal investment amounts required per period, thereby enabling city planners to formulate more informed budgeting decisions in their disaster prevention planning. From our sensitivity analysis, we could identify critical factors (namely, the costs to build the levees, the minimum build height, and the discount rate) that significantly impact the investment amounts and their timing. Planners must carefully consider these parameters to avoid underestimating costs or overestimating risks. Underestimating costs may lead to overspending on infrastructure, costing more than the damages it mitigates. On the other hand, overbuilding for potential sea level rise could restrict the total protected area due to budget depletion. Finally, our experiments show that there will be areas that are not cost-effective to protect. No matter how much budget is available, the investment costs to protect these areas exceed the potential flood damage mitigation. This allows policymakers to assess areas under their control for a potential retreat rather than trying to protect them at any cost.

2 Literature review

The disaster operations management literature has grown substantially in the recent past (Galindo and Batta 2013b, Besiou and Van Wassenhove 2020). Nevertheless, much of this attention skews towards crisis response and logistics with little regarding mitigation policies (Akter and Wamba 2019, Galindo and Batta 2013b, Gupta et al. 2016, Besiou and Van Wassenhove 2020). The emphasis on response operations is justified for several reasons, including the substantial deprivation costs during these operations (Eftekhar et al. 2022), media attention, and donors' sensitivity (Eftekhar et al. 2017).[1] Consequently, most humanitarian assistance donations come with restrictions prioritizing short-term relief operations, thereby limiting opportunities for long-term investment in mitigating potential disasters (Oloruntoba and Gray 2006), resulting in under-financed mitigation strategies.

Looking at the special issues of 2014 *Production and Operations Management*, 2016 *Journal of Operations Management*, and 2018 *European Journal of Operational Research*, Besiou and Van Wassenhove (2020) found only one paper related to mitigation. Likewise, in their seminal review

---

[1] For example, studies show that on average, it takes 38,920 deaths for a "food shortage crisis" to receive media coverage, while major U.S. networks cover news of an earthquake if it leads to two deaths (Eisensee and Strömberg 2007).

of papers published between 1957–2014 on disaster management, Gupta et al. (2016) identified 50 of 268 (18.7%) papers as being in the administrative function of prevention/mitigation, collectively referring to activities aimed at reducing the severity of a disaster's impact or ensuring that a man-made/natural event does not result in disaster. Of these, the majority concentrate on terrorism prevention policies following 9/11, with papers such as allocation of resources for airport screening (Bagchi and Paul 2014), response planning to bioterror attacks in airport terminals (Berman et al. 2012), and strategic terrorism deterrence in two-country frameworks (Roy and Paul 2013). Within these papers, there is a preponderance of papers not focused on specific disaster types (i.e., they treat disasters as a general problem). These studies tend to evaluate overarching methods or frameworks to apply generally to disasters, with some examples including evaluating disaster severity assessments (Rodríguez et al. 2011), representing perceived trade-offs between disaster impact and time to recovery to define disaster resilience (Zobel 2011), and developing a general methodology for inductive rule-building for NGOs involved in responding to natural disasters (Rodríguez et al. 2012). Consequently, Gupta et al. (2016) emphasizes the need for more research in prevention/mitigation.

In digging deeper into the papers labeled as prevention/mitigation, there appear to be scant references centered on planning to mitigate some disaster types, such as flooding, epidemics, and wildfires. In the case of disaster-related research, this includes modeling with specific disaster characteristics to help practitioners develop adequate frameworks for the prevention and mitigation of disasters (Kovacs and Moshtari 2019). For example, although hurricane disaster management has received significant attention (e.g., Uichanco (2022), Galindo and Batta (2013a), Campbell and Jones (2011), Lodree and Taskin (2008) and Davis et al. (2013)), almost all of these studies focus on the response phases of crisis management. Gupta et al. (2016) found only seven papers related to floods, with only two focusing on prevention/mitigation. Of the two papers with some focus on prevention/mitigation, one was modeling disruption to freight transportation networks (Miller-Hooks et al. 2012) and the other was covering optimal deployment for search and rescue operations during disasters (Chen and Miller-Hooks 2012).

Constructing a storm barricade system of levees and dikes is an effective technique for mitigating the risk of coastal flooding. Jonkman et al. (2009) employ an economic optimization approach for a risk-based design of levee systems for the New Orleans metropolitan area. Lund et al. (2010) present an economic decision analysis approach for levee upgrade and repair investments in 34 major islands in California's Sacramento-San Joaquin Delta. Keegan et al. (2011) discuss issues related to the construction and maintenance of locally operated levees, and provide an overview of federal programs addressing them. Eijgenraam et al. (2017) discuss improving the dike infrastructure in the Netherlands to protect more than 55% of the land area below sea level. Perhaps the closest to the current paper is Chakravarty (2018), which proposes an optimization model integrating multiple

decisions pre- and post-disaster to determine how investment in constructing levees can be leveraged in procuring relief items during preparation and response phases. Chakravarty (2018) considers a setting where a governmental agency makes a levee capacity decision at the beginning of a multi-year planning horizon, while humanitarian relief agencies make procurement decisions every year. With this integrated model, Chakravarty (2018) analytically shows how increasing the levee capacity creates more social surplus over time. Nevertheless, depending on the severity of storms, the levees can be damaged or destroyed. An example is the 2005 Hurricane Katrina, which shattered the protective barriers and caused the disaster in New Orleans. Sills et al. (2008) investigate the Southeast Louisiana Flood and Hurricane Protection System that was in place at the time of Hurricane Katrina to further highlight the deficiency of knowledge in the technology and expertise needed to develop levee systems. Given the importance of a levee system reliability, revamping these systems is a common practice (Chakravarty 2018), highlighting the need for continuous investment in flood hazard mitigation from city management. The Climate Ready Boston website (Boston 2023) includes conceptual plans for protecting the entire coastline of Boston with nature-based approaches. Boston aims to implement adaptation plans in the areas most prone to flooding in the present and near term while addressing major obstacles like environmental permitting and financing. Revising the environmental permitting process could enable building protection strategies potentially extending into the coastal waters near the land. Finally, the work proposed herein is done with a preference for landowner cooperation over eminent domain.

Upon evaluating the literature, there is a surprisingly small number of disaster-related papers focused on what many consider to be a slow-motion disaster in the making, coastal flooding caused by rising sea levels (IPCC 2014), and there is scant coverage for addressing the sea level rise in areas where infrastructure is non-existent today. In light of these limitations, our research aims to contribute to the literature by building a model that supports an adaptive strategic approach to mitigate potential disasters caused by coastal city flooding. This article highlights the need for local and national government investment in infrastructure to lessen the impending risk of climate-change-induced flooding. To our knowledge, this is the first study that uses network-based modeling and linear algebra logic to represent complex water movement dynamics on land for detecting regions at risk of flooding. Moreover, our model is more general than the existing methods because it incorporates both permanent and temporary flood damages along with investment costs, can be used in regions without any preexisting infrastructure, and can be built by using only open-source data. Lastly, another important contribution of this work is the model's ability to identify areas that are not cost-effective to protect. This capability is particularly relevant in cities like New Orleans, where many parts of the city have elevations below sea level. City planners should be aware of the fact that not actively protecting certain areas from floods may necessitate revising construction codes.

3 Model, complexity, and solution

We model the Flood Risk Mitigation (FRM) problem as a multistage stochastic program with recourse. To present the model, we will define some sets, parameters and variables in this section. A list summarizing all these defined sets, parameters and variables is presented in the electronic companion Section EC.3. The proposed model incorporates the risk of flooding over time, with t_{max} periods within the planning horizon $t \in \mathcal{T} = \{1, \ldots, t_{max}\}$, on a network of interconnected land grids. We first address the input parameters (i.e., associated with the sea level rise, grid partitioning, investment costs, flood damages, and available budget) and the necessary assumptions in section 3.1, and then present the full model in section 3.2. Then, we discuss the FRM problem's computational complexity and solution in section 3.3.

3.1 Input parameters and assumptions

3.1.1 Sea level states and their probabilities

Given that we are only focusing on flooding caused by SLR and hurricane storm surge along the sea coast, we model the state of the sea level during a period (denoted by $\mathcal{S}$) using two components. The first component, denoted by s, represents the sea level during a period solely due to the climate change effects. The second one, denoted by $\hat{s}$, indicates the sea level during a period due to both climate change effects and hurricane storm surge factors. Notice that we assume climate change effects and hurricane storm surge factors are independent of each other. We also assume that the change in s and $\hat{s}$ happens at the start of a given period, and these two components stay unchanged during the period. These two components together shape the sea level state during a period (i.e., $\mathcal{S} = (s, \hat{s})$), and the set containing all possible sea level states during a period t is denoted by Ξ_t. At time zero, we assume that both components of the sea level state are zero (i.e., $(s = 0, \hat{s} = 0)$), and define the set containing this sea level state as $\Xi_0 = \{(0,0)\}$. Since the hurricane storm surges increase the sea level temporarily within a period, they pose even higher sea levels during the period, i.e., $s \leq \hat{s}$ for all $t \in \mathcal{T}$ and $\mathcal{S} \in \Xi_t$. Given $t \in \{0, \ldots, t_{max} - 1\}$, $\mathcal{S} \in \Xi_t$ and $\mathcal{S}' \in \Xi_{t+1}$, let $p_t^{\mathcal{S}\mathcal{S}'}$ denote the probability that the sea level state during period t is $\mathcal{S}$ and during period $t+1$ is $\mathcal{S}'$. We assume that probabilities $p_t^{\mathcal{S}\mathcal{S}'}, \forall t \in \{0, \ldots, t_{max} - 1\}, \mathcal{S} \in \Xi_t, \mathcal{S}' \in \Xi_{t+1}$, are known.

3.1.2 Grid-based partitioning

To model the SLR and hurricane storm flooding system as a network, we use a grid partitioning that segments a coastal region into hexagonal grids. More precisely, let us denote the coastal area in which we have control to create dikes and levees by elevating the land and we are also responsible for the cost of land elevation and flooding as the "region of interest." We only concern ourselves with

areas within the region of interest that might get flooded during the planning horizon. Some parts of the region of interest might be adjacent to the sea at the start of the planning horizon (referred to as "time zero") and might get flooded directly from the sea. Depending on the land formations, other areas of the region of interest that are not adjacent to the sea may also get flooded due to water passing through the surrounding region during future time periods. To account for this possibility, we must also consider the portions of the region surrounding the region of interest that might experience flooding in the future. Figure 1(a) illustrates the sea, the region of interest, and its surrounding region at the beginning of the planning horizon in a simple example.
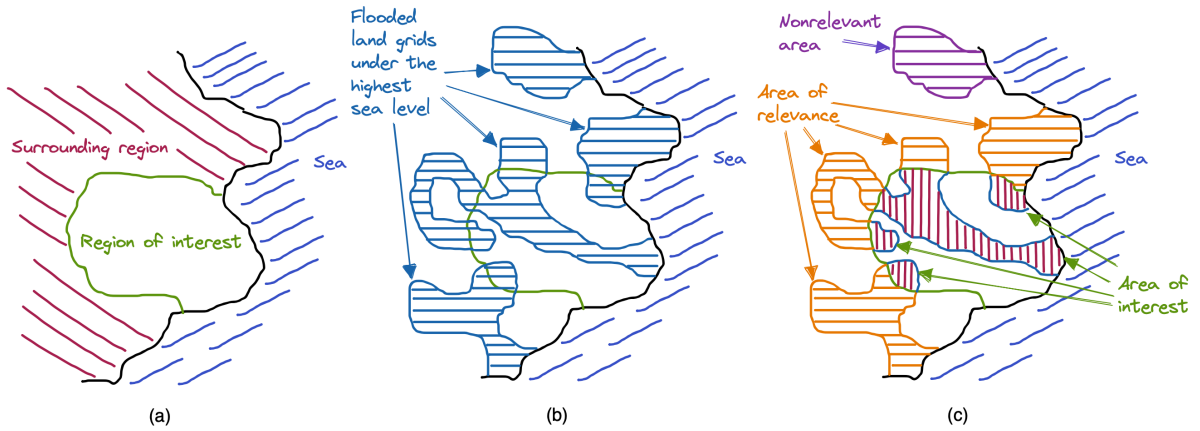

Figure 1   (a) An illustration of the sea, region of interest and its surrounding region at the beginning of the planning horizon. (b) An illustration of the flooded land grids under the highest sea level across all sea level states (i.e., $\hat{s}_{max} = \max\{\hat{s} : (s, \hat{s}) \in \cup_{t \in \mathcal{T}} \Xi_t\}$). (c) An illustration of the areas of interest and relevance identified under the highest sea level. Note that all land grids in the area of relevance are flooded under the highest sea level and have a water path to some flooded land grid in the region of interest without going through the sea. The area marked as "Nonrelevant area" is also flooded under the highest sea level but any water path from this area to the region of interest passes through the sea.

To identify parts of the region of interest and the surrounding region that are at risk of flooding during the planning horizon, we first partition the land in these two regions into hexagonal grids. We assume that the elevation of the land on the surface of a grid is uniform and constant, and is equal to the average elevation of all points across the surface of that grid. We then consider the highest sea level across all sea level states (i.e., $\hat{s}_{max} = \max\{\hat{s} : (s, \hat{s}) \in \cup_{t \in \mathcal{T}} \Xi_t\}$), and identify land grids within the region of interest and the surrounding region at time zero that will get flooded under this sea level (i.e., the land grid elevation is below $\hat{s}_{max}$). A flooded land grid in the surrounding region will be considered in our model if it has a water path to a flooded land grid in the region of interest without going through the sea under the highest sea level $\hat{s}_{max}$. Let us refer to the flooded land grids in the region of interest under sea level $\hat{s}_{max}$ as the "area of interest" and denote the set containing

these grids as Φ. We also refer to the flooded land grids in the surrounding region with a water path to some flooded land grid in the region of interest without going through the sea under sea level $\hat{s}_{max}$ as the "area of relevance." The set of land grids in the area of relevance is denoted by Ψ. Figure 1 parts (b) and (c) show the process of identifying the areas of interest and relevance in our example.

Land grids $i \in \Phi$ start with an initial elevation denoted by h_i. In our model, building levees and dikes within the area of interest is synonymous with raising the elevations of some land grids in set Φ incrementally over time throughout the planning horizon to prevent flooding within the area of interest. However, the elevations of land grids $i \in \Psi$ (also denoted by h_i) are going to stay unchanged throughout the planning horizon as we do not have control over these grids and we are not responsible for their flooding. The only reason grids in set Ψ are incorporated in our model is that these grids might create pathways for the sea to approach the area of interest. Notice that for some $i \in \Phi \cup \Psi$, we might have $h_i < 0$, which indicates that the elevation of the land grid i at time zero is below the sea level state at time zero (i.e., $(s = 0, \hat{s} = 0)$). We also similarly partition the sea at time zero into hexagonal grids designated as set O. These sea-based grids start with an elevation of zero, and rise accordingly with sea level changes over time.

To focus our modeling approach on the land grids subject to flooding during a given period t and under a given sea level state $\mathcal{S} \in \Xi_t$, we further segment the grids in sets Φ and Ψ into those grids at risk of temporary (hurricane storm surge related) flooding or permanent inundation flooding versus those grids that are not at risk of any flooding during period t and under sea level state $\mathcal{S}$. Assuming water can only flow between grids that share a physical border, we define the land grids at risk during a period t and under sea level state $\mathcal{S} \in \Xi_t$ as follows:

DEFINITION 1. Let $R_t^{\mathcal{S}}$ denote the subset of land grids in Φ at risk of permanent inundation flooding during period t and under sea level state $\mathcal{S} \in \Xi_t$. Similarly, let $Q_t^{\mathcal{S}}$ denote the subset of land grids in Ψ at risk of permanent inundation flooding during period t and under sea level state $\mathcal{S} \in \Xi_t$. Given $t \in \mathcal{T}$ and $\mathcal{S} = (s, \hat{s}) \in \Xi_t$, a land grid $i \in \Phi$ is in $R_t^{\mathcal{S}}$ if and only if it has an initial elevation h_i below the permanent sea level s during period t, and at least one of its neighbors is in set $O \cup R_t^{\mathcal{S}} \cup Q_t^{\mathcal{S}}$. Similarly, a land grid $i \in \Psi$ is in $Q_t^{\mathcal{S}}$ if and only if it has an elevation h_i below the permanent sea level s during period t, and at least one of its neighbors is in set $O \cup R_t^{\mathcal{S}} \cup Q_t^{\mathcal{S}}$. Notice that land grids in $R_t^{\mathcal{S}} \cup Q_t^{\mathcal{S}}$ are also logically at risk of temporary flooding.

DEFINITION 2. Let $\hat{R}_t^{\mathcal{S}}$ denote the subset of land grids in Φ only at risk of temporary flooding during period t and under sea level state $\mathcal{S} \in \Xi_t$. Similarly, let $\hat{Q}_t^{\mathcal{S}}$ denote the subset of land grids in Ψ only at risk of temporary flooding during period t and under sea level state $\mathcal{S} \in \Xi_t$. Given $t \in \mathcal{T}$ and $\mathcal{S} = (s, \hat{s}) \in \Xi_t$, a land grid $i \in \Phi$ is in $\hat{R}_t^{\mathcal{S}}$ if and only if one of the two following mutually exclusive cases happens: (1) It has an initial elevation h_i below the temporary sea level $\hat{s}$ and above

(or equal to) the permanent sea level s during period t, and at least one of its neighbors belongs to set $O \cup R_t^{\mathcal{S}} \cup Q_t^{\mathcal{S}} \cup \hat{R}_t^{\mathcal{S}} \cup \hat{Q}_t^{\mathcal{S}}$, or (2) It has an initial elevation h_i below the permanent sea level s during period t, none of its neighbors belongs to set $O \cup R_t^{\mathcal{S}} \cup Q_t^{\mathcal{S}}$, and at least one of its neighbors belongs to set $\hat{R}_t^{\mathcal{S}} \cup \hat{Q}_t^{\mathcal{S}}$. Similarly, a land grid $i \in \Psi$ is in $\hat{Q}_t^{\mathcal{S}}$ if and only if one of the above mentioned mutually exclusive cases happens for land grid i.
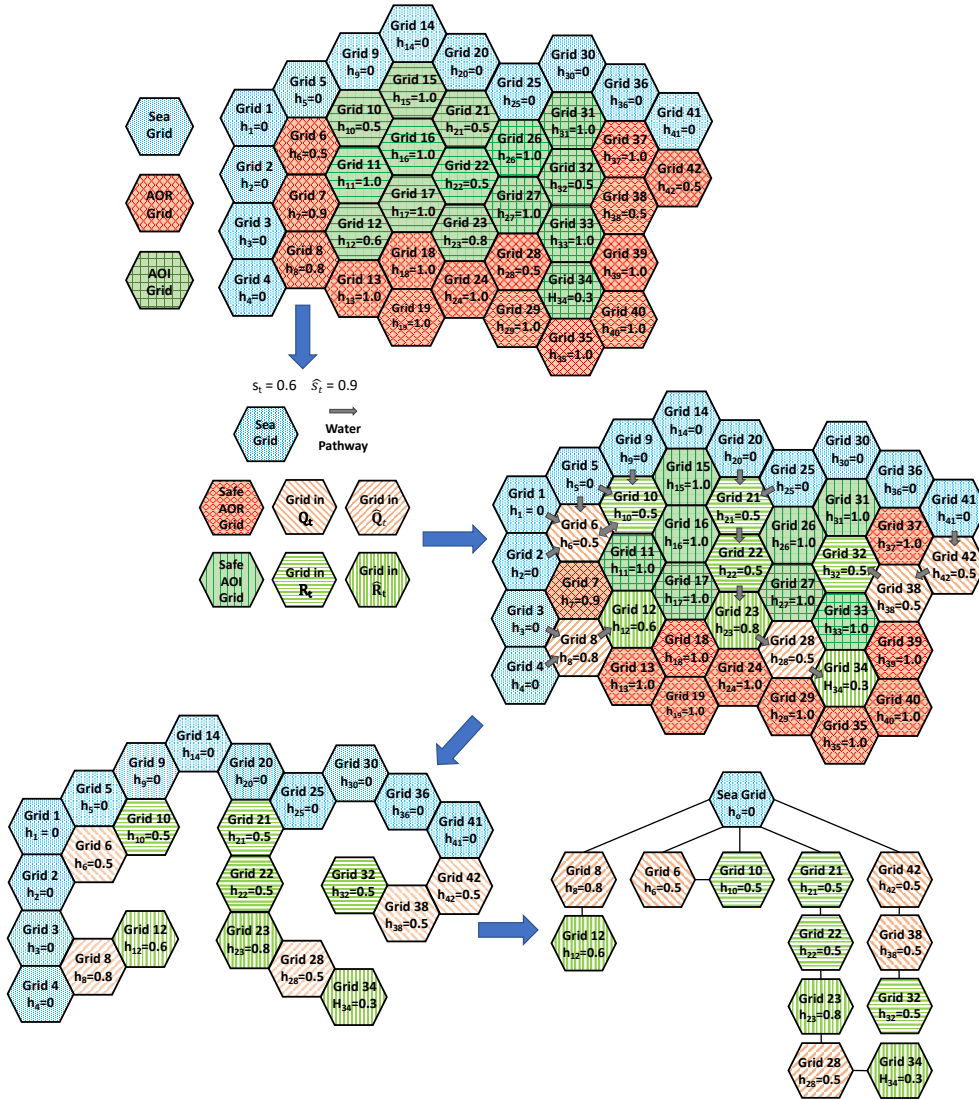
Figure 2 Example transformation of a full grid layout of the areas of interest and relevance along with the sea into an at-risk network for a given period t and a given sea level state $(s = 0.6m, \hat{s} = 0.9m) \in \Xi_t$.

As illustrated in Figure 2, given a period t and a sea level state $\mathcal{S} \in \Xi_t$, the land grids in set $R_t^{\mathcal{S}} \cup \hat{R}_t^{\mathcal{S}} \cup Q_t^{\mathcal{S}} \cup \hat{Q}_t^{\mathcal{S}}$ represent the vertices in a network (referred to as the "at-risk network during period t and under sea level state $\mathcal{S}$"), and the grids that share borders are made adjacent via edges within the network. In Figure 2, a full grid layout of the areas of interest and relevance along

with the sea is transformed into an at-risk network during a period t and under a sea level state $\mathcal{S} = (0.6, 0.9) \in \Xi_t$ in meters. The starting elevations are labeled in each land grid and the sea-based grids are highlighted in blue. Highlighting the grids at risk during this time period and under this sea level state results in the middle image with sets $R_t^{\mathcal{S}}$, $\hat{R}_t^{\mathcal{S}}$, $Q_t^{\mathcal{S}}$ and $\hat{Q}_t^{\mathcal{S}}$ identified. To create the associated at-risk network using the identified at-risk land grids, we collapse all sea-based grids into one vertex (denoted by vertex "o"), and build the network with the at-risk grids and edges based on shared borders. The at-risk network basically highlights which grids will flood during the given time step and under the given sea level state, if no elevation increase is made for flood protection throughout the planning horizon. As shown in the At-Risk Network in Figure 2, the set of vertices includes a risk vertex for each risk grid in set $R_t^{\mathcal{S}} \cup \hat{R}_t^{\mathcal{S}} \cup Q_t^{\mathcal{S}} \cup \hat{Q}_t^{\mathcal{S}}$ and a single sea vertex. This means that we will have a total number of $|R_t^{\mathcal{S}} \cup \hat{R}_t^{\mathcal{S}} \cup Q_t^{\mathcal{S}} \cup \hat{Q}_t^{\mathcal{S}}| + 1$ vertices. Note that if a risk grid shares a border with the sea, we also add an edge between its corresponding vertex and the sea vertex (i.e., vertex o). Given the at-risk network during a period t and under a sea level state $\mathcal{S} \in \Xi_t$, the set containing vertices that are adjacent to a vertex $i \in R_t^{\mathcal{S}} \cup \hat{R}_t^{\mathcal{S}} \cup Q_t^{\mathcal{S}} \cup \hat{Q}_t^{\mathcal{S}}$ is referred to as the neighbors of i within the at-risk network, and is denoted by $N_t^{\mathcal{S}}(i)$.

3.1.3 Grid costs for investment and flood damage

There are four inputs required to model the costs associated with the FRM problem. The first parameter is related to the investment cost to elevate grids in set Φ by building dikes and levees on them. The cost c is what it takes to elevate a grid in Φ by one meter at the start of a given a period. We assume that investment costs are uniform across grids, independent of the grid's surface structure, and do not vary much over the planning horizon. The units of c are in terms of dollars per meter of elevation raise. Similar to the case of the sea level rise, we assume that the increase in grids' elevations happens at the start of a given period before realization of the sea level state at the start of that period, and the grids' elevations stay unchanged during the period.

The next two inputs provide the information needed to determine flood-related damages. The first parameter is the cost g_i of losing a grid $i \in \Phi$ due to inundation if the grid is in $R_t^{\mathcal{S}}$ during a period t and under a sea level state $\mathcal{S} \in \Xi_t$, and is permanently flooded. We assume the inundation cost is a constant value representing the full grid loss during a given period. We also assume that once a grid is inundated (permanently flooded) during a period, it is possible to raise the elevation of that grid at the start of the next period and pull it out of the inundation (full loss) state. This is specifically possible when the investment budget in early periods is limited. Notice that during a period t and under a sea level state $\mathcal{S} \in \Xi_t$, a grid may be in $R_t^{\mathcal{S}}$ but not be permanently flooded because that grid has been elevated at the start of period t before realization of $\mathcal{S}$ or during the previous periods, or there is no path to it from the sea due to other grids being elevated. We assume g_i is strictly positive,

and its units are in dollars per time period for a given grid $i \in \Phi$. The second flood-cost related parameter is the cost for one meter of hurricane storm surge flood damage f_i to a grid i in $R_t^{\mathcal{S}} \cup \hat{R}_t^{\mathcal{S}}$ during a period t and under a sea level state $\mathcal{S} \in \Xi_t$ when the grid is temporarily flooded. Notice that we assume a grid will not experience hurricane storm surge related costs if it is permanently inundated during a given period. This is due to the fact that when a grid i is permanently inundated during a period, the total value of the grid (i.e., g_i) is lost during that period, but the storm surge only causes partial grid value loss (e.g., only first floors of buildings being damaged) during a period. Therefore, during a period t and under a sea level state $\mathcal{S} \in \Xi_t$, a grid might be in $R_t^{\mathcal{S}} \cup \hat{R}_t^{\mathcal{S}}$, but not be temporarily flooded because it is permanently flooded, or it has been elevated at the start of period t or during previous periods, or there is no path to it from the sea due to other grids being elevated. Hurricane storm surge flood cost in a given grid is based on a linear depth damage curve for that grid. Similarly, we assume f_i is strictly positive, and its units are in dollars per time period per meter of sea level elevation above a grid i elevation.

The final input to incorporate realistic costs over time is to apply a discount rate per period, denoted by λ. The discount rate systematically adjusts the value of costs and benefits during future periods. Notice that to get λ, the standard annual discount rate (i.e., d) will need to be adjusted to match the time frame used for a period in our model.

3.1.4 Budget

We consider a fixed construction and maintenance budget for each period t (denoted by b_t) that does not carry over into other periods, where b_t is given for $t \in \mathcal{T}$. Coastal cities' resources are limited, and so this budget imposes a constraint on the amount of investment and construction in a given period. Inclusion of this budget constraint in the FRM problem makes this problem more realistic, but imposes significant computational challenge for its solution. We further discuss the FRM problem's complexity and solution in Section 3.3.

3.2 Model development

3.2.1 Decision variable

The main decision variables for the FRM model are the heights of each grid $i \in \Phi$ during each period $t \in \mathcal{T}$. As mentioned before, we assume that the decisions on the heights of the grids in Φ during a period t are made at the start of period t before disclosure of the sea level change at the start of this period. We also assume that the decisions on the heights of the grids in Φ at the start of any period $t \in \{1, \ldots, t_{max}\}$ only depend on the sea level state during period $t-1$, which is known to the decision maker at the time of decision making. This means that the heights of the grids during the first period (first-stage decisions) are decided while the only piece of information available is the sea

level state at time zero (i.e., $(s = 0, \hat{s} = 0)$). So, given a period $t \in \mathcal{T}$ and a sea level state $\mathcal{S} \in \Xi_{t-1}$, we use notation $x_{it\mathcal{S}}$ to represent the decision variable associated with the height of a grid $i \in \Phi$ during period t if the sea level state during period $t-1$ is $\mathcal{S}$.

It is important to note that elevating grids by building dikes and levees on them cannot be done in small increments across the years. In practice, if the decision maker decides to elevate a grid in Φ during a time period, the elevation increase should be done up to a minimum threshold to justify the initial setup cost. Therefore, we incorporate a parameter m in our model that represents the minimum threshold of elevation increase in any grid in Φ during a period. Moreover, to model the FRM problem, we need to find a valid upper bound on the elevation increase in any grid in Φ during a period (denoted by M). One such valid upper bound is $M = \max\{\hat{s}_{max} - \min\{h_i : i \in \Phi \cup \Psi\}, m\}$, which is used in our model.

3.2.2 Objective function

This model's main objective is to minimize the total cost, with two primary components to address. The first is the expected investment cost for building dikes and levees by increasing the elevation of grids to protect themselves and possibly other grids in the network. The second is the expected flood cost when grids are affected by either permanent inundation or hurricane storm surge flooding.

The cost for investment is evaluated on a per grid basis, and the overall cost for each grid is determined by looking at a grid's height change throughout the planning horizon. Equation (1) below captures the expected investment cost (denoted by EIC) for all at-risk grids during the planning horizon. To account for discounted future periods, we incorporate the adjusted discount rate λ in this equation.

$$EIC = c\sum_{i \in \Phi}(x_{i1(0,0)} - h_i) + c\sum_{i \in \Phi}\sum_{t=1}^{t_{max}-1}\sum_{\mathcal{S} \in \Xi_{t-1}}\sum_{\mathcal{S}' \in \Xi_t} p_{(t-1)}^{\mathcal{S}\mathcal{S}'}\frac{(x_{i(t+1)\mathcal{S}'} - x_{it\mathcal{S}})}{\lambda^t} \tag{1}$$

A grid $i \in \Phi \cup \Psi$ faces two mutually exclusive possibilities of flooding during a period and under a sea level state: (1) permanent inundation where the grid is deemed underwater (at least during daily high tides) for the full period t, and (2) temporary hurricane storm surge flooding where the grid only faces damage due to short duration flooding within the period. During a period $t \in \mathcal{T}$ and under sea level states $\mathcal{S} \in \Xi_{t-1}$ and $\mathcal{S}' \in \Xi_t$ for which $p_{t-1}^{\mathcal{S}\mathcal{S}'} > 0$, to capture if a grid $i \in R_t^{\mathcal{S}'} \cup Q_t^{\mathcal{S}'}$ is inundated, we designate a binary variable $w_{it\mathcal{S}\mathcal{S}'}$, where $w_{it\mathcal{S}\mathcal{S}'} = 0$ if the grid is not inundated, and $w_{it\mathcal{S}\mathcal{S}'} = 1$ otherwise. If a grid $i \in R_t^{\mathcal{S}'} \cup Q_t^{\mathcal{S}'} \cup \hat{R}_t^{\mathcal{S}'} \cup \hat{Q}_t^{\mathcal{S}'}$ is not inundated but faces hurricane storm surge related flooding during period t and under sea level states $\mathcal{S} \in \Xi_{t-1}$ and $\mathcal{S}' \in \Xi_t$ for which $p_{t-1}^{\mathcal{S}\mathcal{S}'} > 0$, we designate the water depth used to calculate the flood cost by a continuous variable $z_{it\mathcal{S}\mathcal{S}'}$. As mentioned before, if a grid $i \in R_t^{\mathcal{S}'} \cup Q_t^{\mathcal{S}'}$ is inundated, then it is assumed to be only subject

to the permanent flooding cost, and not the hurricane storm surge cost. This means that if $w_{itSS'} = 1$ for some $t \in \mathcal{T}$, $\mathcal{S} \in \Xi_{t-1}$, $\mathcal{S}' \in \Xi_t$, and $i \in R_t^{\mathcal{S}'} \cup Q_t^{\mathcal{S}'}$, then $z_{itSS'}$ is assumed to be zero.

If a grid $i \in \Phi$ is inundated during a period (permanent flooding), there is a fixed cost (i.e., g_i) for losing that grid during that period. If a grid $i \in \Phi$ is not inundated but is affected by hurricane storm surge level during a period (temporary flooding), then the cost is assumed to be a linear depth damage curve (using parameter f_i) that depends on the depth of the flood in grid i during that period. Using variables $w_{itSS'}$ and $z_{itSS'}$, and incorporating the discount rate for each period, we have the expected flood cost (denoted by EFC) as shown in Equation (2).

$$EFC = \sum_{t=1}^{t_{max}} \sum_{\mathcal{S} \in \Xi_{t-1}} \sum_{\mathcal{S}' \in \Xi_t} \frac{p_{t-1}^{\mathcal{SS}'}}{\lambda^t} \left(\sum_{i \in R_t^{\mathcal{S}'} \cup \hat{R}_t^{\mathcal{S}'}} f_i z_{itSS'} + \sum_{i \in R_t^{\mathcal{S}'}} g_i w_{itSS'} \right) \tag{2}$$

3.2.3 Associated constraints and the full model

Minimize $\qquad\qquad\qquad\qquad\qquad EIC + EFC \qquad\qquad\qquad\qquad\qquad$ (3)

Subject to:

$x_{i1(0,0)} \geq h_i + m v_{i1(0,0)}$ $\qquad\qquad\qquad\qquad\qquad\qquad\qquad\qquad\qquad \forall i \in \Phi$ (4)

$x_{i1(0,0)} \leq h_i + M v_{i1(0,0)}$ $\qquad\qquad\qquad\qquad\qquad\qquad\qquad\qquad\qquad \forall i \in \Phi$ (5)

$x_{i(t+1)\mathcal{S}'} \geq x_{it\mathcal{S}} + m v_{i(t+1)\mathcal{SS}'}$ $\qquad\qquad \forall i \in \Phi, \forall t \in \{1, \ldots, t_{max}-1\}, \forall \mathcal{S} \in \Xi_{t-1}, \mathcal{S}' \in \Xi_t : p_{t-1}^{\mathcal{SS}'} > 0$ (6)

$x_{i(t+1)\mathcal{S}'} \leq x_{it\mathcal{S}} + M v_{i(t+1)\mathcal{SS}'}$ $\qquad\qquad \forall i \in \Phi, \forall t \in \{1, \ldots, t_{max}-1\}, \forall \mathcal{S} \in \Xi_{t-1}, \mathcal{S}' \in \Xi_t : p_{t-1}^{\mathcal{SS}'} > 0$ (7)

$c \sum_{i \in \Phi} (x_{i1(0,0)} - h_i) \leq b_1$ $\qquad\qquad\qquad\qquad\qquad\qquad\qquad\qquad\qquad\qquad$ (8)

$c \sum_{i \in \Phi} \dfrac{(x_{i(t+1)\mathcal{S}'} - x_{it\mathcal{S}})}{\lambda^t} \leq b_{(t+1)}$ $\qquad\qquad \forall t \in \{1, \ldots, t_{max}-1\}, \forall \mathcal{S} \in \Xi_{t-1}, \mathcal{S}' \in \Xi_t : p_{t-1}^{\mathcal{SS}'} > 0$ (9)

$w_{itSS'} \geq \dfrac{(s' - x_{it\mathcal{S}})}{M} - (1 - y_{itSS'})$

$\qquad\qquad\qquad \forall t \in \{1, \ldots, t_{max}\}, \forall \mathcal{S} \in \Xi_{t-1}, \forall \mathcal{S}' = (s', \hat{s}') \in \Xi_t : p_{t-1}^{\mathcal{SS}'} > 0, \forall i \in R_t^{\mathcal{S}'}$ (10)

$w_{itSS'} \geq \dfrac{(s' - h_i)}{M} - (1 - y_{itSS'})$

$\qquad\qquad\qquad \forall t \in \{1, \ldots, t_{max}\}, \forall \mathcal{S} \in \Xi_{t-1}, \forall \mathcal{S}' = (s', \hat{s}') \in \Xi_t : p_{t-1}^{\mathcal{SS}'} > 0, \forall i \in Q_t^{\mathcal{S}'}$ (11)

$\sum_{i' \in N_t^{\mathcal{S}'}(i) \cap (R_t^{\mathcal{S}'} \cup Q_t^{\mathcal{S}'})} w_{i'tSS'} \leq |N_t^{\mathcal{S}'}(i)| \, y_{itSS'}$

$\qquad\qquad\qquad \forall t \in \{1, \ldots, t_{max}\}, \forall \mathcal{S} \in \Xi_{t-1}, \forall \mathcal{S}' \in \Xi_t : p_{t-1}^{\mathcal{SS}'} > 0, \forall i \in R_t^{\mathcal{S}'} \cup Q_t^{\mathcal{S}'} : o \notin N_t^{\mathcal{S}'}(i)$ (12)

$y_{itSS'} = 1$

$\qquad\qquad\qquad \forall t \in \{1, \ldots, t_{max}\}, \forall \mathcal{S} \in \Xi_{t-1}, \forall \mathcal{S}' \in \Xi_t : p_{t-1}^{\mathcal{SS}'} > 0, \forall i \in R_t^{\mathcal{S}'} \cup Q_t^{\mathcal{S}'} : o \in N_t^{\mathcal{S}'}(i)$ (13)

$$z_{itSS'} \geq (\hat{s}' - x_{itS}) - M(1 - \hat{y}_{itSS'} + w_{itSS'})$$

$$\forall t \in \{1, \ldots, t_{max}\}, \ \forall \mathcal{S} \in \Xi_{t-1}, \ \forall \mathcal{S}' = (s', \hat{s}') \in \Xi_t : p_{t-1}^{SS'} > 0, \ \forall i \in R_t^{S'} \tag{14}$$

$$z_{itSS'} \geq (\hat{s}' - h_i) - M(1 - \hat{y}_{itSS'} + w_{itSS'})$$

$$\forall t \in \{1, \ldots, t_{max}\}, \ \forall \mathcal{S} \in \Xi_{t-1}, \ \forall \mathcal{S}' = (s', \hat{s}') \in \Xi_t : p_{t-1}^{SS'} > 0, \ \forall i \in Q_t^{S'} \tag{15}$$

$$z_{itSS'} \geq (\hat{s}' - x_{itS}) - M(1 - \hat{y}_{itSS'})$$

$$\forall t \in \{1, \ldots, t_{max}\}, \ \forall \mathcal{S} \in \Xi_{t-1}, \ \forall \mathcal{S}' = (s', \hat{s}') \in \Xi_t : p_{t-1}^{SS'} > 0, \ \forall i \in \hat{R}_t^{S'} \tag{16}$$

$$z_{itSS'} \geq (\hat{s}' - h_i) - M(1 - \hat{y}_{itSS'})$$

$$\forall t \in \{1, \ldots, t_{max}\}, \ \forall \mathcal{S} \in \Xi_{t-1}, \ \forall \mathcal{S}' = (s', \hat{s}') \in \Xi_t : p_{t-1}^{SS'} > 0, \ \forall i \in \hat{Q}_t^{S'} \tag{17}$$

$$\sum_{i' \in N_t^{S'}(i)} z_{i'tSS'} + \sum_{i' \in N_t^{S'}(i) \cap (R_t^{S'} \cup Q_t^{S'})} w_{i'tSS'} \leq |N_t^{S'}(i)| \, (M+1)\hat{y}_{M{itSS'}}$$

$$\forall t \in \{1, \ldots, t_{max}\}, \ \forall \mathcal{S} \in \Xi_{t-1}, \ \forall \mathcal{S}' \in \Xi_t : p_{t-1}^{SS'} > 0, \ \forall i \in R_t^{S'} \cup Q_t^{S'} \cup \hat{R}_t^{S'} \cup \hat{Q}_t^{S'} : o \notin N_t^{S'}(i) \tag{18}$$

$$\hat{y}_{itSS'} = 1$$

$$\forall t \in \{1, \ldots, t_{max}\}, \ \forall \mathcal{S} \in \Xi_{t-1}, \ \forall \mathcal{S}' \in \Xi_t : p_{t-1}^{SS'} > 0, \ \forall i \in R_t^{S'} \cup Q_t^{S'} \cup \hat{R}_t^{S'} \cup \hat{Q}_t^{S'} : o \in N_t^{S'}(i) \tag{19}$$

$$z_{itSS'} \geq 0 \qquad \forall t \in \{1, \ldots, t_{max}\}, \ \forall \mathcal{S} \in \Xi_{t-1}, \ \forall \mathcal{S}' \in \Xi_t : p_{t-1}^{SS'} > 0, \ \forall i \in R_t^{S'} \cup Q_t^{S'} \cup \hat{R}_t^{S'} \cup \hat{Q}_t^{S'} \tag{20}$$

$$w_{itSS'} \in \{0,1\} \qquad \forall t \in \{1, \ldots, t_{max}\}, \ \forall \mathcal{S} \in \Xi_{t-1}, \ \forall \mathcal{S}' \in \Xi_t : p_{t-1}^{SS'} > 0, \ \forall i \in R_t^{S'} \cup Q_t^{S'} \tag{21}$$

$$v_{i1(0,0)} \in \{0,1\} \qquad \forall i \in \Phi \tag{22}$$

$$v_{itSS'} \in \{0,1\} \qquad \forall t \in \{2, \ldots, t_{max}\}, \ \forall \mathcal{S} \in \Xi_{t-2}, \ \forall \mathcal{S}' \in \Xi_{t-1} : p_{t-2}^{SS'} > 0, \ \forall i \in \Phi \tag{23}$$

$$y_{itSS'} \in \{0,1\} \qquad \forall t \in \{1, \ldots, t_{max}\}, \ \forall \mathcal{S} \in \Xi_{t-1}, \ \forall \mathcal{S}' \in \Xi_t : p_{t-1}^{SS'} > 0, \ \forall i \in R_t^{S'} \cup Q_t^{S'} \tag{24}$$

$$\hat{y}_{itSS'} \in \{0,1\} \qquad \forall t \in \{1, \ldots, t_{max}\}, \ \forall \mathcal{S} \in \Xi_{t-1}, \ \forall \mathcal{S}' \in \Xi_t : p_{t-1}^{SS'} > 0, \ \forall i \in R_t^{S'} \cup Q_t^{S'} \cup \hat{R}_t^{S'} \cup \hat{Q}_t^{S'} \tag{25}$$

The elevation of a grid $i \in \Phi$ is assumed to stay constant or increase due to an investment in building dikes and levees on the grid. Using Inequalities (4)-(7), the model ensures that a grid $i \in \Phi$ cannot be lowered in elevation from its initial elevation h_i or any subsequent elevation it may be raised to in the planning horizon. These equations also ensure that if a grid $i \in \Phi$ is elevated at the start of a period, the increase in elevation is at least equal to the minimum required threshold m. Notice that Inequalities (6)-(7) are written for any possible transition of water level states from a period $t-1$ to a period t (with positive probability) as we do not need to enforce these requirements on impossible water level state transitions. This is the case for many of the constraints in our proposed model. Inequalities (8) and (9) limit the amount of money spent at the start of a given period t for raising the elevations of grids in Φ by a user-specified parameter b_t.

Given a period t and water level states $\mathcal{S} \in \Xi_{t-1}$ and $\mathcal{S}' = (s', \hat{s}') \in \Xi_t$ with positive transition probabilities, a grid $i \in R_t^{S'} \cup Q_t^{S'}$ is protected from inundation during period t, if its elevation (i.e.,

$x_{it\mathcal{S}}$ for $i \in R_t^{\mathcal{S}'}$, and h_i for $i \in Q_t^{\mathcal{S}'}$) is higher than permanent sea level s'. Grid i is also protected if it does not have a hydraulic connection to the sea via one or more paths through inundated grids in $R_t^{\mathcal{S}'} \cup Q_t^{\mathcal{S}'}$. This secondary protection is determined by checking if grid i is a neighbor of the sea grid or it has any adjacent grid $i' \in N_t^{\mathcal{S}'}(i) \cap (R_t^{\mathcal{S}'} \cup Q_t^{\mathcal{S}'})$ that is inundated, and is represented by a binary variable $y_{it\mathcal{S}\mathcal{S}'}$ in the model. If grid i is safe from inundation due to not being a neighbor of the sea grid and also due to the absence of a hydraulic connection to the ocean through inundated grids in $R_t^{\mathcal{S}'} \cup Q_t^{\mathcal{S}'}$, $y_{it\mathcal{S}\mathcal{S}'}$ is zero, and one otherwise. Using variables $y_{it\mathcal{S}\mathcal{S}'}$, Inequalities (10)-(13) along with the objective function guarantee that grid $i \in R_t^{\mathcal{S}'} \cup Q_t^{\mathcal{S}'}$ is inundated during period t (i.e., $w_{it\mathcal{S}\mathcal{S}'} = 1$) if and only if its elevation is below the sea level s' and it is a neighbor of the sea grid or has a hydraulic path through inundated grids to the sea (i.e., $y_{it\mathcal{S}\mathcal{S}'} = 1$).

With the temporary flooding during a period t and under water level states $\mathcal{S} \in \Xi_{t-1}$ and $\mathcal{S}' = (s', \hat{s}') \in \Xi_t$ with positive transition probabilities, a grid $i \in R_t^{\mathcal{S}'} \cup Q_t^{\mathcal{S}'} \cup \hat{R}_t^{\mathcal{S}'} \cup \hat{Q}_t^{\mathcal{S}'}$ incurs hurricane storm surge flooding, if and only if its elevation (i.e., $x_{it\mathcal{S}}$ for $i \in R_t^{\mathcal{S}'} \cup \hat{R}_t^{\mathcal{S}'}$, and h_i for $i \in Q_t^{\mathcal{S}'} \cup \hat{Q}_t^{\mathcal{S}'}$) is below water level $\hat{s}'$, it is a neighbor of the sea grid or has a hydraulic connection to the sea via a path through flooded grids (permanent or temporary), and it is not inundated. A grid $i \in R_t^{\mathcal{S}'} \cup Q_t^{\mathcal{S}'} \cup \hat{R}_t^{\mathcal{S}'} \cup \hat{Q}_t^{\mathcal{S}'}$ being a neighbor of the sea grid or existence of a hydraulic path to the sea from this grid is captured by the binary variable $\hat{y}_{it\mathcal{S}\mathcal{S}'}$, which is equal to one if grid i is a neighbor of the sea or such a path exists, and zero otherwise. Inequalities (14)-(20) along with the objective function, use variables $\hat{y}_{it\mathcal{S}\mathcal{S}'}$ to assure that a grid $i \in R_t^{\mathcal{S}'} \cup Q_t^{\mathcal{S}'} \cup \hat{R}_t^{\mathcal{S}'} \cup \hat{Q}_t^{\mathcal{S}'}$ is temporarily flooded during period t (i.e., $z_{it\mathcal{S}\mathcal{S}'} > 0$) if and only if its elevation is below the sea level $\hat{s}'$, it is a neighbor of the sea grid or has a hydraulic path through flooded grids to the sea (i.e., $\hat{y}_{it\mathcal{S}\mathcal{S}'} = 1$), and it is not inundated (i.e., $w_{it\mathcal{S}\mathcal{S}'} = 0$ if $i \in R_t^{\mathcal{S}'} \cup Q_t^{\mathcal{S}'}$).

3.3 Computational complexity and solution approach

Having defined the FRM problem to this point in Section 3, we address its computational complexity in Theorem 1 below, and establish that the decision version of this problem is indeed NP-complete.

THEOREM 1. *The decision version of the FRM problem is NP-complete.*

We present the proof of Theorem 1 in the electronic companion Section EC.1 by reducing the well-known Knapsack problem (Karp 1972) to a special case of the FRM decision version. Given the intractability of the FRM problem and considering the extremely large number of variables and constraints in Formulation (3)-(25), solving this problem by classical branch-and-cut algorithms available via commercial solvers is impractical and computationally expensive. In our case study in Section 4, to solve the FRM problem within practical time limits and obtain managerial insights, we employed two different methods: a simulation-based approach and a scenario-based approach. The reader is referred to Sections 4.2 and 4.3 for the details of these proposed methods.

4 Case study

In this section, we employ our proposed model to develop a decision-support system for building levees to protect Boston, using only publicly available data. This research is the fifth paper of a series of articles on climate change adaptation in Boston. Douglas et al. (2012) identified major obstacles and incentives for adaptation based upon representative focus groups, Kuhl et al. (2014) examined in more details some of the challenges and implementation barriers for evacuation in an environmental-justice community, Kirshen et al. (2018a) addressed how to involve vulnerable exposed populations in urban adaptation strategy planning and the use of multi-stakeholder collaborative processes, and Zandvoort et al. (2019) studied how pathway thinking can be used to inform landscape architects to design sustainable and adaptive landscapes.

4.1 Data and experiment settings

As shown in Figure 3(a), a neighborhood in Boston marked within the solid boundary line is the region of interest in our case study. This region presents a large coastal front with a relatively dense population and a variety of building structures. The surrounding region includes the neighboring towns of Winthrop and Revere, as well as Boston Logan Airport owned by MassPort and not under the control of the city (Aloisi 2017). By following the procedure outlined in Section 3.1.2, we create the network for our model by overlaying the grids as shown in Figure 3(b), and then Figure 3(c) shows the identified areas of interest and relevance in our case study. This region has a nonuniform topography with several hilly areas shown by black hexagons in Figure 3(c) that overlook the city and are not at risk of flooding because of their higher elevations. In creating the grid attributes (i.e., h_i, f_i, and g_i), we use open source tax appraisal data from the City of Boston (Boston 2020, BostonGIS 2016) and Light Detection and Radar (LIDAR) elevation data from the Massachusetts Commonwealth (MassGIS 2017). Full details of the data sources and transformations conducted to create the network and estimate grid parameters h_i, f_i, and g_i are found in the electronic companion Section EC.2.2.

Given that the model's parameters are estimated based on available open-source data, there might be inaccuracies associated with the estimated values. Therefore, we used a range of possible values for some of the primary parameters as shown in Table 1, and conducted a sensitivity analysis in our experiments to show the behavior of the optimal objective as the values for these parameters change. We justify the range of values chosen for each one of these primary parameters as follows. In evaluating flooding of coastal mega-cities, Aerts et al. (2014) provide multiple sources and a range of discount rates (d) applicable to studies evaluating flood protection investment, leading to our chosen values of 3, 5, and 7 percent. As mentioned before, raising a grid requires initial setup costs, including
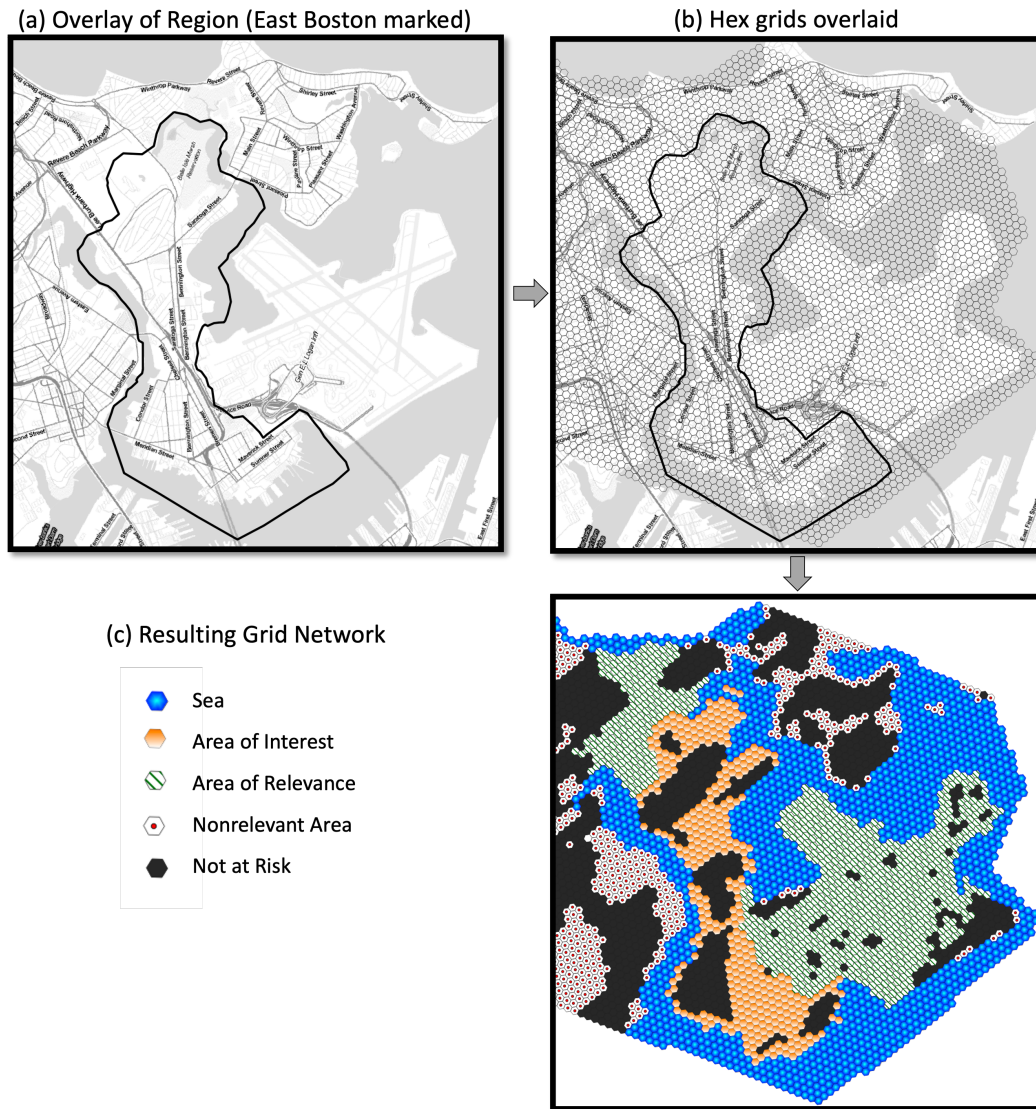
(a) Overlay of Region (East Boston marked)

(b) Hex grids overlaid

(c) Resulting Grid Network

- 🔷 Sea
- ⬡ Area of Interest
- ⬡ Area of Relevance
- ⦿ Nonrelevant Area
- ⬢ Not at Risk

Figure 3 Map of Boston and overlays to make the network.

field investigation, surface exploration, field testing, and foundation construction. As a result, in practice, grids are not raised cm-by-cm over the years; instead, they are elevated via large discrete investments. We incorporate this in our model by introducing the minimum threshold for elevation increase in a land grid parameter (m). We chose values of 1, 3, and 5 meters for parameter m, which is also based on past studies showing a breakdown of heights for levee projects around the globe as discussed in Jonkman et al. (2013). To determine the levee build cost (c), we initially started with a linear estimate of \$450 per foot build-up per linear foot of wall (Hecht and Kirshen 2019) as a potential lower value. In order to provide for assessing sensitivity, we evaluated and chose values of \$5M, \$15M, and \$25M per kilometer of wall built one meter in height based on historical and regional factors affecting these values as discussed in Jonkman et al. (2013). To conduct sensitivity analysis on

the values used for storm surge flooding, we shift the slope of the estimated depth damage function curve ($\bar{f}_i$) by $\pm 25\%$ to attain f_i. Finally, we determined the budget values (b_t) by initially running the full range of simulations with an unlimited budget. We then looked for clear breakpoints for the initial period spends across all scenarios to use them as possible values for budgets.

Table 1 Parameter values used to conduct sensitivity analysis

Parameter	Values used	Units
Discount rate (d)	3, 5, 7	%
Minimum elevation increase (m)	1, 3, 5	meters
Grid elevation cost (c)	5, 15, 25	\$M/km per m
Storm flood damage curve (f_i)	$0.75\bar{f}_i$, $\bar{f}_i$, $1.25\bar{f}_i$	\$M/m
Budget per period (b_t)	0, 25, 50, 75, 100, 150, 200, 400, 600	\$M

As discussed in Section 3.3, given the intractability and impracticality of solving the FRM model, we employ two different approaches, namely a simulation-based approach and a scenario-based approach to handle this challenge. In both methods, we built the related models using Python 3.8.5 and used Gurobi version 9.5.2 as the commercial solver. The experiments were conducted on Amazon Web Services EC2 c5n.4xlarge instances (AWS 2023). Given more than 100K individual optimization runs for the case study, we set the termination condition for each optimization run as either one percent optimality gap or one hour running time limit, whichever is observed first. Most (98.5%) of the runs completed by reaching the one percent optimality gap. In the remainder of this article, we refer to the best solution found before reaching the termination condition in each optimization run as the "optimal" solution. We discuss the details of our simulation- and scenario-based methods next.

4.2 Simulation-based approach

The first approach is a simulation-based approach in which we solve the FRM Formulation (3)-(25) for each possible combination of chosen values for the model's parameters on simulated sea level states sample paths each composed of a collection of possible sea level states over the next five decades. In this approach, each run of the model is done on a single simulated sea level states path (i.e., we assume $\Xi_t = \{\mathcal{S}_t\}$, where $\mathcal{S}_t$ is the sea level state on the considered path during period $t \in \{1, \ldots, 5\}$), which makes this solution approach computationally practical. Then, incorporating the probability associated with each simulated sea level state path, we compute and analyze the expected optimal objective of the FRM Formulation (3)-(25) across all simulation runs.

To sample sea level states paths over the next five decades in our simulation, we use a collection of four greenhouse gas emission pathways (also known as Representative Concentration Pathways or RCPs) (IPCC 2014), nine probabilistic sea level rise curves per RCP (Kopp et al. 2017), and four

potential hurricane storm surge levels (NOAA 2018). The sampling is done by first randomly selecting one of the four RCPs, followed by a random selection of one of the nine possible sea level rise curves associated with the chosen RCP (results in components s for all five sea level states) and a random selection of one of the four potential hurricane storm surge levels (results in components $\hat{s}$ for all five sea level states). We assume that all four RCPs are equally likely to happen. We also estimate the probabilities for all sea level rise curves under all RCPs and the four storm surge levels using a linear interpolation method on corresponding exceedance curves. We provide the details of these probability estimations in the electronic companion Section EC.2.1. Using this sampling approach, we can derive the actual distribution for all possible simulated five-period sea level states paths. This distribution contains a total of 144 five-period sea level states paths and their probabilities of occurrence as shown in Table EC.4 in Section EC.2.1. We use Ω to denote the set containing these 144 paths, and $p(\boldsymbol{S})$ to represent the probability associated with a path $\boldsymbol{S} \in \Omega$.

Assuming that the distribution of all possible simulated sea level states paths is given by Table EC.4, we solve the FRM Formulation (3)-(25) for a possible combination of chosen values for the model's parameters 144 times, each time on a distinct five-period simulated sea level states path, and compute the expected optimal objective for the chosen parameters' combination in our simulation experiment as $\sum_{\boldsymbol{S} \in \Omega} p(\boldsymbol{S}) z_{\boldsymbol{S}}^*$, where $z_{\boldsymbol{S}}^*$ is the optimal objective of the FRM Formulation (3)-(25) for the chosen parameters' combination using path $\boldsymbol{S} \in \Omega$. We discuss key takeaways from our simulation-based approach below, and refer the reader to the electronic companion Section EC.4 for the full set of simulation results.

Figure 4 presents three simulation results with expected optimal costs reported for two extreme parameter settings and the mid-point of these settings, as shown in the inset table in this figure. In Figure 4, charts (a) and (b), the parameters selection results in the worst-case combination (i.e., highest overall costs). The "do nothing" (zero budget) expected costs nearly reach $340M. The optimal expected investment is $88.7M with a per-period budget of at least $400M. Notice that $88.7M is an expected value and there might be a sea level states path under which the build cost could be substantially more in a given period, but due to the low probability for such sea level states path, the expected value is much lower. This is the reason that with budgets less than $400M, the overall expected costs are higher. It is also important to note that even with budget values of more than $400M, there are combined expected storm surge and inundation costs tallying more than $70M. This is due to the fact that given the highest build costs (i.e., c) and the largest increments in levee heights (i.e., m) in this worst-case parameters setting, more grids are sacrificed to flooding and inundation over the planning horizon. This simulation's discounted flooding costs are higher due to the low discount rate causing future flooding to be more expensive at today's rates. Figure 4(b) provides a percentage by type breakdown of costs. Storm-surge flooding under lower budgets makes

Figure 4 Overall expected optimal costs and their percentage breakdown by per-period budget for worst-case (charts (a) & (b)), mid-case (charts (c) & (d)), and best-case (charts (e) & (f)) parameter settings across full 144 simulated sea level states paths.

Parameter values used in each chart	Chart		
Parameter	(a) & (b)	(c) & (d)	(e) & (f)
Discount rate (d) [%]	3	5	7
Minimum elevation increase (m) [meters]	5	3	1
Grid elevation cost (c) [\$M/km per m]	25	15	5
Storm flood damage curve (f_i) [\$M/m]	$1.25\bar{f_i}$	$\bar{f_i}$	$0.75\bar{f_i}$

up the bulk of costs. Not until the model reaches a \$400M per-period budget does the expected investment cost stabilize at an optimal point where an \$88.7M expected investment reduces total expected costs from "do nothing" by 52.3% while also reducing total expected flood-related damages by 78.5% (expected flooding cost of doing nothing is \$338.4M). On the other extreme parameters setting, Figure 4 charts (e) and (f) show that with lower minimum levee heights (i.e., m) and building costs (i.e., c), expected costs are the same under all budget values. Only in the "do nothing" case does the model reach total expected costs of \$82.8M, with inundated grids making up nearly 40% of those

costs. With just a \$10.6M expected investment over the planning horizon, the total expected costs
are reduced by 81.0%, while total expected flood-related damages are reduced by 94.3% (expected
flooding cost of doing nothing is \$82.8M). Of note, even at these investment costs, the model still
sacrifices some grids to storm-surge flooding and inundation, meaning they are not protected even
with the extra funding available to build. The behaviour of the expected optimal costs is in between
the two extreme cases for the mid-point parameters setting as shown in Figure 4 charts (c) and
(d). As mentioned before, Section EC.4 shows the full breakdown of expected costs and percentages
observed for all possible parameter combinations. The best overall expected cost reduction compared
to a "do nothing" policy is 92.2% across all parameter combinations and budget values (attained
when $d = 3\%$, $m = 1$m, $c = \$5$M/km per m, $f_i = 1.25 \bar{f}_i$, and $b_t \geq \$25M$ with a "do nothing" cost
of \$338.4M), while the average cost reduction is 63.2% (average cost of doing nothing is \$182.7M).
Across the board, investment shows a meaningful reduction in flood damages, but only until further
investment is no longer cost-beneficial.

In Figure 5, we show overall expected costs across per-period budgets with combinations of min-
imum levee heights (m) and levee costs (c) while holding the discount rate ($d = 3\%$) and the depth
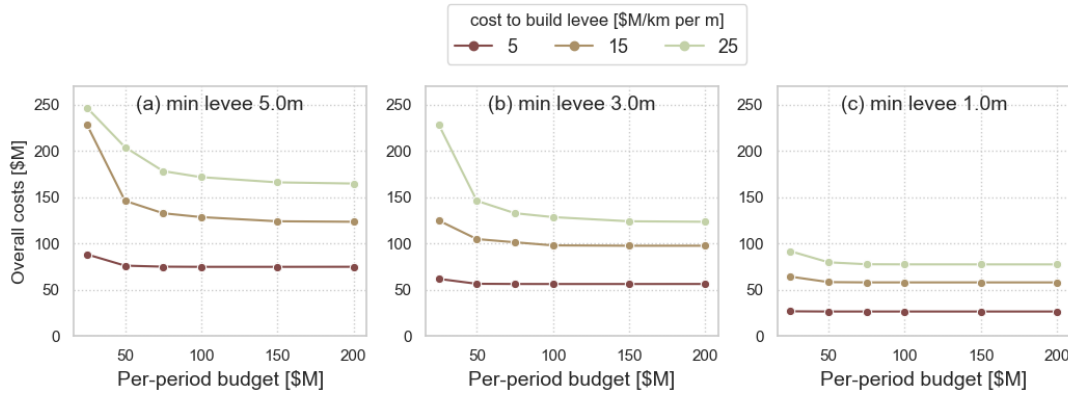damage function ($f_i = 1.25 \bar{f}_i$) constant.

Figure 5   Effects of varying minimum levee heights (m) and levee costs (c) on expected optimal costs for varying

per-period budgets ranging from \$25M to \$200M

(discount rate (d) at 3% and storm depth damage function slope (f_i) at $1.25 \bar{f}_i$).

In Figure 5(c), with $m = 1$m and $c = \$5$M/km per m, the lowest curve is constant regardless of
budget. As the value of c increases, the other curves begin increasing when the budget falls below
\$75M. In Figure 5(b), with $m = 3$m, the $c = \$5$M/km per m line remains constant until the budget
falls to \$25M. With higher values of c, the overall expected costs increase as the per-period budgets
fall. At the lowest budget of \$25M, there is a significant uptick in overall costs due to the inability

of the model to build up enough grids to protect the network overall. Finally, in Figure 5(a), the expected costs are rising again, especially at the lower budgets. At $m =$ 5m, both the \$15M/km per m and \$25M/km per m values of c show increased overall costs when falling below the \$200M per-period budget. At these higher values of m and c, the model hinders building levees on enough grids to provide adequate protection within the network overall. It uses constrained funding to protect the most valuable grids and initially requires higher funding to protect the network more broadly.

Figure 6 shows expected overall, build, storm surge, and inundation cost distributions for the three values of each parameter d, c, m, and f_i when holding the budget constant at \$50M.

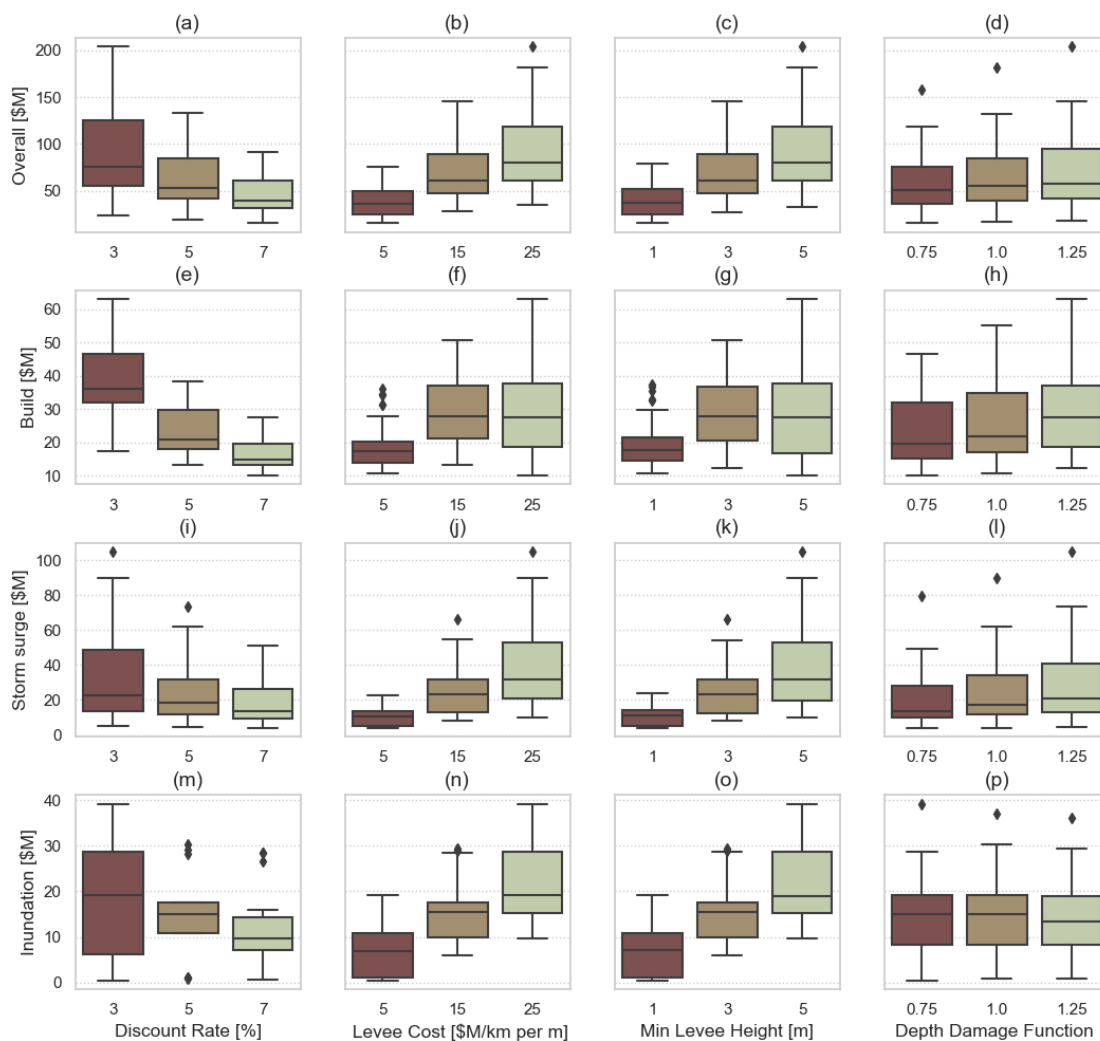**Figure 6**   Boxplots showing effects of changing parameters on expected costs for all \$50M budget runs.

The top row shows overall expected cost distributions for the simulations when varying each parameter. As anticipated, increasing discount rate reduces the expected overall costs, while increasing the other parameters causes higher overall expected costs. The discount rate has the largest overall effect

across model runs. In contrast, changes to the depth damage function (f_i) have the smallest effect, which makes sense given that it primarily affects storm surge flooding costs. Looking at individual cost charts is where we see some interesting effects. For instance, in Figure 5, we saw that changes to m and c result in significantly more flood-related damage at lower budgets. Figures 6 (f) and (g) show substantially lower build costs for levee costs of $c = \$5\text{M/km}$ per m and minimum levee height of $m = 1\text{m}$ than for the higher values of each parameter. Additionally, the median build cost for $m = 3\text{m}$ is higher than when $m = 5\text{m}$. The combination of c and m values are critical factors in evaluating building a levee system that can protect as much of the network as possible. At the lower values, adequate funding exists to leverage the network effect and build levees that protect as many grids as possible. However, at higher levee costs with higher minimum levee heights, the model shifts to protecting the most valuable grids in the network because the investment to protect more of the network is too costly.

When evaluating discount rate sensitivity in Figures 6 (e) and (m), there are notable observations in the individual build and inundation costs. At the 3% discount rate, the build costs' boxplot stretches upward, with its lower quartile higher than the upper quartile of the 5% boxplot. Similarly, at 3%, the inundation costs cover a wider range of values, while at 5%, the inundation cost distribution is much smaller, with a handful of outliers. The smaller discount rates cause future storm surge and flood costs to be higher in discounted terms. So, we interpret these observations to mean that the model is inclined to protect against inundation when those costs can be higher due to lower discount rates. The model invests earlier to protect those grids from future damages. However, with the higher discount rate of 5%, the model invests less because the discounted inundation costs are lower in future periods. Essentially, the lower discount rate tends to cause earlier investments due to flooding and inundation costs in future periods having a more considerable effect on costs in discounted terms.

Some key takeaways from the simulation experiment and its sensitivity analysis are:

1. From Figure 4, potential overall expected costs can be significantly reduced by investing only a small fraction of the "do nothing" flood-related costs independent of parameters' values. This quantifiably proves the effectiveness of a mitigation policy in dollar values and shows the extent of the loss for following a response-type strategy.

2. From Figure 4, some grids appear too expensive to protect through the network effect (or individually) and incur storm-surge flooding and inundation costs even when a surplus budget is available. Identifying such grids for planning purposes is not a trivial task and our proposed model can be an effective tool for this purpose. These grids form areas in which following a retreat-like policy is preferred. Building codes in these areas also need to be revised to ensure critical facilities are not on the lower levels in these areas.

3. From Figures 4 and 5, our model can be used to find optimal budget per period values that yield the minimum expected overall costs for a given combination of input parameters. We also observed that the levee cost (c) and minimum levee height (m) have the biggest effect on the amount of budget needed to reach the minimum expected overall cost before no further spending occurs. Our proposed model is a powerful tool for determining such meaningful budget values and can be used in financial planning for development of a levee system.

4. From Figure 6, the discount rate (d) has the largest effect on overall expected costs while the changes to the storm depth damage function (f_i) has the smallest effect. This is an important capability of our model as it can be used to identify parameters that require more accurate estimations because of their significant effects on levee construction planning and timing.

4.3 Scenario-based approach

Given the uncertainty associated with the expected sea level rise used in the model, policymakers might be interested in adopting a scenario-based approach by investigating individual scenarios ranging from the best- to the worst-case sea level rise predictions. For example, a policymaker might want to highlight the range of values for investment and flood cost across four different scenarios, namely optimistic, expected-low, expected-high, and high sea level rise scenarios for the next five periods (50 years). This scenario-based approach provides policymakers with meaningful insights to make decisions based on their judgment on anticipated future sea levels. To this aim, in this section, we focus on solving the FRM Formulation (3)-(25) on four scenarios (i.e., optimistic, expected-low, expected-high, and high sea level rise scenarios) chosen from the 144 simulated sea level states paths mentioned in Section 4.2. The chosen scenarios are paths numbered 114 (high), 130 (expected-high),85 (expected-low) and 64 (optimistic) in Table EC.4 of Section EC.2.1, respectively. The optimistic and high scenario values represent points near the extremes of the 144 simulated sea level states paths, while the expected-high and expected-low scenarios represent points near the middle. Similar to the case of the simulation-based method, we use the same ranges of values for the model's parameters to conduct a sensitivity analysis for each of the four scenarios considered. Figure 7 shows the results for these four chosen scenarios using the same worst-, mid-, and best-case parameter settings as in Section 4.2.

We see similar patterns in Figure 7 compared to Figure 4. In the best-case parameters column, all four scenarios show minimal change in total costs across all non-zero budgets. Therefore, the model mitigates the "do nothing" damages with funding available in the $25M per-period budget. For example, in the optimistic scenario (Figure 7(l)), when faced with $26.4M of "do nothing" costs, investing only 3.5% of that $26.4M results in a total overall cost reduction of 79.6%. We see similar effects across the other scenarios where an investment of a small percentage of the "do
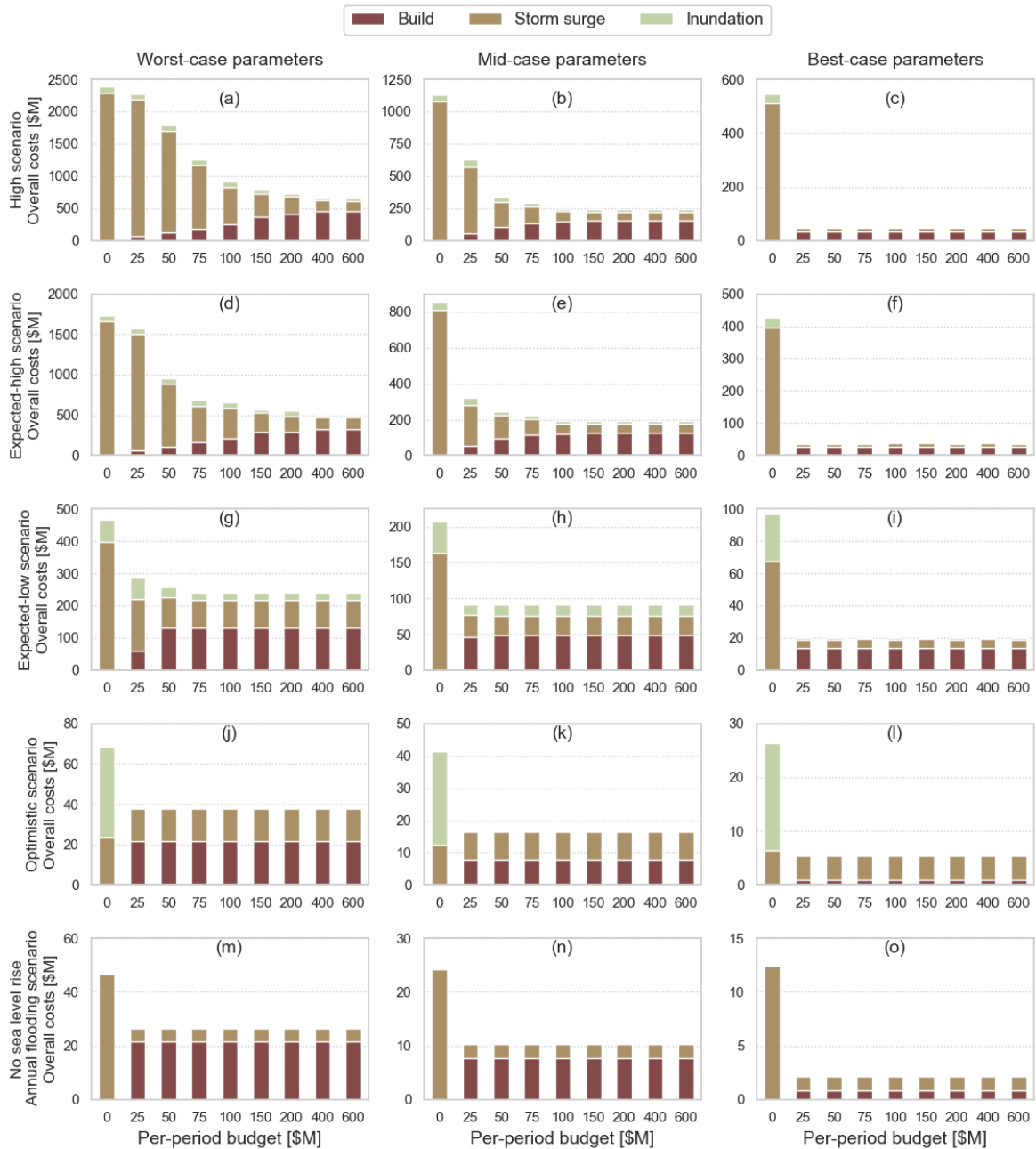
Figure 7   Overall optimal costs by per-period budget for worst-case, mid-case, and best-case parameter settings for no SLR with annual flooding, optimistic, expected-low, expected-high, and high sea level rise scenarios.

nothing" costs results in substantial overall cost reductions. Specifically, in the expected-low scenario (Figure 7(i)), investing 14.1% of \$96.6M leads to a 79.2% overall reduction; in the expected-high scenario (Figure 7(f)), investing 6.2% of \$426.7M results in a 91.1% overall reduction; and in the high scenario (Figure 7(c)), investing 6.1% of \$545.5M leads to a 91.3% overall reduction. Contrasting that with the worst-case parameters column, we observe that the overall costs increase significantly due to 1) higher investment required due to higher and more expensive levees and 2) more costly damages due to a lower discount rate and steeper depth damage function. In the high scenario and under the worst-case parameters, the overall costs of a "do nothing" policy nearly reach \$2.4B over 50 years. A substantial investment of \$454.8M is only 19.1% of the "do nothing" total costs but reduces overall costs by 72.4%. Section EC.4 shows the full breakdown of costs and percentages observed for all possible parameter combinations for each of the four sea level rise scenarios. In all four scenarios, investing in flood protection infrastructure at a fraction of the potential flood-related damages results in a meaningful reduction in overall costs.

While evaluating the costs under the four scenarios, we observed consistent sensitivity analysis behavior to that seen previously in Figure 6. The main difference in the scenario-based analysis is the extensive range of investment costs and flood damages. This wide range of sea level states causes substantial variation across the four scenarios, with the "do nothing" overall costs in the high scenario being 27.3 times larger than in the optimistic scenario when averaged across the different parameter settings. Investigating this range for an individual scenario and across different parameter settings also reveals interesting facts. In the optimistic scenario, when given the best-case parameters, the investment required is \$0.9M to handle the addressable risk, while in the worst-case parameters, the investment required is \$21.7M. This presents a reasonably manageable range for a policymaker trying to address the sensitivity of the optimal investment costs to the parameters' estimation accuracy while protecting Boston from the optimistic flooding. Contrast that with the challenge posed under the high scenario when these numbers go to \$33.0M and \$454.8M, respectively. This presents an extremely risk-averse policymaker with potentially hard trade-offs, and the policymaker must ensure sufficient diligence in estimation of parameters to defend their coastal areas adequately.

In addition to the four sea level rise scenarios discussed above, we also include a no sea level rise (only hurricane storm) flooding scenario in Figures 7 (m)-(o). Comparing this scenario with the other four potential sea level rise scenarios further emphasizes the magnitude of additional flooding costs caused by sea level rise, and calls for more attention to this potential threat. We see investments made in Figure 7 where the costs are balanced in the case of only-storm flooding. However, there are several combinations of parameters for which the model forgoes any investment regardless of the budget amount (see Figure EC.10 in Section EC.4). This happens when investment costs are high due to higher minimum levee heights and construction costs and future flood costs are low due

to higher discount rates. For a policymaker believing that sea levels do not rise, given the proper cost structure and levee scope, there is still considerable financial benefit to building such protection infrastructure. Section EC.4 shows the full breakdown of costs observed for all possible parameter combinations for no sea level rise (only-storm) flooding scenario.

Table 2 shows the per-period spend for the scenario and parameter combination shown in Figure 7(a). In this table, we include per-period budget data only up to $400M, because both the $600M and unlimited budget runs had the same optimal solutions as the $400M case. The investment costs per decade shown in the $400M row are essentially the actual amounts required in each period to reach the optimal solution, because even with the higher per-period budgets ($600M and unlimited cases), the model will only spend up to these levels, and then spends no more. As the per-period budget decreases, however, the budget constraints start enforcing limits on per-period spend. We see that with reduced spending in 2030, the model shifts development costs into future periods to mitigate as much damage as possible. This effect results in total investment decreasing as the per-period budget decreases, while the total flood-related damages proliferate with each reduction in per-period budget. Of note, if possible, investment costs are pushed to future periods at the discounted rate. For instance, in both the $150M and $200M budgets, one can see reduced spending in 2060 compared to 2070. One key takeaway from Table 2 when looking at the $400M row is that an initial influx of cash in the first period can reduce future cash needs while significantly reducing overall total costs experienced throughout the planning horizon.

Table 2 Investment costs per period for the high sea level rise scenario and worst-case parameter combination given for each per-period budget value

Per-period Budget [$M]	Discounted Investment Cost [$M]					Total Investment [$M]	Total Flood Related Costs [$M]
	2030	2040	2050	2060	2070		
0.0	0.0	0.0	0.0	0.0	0.0	0.0	2,379.0
25.0	21.7	16.1	12.0	8.9	6.6	65.3	2,205.0
50.0	43.3	32.2	24.0	17.8	13.3	130.6	1,657.1
75.0	65.0	48.3	36.0	26.8	13.3	189.3	1,064.1
100.0	86.6	64.4	47.9	35.7	26.5	261.2	649.6
150.0	129.9	96.7	71.9	26.8	39.8	365.1	424.8
200.0	173.2	145.0	24.0	26.8	39.8	408.7	319.2
400.0	281.5	80.5	24.0	35.7	33.2	454.8	202.9

In summary, the following are the key takeaways from our scenario-based experiment.

1. From Figure 7, similar to the simulation results, all four scenarios show opportunities to significantly reduce potential overall costs with levels of investment that are a fraction of "do nothing" flood-related costs. This again demonstrates how rewarding a mitigation approach could be compared to a wait-and-see response-type policy.

2. From Figure 7, the wide range of potential investment and flood costs shows the importance of adequately assessing the potential risks and estimating the relevant parameters for making an investment decision. The more risk-averse the decision maker is, the more accurate their estimation of the model's parameters need to be.

3. From Figure 7, sea level rise threat is real, and can potentially increase the storm-only flood damages by several orders of magnitude. Even if policymakers do not believe sea levels are rising, there is still value to invest in protecting against annual storm flooding if the anticipated cost structures and discount rate support building a levee.

4. From Table 2, policymakers get a view into the actual funding required per decade to mitigate flood-related damages, allocating only as much money as needed to address risks over time. This again proves the value of our model when used for budgeting and financial planning purposes.

Before concluding the case study section, we find it necessary to investigate the generalizability of the takeaways from our Boston case study to other coastal areas with different at-risk network structures. To this aim, we conducted the same simulation-based and scenario-based experiments on 50 randomly-generated at-risk networks. After comparing the results from the 50 random network experiments with the Boston case study, we conclude that the key takeaways highlighted in Sections 4.2 and 4.3 are generalizable to any other coastal area. Full details of random network creation and experiment outputs are available in electronic companion Section EC.5.

5   Discussion and conclusion

In this study, we employ networks to model the movement of temporary (storm-related) and permanent sea level rise floods on land and propose a multi-stage stochastic program with recourse for cost-benefit analysis of creating dikes and levees in a coastal city to mitigate climate-change-induced flood damages. According to the experiments in Section 4, our model enables an improved understanding of the costs associated with protecting an urban coastal neighborhood from rising sea levels. A "do nothing" strategy of zero flood protection infrastructure investment incurs significant flooding costs. When evaluating the full range of scenarios, modest investment in the creation of dikes and levees enhances protection significantly, causing a precipitous drop in overall long-term costs. Our model is also a powerful tool for identifying areas where the development of dikes and levees is not financially justified. In this case, decision-makers should consider a retreat-like policy and revise construction codes, taking into account the possibility of flooding in lower levels of buildings in these areas.

Our model provides planners with a powerful budgeting and financial planning tool by including a constrained budget. If faced with limited funding, decision-makers can conduct what-if analysis to evaluate potential flood-related damages. We observed that the cost of levee per meter elevation and

the minimum threshold for levee height are the two most important construction factors affecting the optimal budget allocations. Moreover, our model effectively identifies critical parameters that necessitate precise estimation to prevent substantial costs resulting from poor assumptions. Based on our experiments, the discount rate is one of the parameters that require very accurate estimation as it has the largest effect on overall expected costs.

We observed an extreme range for investment and flooding costs across different sea level rise scenarios and parameters' values in our experiments. Going from an optimistic SLR scenario with low-cost parameters estimation to a high SLR scenario with high-cost parameters estimation, the optimal costs increase more than \$650M, while the "do nothing" costs increase more than \$2,350M. This further emphasizes the importance of accurate sea level rise forecasts and precise estimations of cost parameters. Looking more closely at each SLR scenario, the average cost savings between the model's optimal outcomes versus the "do-nothing strategy" can be substantial. Specifically, in the optimistic scenario (best-case), we see a cost reduction of as much as 85.0% (on \$58.9M in damages for DNS) and average cost reductions of 60.2% (on \$44.5M in average damages for DNS). These same maximum and average cost reductions are 92.5% (on \$465.9M for DNS) and 59.2% (on \$237.3M for DNS) for the expected-low scenario, 96.5% (on \$1,730.1M for DNS) and 78.3% (on \$936.6M for DNS) in the expected-high scenario, and 96.5% (on \$2,379.3M for DNS) and 78.9% (on \$1,255.4M for DNS) in the high (worst-case) scenario. Another interesting conclusion is that even if decision-makers do not believe that sea levels are rising, our experiments prove that investing in the creation of dikes and levees to only protect against annual storm flooding is still financially justified.

Our model's multi-stage structure and recourse feature enable prospective community leaders to adapt their measures to the unfolding sea level rise situation, as recommended in Kirshen et al. (2018b). The model also allows quickly incorporating the latest thinking in sea level rise probabilities, thereby interpreting and applying potential probabilities for a broader range of sea level rise as found in studies by Kopp et al. (2017) and Sweet et al. (2017). The agile nature of our proposed method also enables quick solution adaptation when facing infrastructure changes in built-up areas, new risks in specific locations, and changes in flood protection design and costs.

In pursuing this research, we aimed to build a model that applies to any coastal area using readily available open-source data. Using a collection of 50 randomly generated networks, we showed that our model and the insights from our Boston case are generalizable to any other coastal area with the same data availability. For example, low-lying cities like Miami and New Orleans have publicly available elevation data (through the NOAA Data Access Viewer (NOAA 2021)) and appraised tax data (through local municipal Open Data Hubs (USGSA 2009)). In practice, these cities could similarly use this methodology to evaluate their city's changing situation.

As potential directions for future studies, researchers may focus on potential impacts of hurricane storm and sea level rise flooding on other infrastructure such as roads and transportation networks. Moreover, future research may help mitigate the non-financial impacts of flooding associated with disrupted communities, lost lives, and displacement of people, particularly those from socially or economically marginalized communities. Though we do not currently capture these non-monetary parameters, there is an opportunity to incorporate these considerations in the future development of our proposed model.

References

Abadie, Luis María. 2018. Sea level damage risk with probabilistic weighting of IPCC scenarios: An application to major coastal cities. *Journal of Cleaner Production*, 175, 582-598.

Abel, David. 2021. Costs of floods will soar, study warns: Advocates call for plans to manage a retreat from low-lying coastal areas. *Boston Globe*, https://www.proquest.com/newspapers/costs-floods-will-soar-study-warns/docview/2491776772/se-2 (accessed on 03 Feb 2023).

Aerts, Jeroen C. J. H., W. J. Wouter Botzen, Kerry Emanuel, Ning Lin, Hans de Moel, Erwann O. Michel-Kerjan. 2014. Evaluating Flood Resilience Strategies for Coastal Megacities. *Science*, 344 (6183), 473-475.

Akter, Shahriar, Samuel Fosso Wamba. 2019. Big data and disaster management: a systematic review and agenda for future research. *Annals of Operations Research*, 283 (1), 939-959.

Aloisi, Jim. 2017. *Massport at 60: Shaping the Future Since 1956*. Massport, Boston.

Anguelov, Dragomir, Carole Dulong, Daniel Filip, Christian Frueh, Stéphane Lafon, Richard Lyon, Abhijit Ogale, Luc Vincent, Josh Weaver. 2010. Google Street View: Capturing the World at Street Level. *Computer*, 43 (6), 32-38.

Armal, Saman, Ziyan Chu, Brett Lingle, Michael L. Marston, Jeremy R. Porter, Oliver E. J. Wing. 2020. Assessing Property Level Economic Impacts of Climate in the US, New Insights and Evidence from a Comprehensive Flood Risk Assessment Tool. *Climate*, 8 (10), 116.

AWS. 2023. Amazon EC2 z1d Instances. https://aws.amazon.com/ec2/instance-types/c5/ (accessed on 15 Feb 2023).

Bagchi, Aniruddha, Jomon Aliyas Paul. 2014. Optimal Allocation of Resources in Airport Security: Profiling vs. Screening. *Operations Research*, 62 (2), 219-233.

Baranes, H.E., J.D. Woodruff, S.A. Talke, R.E. Kopp, R.D. Ray, R.M. DeConto. 2020. Tidally driven interannual variation in extreme sea level frequencies in the Gulf of Maine. *Journal of Geophysical Research: Oceans*, 125 (10), e2020JC016291.

Berman, Oded, Arieh Gavious, Mozart B. C. Menezes. 2012. Optimal response against bioterror attack on airport terminal. *European Journal of Operational Research*, 219 (2), 415-424.

Besiou, Maria, Luk N. Van Wassenhove. 2020. Humanitarian Operations: A World of Opportunity for Relevant and Impactful Research. *Manufacturing & Service Operations Management*, 22 (1), 135-145.

Birch, Colin P. D., Sander P. Oom, Jonathan A. Beecham. 2007. Rectangular and hexagonal grids used for observation, experiment and simulation in ecology. *Ecological Modelling*, 206 (3), 347-359.

Boston. 2016. Climate Ready Boston - Final Report. Tech. rep., City of Boston. https://www.boston.gov/departments/environment/preparing-climate-change (accessed on 18 Aug 2018).

Boston, City of. 2020. Property Assessment FY2016 Data Key. https://data.boston.gov/dataset/property-assessment/resource/dbdc1bd8-60af-4913-a788-5f91cb68541b (accessed on 04 Apr 2020).

Boston, City of. 2023. Climate Ready Boston: Coastal Resilience. https://www.boston.gov/environment-and-energy/climate-ready-bostoncoastal-resilience (accessed on 31 Jul 2023).

BostonGIS. 2016. Boston Tax Parcel Data. https://bostonopendata-boston.opendata.arcgis.com/datasets/f3d274161b4a47aa9acf48d0d04cd5d4 (accessed on 22 Mar 2020).

Campbell, A M, P C Jones. 2011. Prepositioning supplies in preparation for disasters. *European Journal of Operational Research*, 209 (2), 156-165.

Chakravarty, Amiya K. 2018. Humanitarian response to hurricane disasters: Coordinating flood-risk mitigation with fundraising and relief operations. *Naval Research Logistics*, 65 (3), 275-288.

Chen, Lichun, Elise Miller-Hooks. 2012. Optimal team deployment in urban search and rescue. *Transportation Research Part B: Methodological*, 46 (8), 984-999.

Davis, L B, F Samanlioglu, X Qu, S Root. 2013. Inventory planning and coordination in disaster relief efforts. *International Journal of Production Economics*, 141 (2), 561-673.

De Sousa, Luís, Mike Gibson, Albert Chen, Dragan Savic, João Leitão. 2017. Exploring the advantages of hexagonal raster for flood modelling using cellular automata. *14th IWA/IAHR International Conference on Urban Drainage ICUD, Prague*.

Douglas, Ellen, Paul Kirshen. 2022. Climate change impacts and projections for the Greater Boston area. Tech. rep., University of Massachusetts Boston. Retrieved on January 23, 2023 from `https://greenribboncommission.org/wp-content/uploads/2022/06/GBRAG_report_05312022@1915.pdf`.

Douglas, Ellen M., Paul H. Kirshen, Michael Paolisso, Chris Watson, Jack Wiggin, Ashley Enrici, Matthias Ruth. 2012. Coastal flooding, climate change and environmental justice: Identifying obstacles and incentives for adaptation in two metropolitan Boston Massachusetts communities. *Mitigation and Adaptation Strategies for Global Change*, 17 (5), 537-562.

Eftekhar, M., J. Song, S. Webster. 2022. Optimal pre-positioning and local-purchasing for emergency operations under budget and supply uncertainty. *Manufacturing & Service Operations Management*, 24 (1), 315-332.

Eftekhar, Mahyar, Hongmin Li, Luk N. Van Wassenhove, Scott Webster. 2017. The Role of Media Exposure on Coordination in the Humanitarian Setting. *Production and Operations Management*, 26 (5), 802-816.

Eijgenraam, Carel, Ruud Brekelmans, Dick den Hertog, Kees Roos. 2017. Optimal Strategies for Flood Prevention. *Management Science*, 63 (5), 1644-1656.

Eisensee, Thomas, David Strömberg. 2007. News Droughts, News Floods, and U.S. Disaster Relief. *The Quarterly Journal of Economics*, 122 (2), 693-728.

EM-DAT. 2020. OFDA/CRED International Disaster Database. Tech. rep., Universite catholique de Louvain – Brussels - Belgium. Available at http://www.emdat.be/ (accessed on 14 Apr 2022).

Galindo, G., R. Batta. 2013a. Prepositioning of supplies in preparation for a hurricane under potential destruction of prepositioned supplies. *Socio-Economic Planning Sciences*, 47 (1), 20-37.

Galindo, Gina, Rajan Batta. 2013b. Review of recent developments in OR/MS research in disaster operations management. *European Journal of Operational Research*, 230 (2), 201-211.

Garner, Andra J., Jeremy L. Weiss, Adam Parris, Robert E. Kopp, Radley M. Horton, Jonathan T. Overpeck, Benjamin P. Horton. 2018. Evolution of 21st Century Sea Level Rise Projections. *Earth's Future*, 6 (11), 1603-1615.

Gesch, Dean B. 2018. Best Practices for Elevation-Based Assessments of Sea-Level Rise and Coastal Flooding Exposure. *Frontiers in Earth Science*, 6, 230.

Gupta, Sushil, Martin K. Starr, Reza Zanjirani Farahani, Niki Matinrad. 2016. Disaster Management from a POM Perspective: Mapping a New Domain. *Production and Operations Management*, 25 (10), 1611-1637.

Hecht, Jory S., Paul H. Kirshen. 2019. Minimizing Urban Floodplain Management Regrets under Deeply Uncertain Climate Change. *Journal of Water Resources Planning and Management*, 145 (2), 04018096.

IPCC. 2014. *AR5 Climate Change 2014: Mitigation of Climate Change.* The Intergovernmental Panel on Climate Change, United Nations.

Jonkman, Sebastiaan N, Marten M Hillen, Robert J Nicholls, Wim Kanning, Mathijs van Ledden. 2013. Costs of adapting coastal defences to sea-level rise—new estimates and their implications. *Journal of Coastal Research*, 29 (5), 1212-1226.

Jonkman, S.N., M. Kok, M. Van Ledden, J.K. Vrijling. 2009. Risk-based design of flood defence systems: a preliminary analysis of the optimal protection level for the New Orleans metropolitan area. *Journal of Flood Risk Management*, 2 (3), 170-181.

Karp, Richard M. 1972. Reducibility among Combinatorial Problems. *Complexity of Computer Computations.* Springer, Boston, MA, 85-103.

Keegan, N., R. King, N. Carter, M. Stubbs. 2011. Locally operated levees: Issues and federal programs. Tech. rep., Congressional Research Service, 7–5700. Retrieved from https://www.fas.org/sgp/crs/misc/R41752.pdf (accessed on 10 Feb 2023).

Kirshen, Paul, Thomas Ballestero, Ellen Douglas, Christine D Miller Hesed, Matthias Ruth, Michael Paolisso, Chris Watson, Phil Giffee, Kim Vermeer, Kirk Bosma. 2018a. Engaging vulnerable populations in multi-level stakeholder collaborative urban adaptation planning for extreme events and climate risks—a

case study of east boston usa. *Journal of Extreme Events*, 5 (02n03), 1850013.

Kirshen, Paul, Mark Borrelli, Jarrett Byrnes, Robert Chen, Lucy Lockwood, Chris Watson, Kimberly Starbuck, Jack Wiggin, Allison Novelly, Kristin Uiterwyk, Kelli Thurson, Brett McMann, Carly Foster, Heather Sprague, Hugh J. Roberts, Kirk Bosma, Di Jin, Rebecca Herst. 2018b. Feasibility of Harbor-wide Barrier Systems: Preliminary Analysis for Boston Harbor. Tech. rep., Sustainable Solutions Lab, University of Massachusetts Boston. http://blogs.umb.edu/capelab/files/2018/07/umb_rpt_BosHarbor_5.18_15-optimized-2dxu5cr.pdf (accessed on 10 Jul 2019).

Kirshen, Paul, Samuel Merrill, Peter Slovinsky, Norman Richardson. 2012. Simplified method for scenario-based risk assessment adaptation planning in the coastal zone. *Climatic Change*, 113 (3-4), 919-931.

Kopp, Robert E., Robert M. DeConto, Daniel A. Bader, Carling C. Hay, Radley M. Horton, Scott Kulp, Michael Oppenheimer, David Pollard, Benjamin H. Strauss. 2017. Evolving Understanding of Antarctic Ice-Sheet Physics and Ambiguity in Probabilistic Sea-Level Projections. *Earth's Future*, 5 (12), 1217-1233.

Kovacs, Gyöngyi, Mohammad Moshtari. 2019. A roadmap for higher research quality in humanitarian operations: A methodological perspective. *European Journal of Operational Research*, 276 (2), 395-408.

Kuhl, Laura, Paul H. Kirshen, Matthias Ruth, Ellen M. Douglas. 2014. Evacuation as a climate adaptation strategy for environmental justice communities. *Climatic Change*, 127 (3), 493-504.

Lodree, E J, S Taskin. 2008. An insurance risk management framework for disaster relief and supply chain disruption inventory planning. *Journal of Operational Research Society*, 59 (5), 674-684.

Lund, Robyn J, J. R. Suddeth, Jeff Mount, Jay R Lund. 2010. Levee decisions and sustainability for the Sacramento-San Joaquin delta. *San Francisco Estuary and Watershed Science*, 8 (2), 1-23.

Martyr-Koller, Rosanne, Adelle Thomas, Carl-Friedrich Schleussner, Alexander Nauels, Tabea Lissner. 2021. Slow-onset events: a review of the evidence from the IPCC Special Reports on Land, Oceans and Cryosphere. *Current Opinion in Environmental Sustainability*, 50, 109-120.

MassGIS. 2017. MassGIS LIDAR Data. https://docs.digital.mass.gov/dataset/massgis-data-lidar-terrain-data (accessed on 16 Mar 2020).

Mechler, Reinhard, Jeffrey Czajkowski, Howard Kunreuther, Erwann Michel-Kerjan, Wouter Botzen, Adriana Keating, Colin McQuistan, Nathan Cooper, Ian O'Donnell. 2014. Making Communities More Flood Resilient: The Role of Cost Benefit Analysis and Other Decision-Support Tools in Disaster Risk Reduction. Tech. rep., Zurich Flood Resilience Alliance.

Miller-Hooks, Elise, Xiaodong Zhang, Reza Faturechi. 2012. Measuring and maximizing resilience of freight transportation networks. *Computers & Operations Research*, 39 (7), 1633-1643.

Molenaar, Martien. 1998. *An Introduction to the Theory of Spatial Object Modelling for GIS*. CRC Press.

Nicholls, Robert J., Poh Poh Wong, Virginia R. Burkett, Jorge Codignotto, John E. Hay, Roger F. McLean, Sachooda Ragoonaden, Colin D. Woodroffe, Pamela Abuodha, Julie Arblaster, Barbara Brown, Don Forbes, Jim Hall, Sari Kovats, Jason Lowe, Kathy McInnes, Susanne Moser, Susanne Rupp-Armstrong,

Yoshiki Saito, Richard S. J. Tol. 2007. Coastal systems and low-lying areas. Climate Change 2007: Impacts, Adaptation and Vulnerability. Contribution of Working Group II to the Fourth Assessment Report of the Intergovernmental Panel on Climate Change.

NOAA. 2018. National Oceanic and Atmospheric Administration Tides and Currents: Extreme Water Levels. https://tidesandcurrents.noaa.gov/stationhome.html?id=8443970 (accessed on 10 Mar 2020).

NOAA. 2021. National Oceanic and Atmospheric Administration Data Access Viewer. https://coast.noaa.gov/dataviewer/#/ (accessed on 04 Aug 2021).

Oloruntoba, Richard, Richard Gray. 2006. Humanitarian aid: an agile supply chain? *Supply Chain Management: An International Journal*, 11 (2), 115-120.

Oppenheimer, Glavovic B.C. Hinkel J. van de Wal R. Magnan A.K. Abd-Elgawad A. Cai R. M. C. DeConto R.M. Ghosh T. Hay J. Isla F. Marzeion B. Meyssignac B., M. 2019. Sea level rise and implications for low-lying islands, coasts and communities. Tech. rep., IPCC Special Report on the Ocean and Cryosphere in a Changing Climate, 2019.

Rodríguez, J. Tinguaro, Begoña Vitoriano, Javier Montero. 2012. A general methodology for data-based rule building and its application to natural disaster management. *Computers & Operations Research*, 39 (4), 863-873.

Rodríguez, J. Tinguaro, Begoña Vitoriano, Javier Montero, Vojislav Kecman. 2011. A disaster-severity assessment DSS comparative analysis. *OR Spectrum*, 33 (3), 451-479.

Roy, Abhra, Jomon Aliyas Paul. 2013. Terrorism deterrence in a two country framework: strategic interactions between R&D, defense and pre-emption. *Annals of Operations Research*, 211 (1), 399-432.

Ruckert, Kelsey L., Vivek Srikrishnan, Klaus Keller. 2019. Characterizing the deep uncertainties surrounding coastal flood hazard projections: A case study for Norfolk, VA. *Scientific Reports*, 9 (1), 11373.

Sills, G. L., N. D. Vroman, R. E. Wahl, N. T. Schwanz. 2008. Overview of New Orleans levee failures: Lessons learned and their impact on national levee design and assessment. *Journal of Geotechnical and Geoenvironmental Engineering*, 134 (5), 556-565. https://ascelibrary.org/doi/abs/10.1061/ (accessed on 10 Feb 2023).

Sodhi, ManMohan S., Christopher S. Tang. 2014. Buttressing Supply Chains against Floods in Asia for Humanitarian Relief and Economic Recovery. *Production and Operations Management*, 23 (6), 938-950.

Sweet, William V., Robert E. Kopp, Christopher P. Weaver, Jayantha Obeysekera, Radley M. Horton, E. Robert Thieler, Chris Zervas. 2017. Global and Regional Sea Level Rise Scenarios for the United States. Tech. Rep. NOAA Technical Report NOS CO-OPS 083, National Oceanic and Atmospheric Administration. https://tidesandcurrents.noaa.gov/publications/techrpt83_Global_and_Regional_SLR_Scenarios_for_the_US_final.pdf (accessed on 15 Feb 2019).

Thompson, P.R., M.J. Widlansky, M.A. Merrifield, J.M. Becker, J.J. Marra. 2019. A statistical model for frequency of coastal flooding in Honolulu, Hawaii, during the 21st century. *Journal of Geophysical Research: Oceans*, 124 (4), 2787-2802.

Uichanco, Joline. 2022. A model for prepositioning emergency relief items before a typhoon with an uncertain trajectory. *Manufacturing & Service Operations Management*, 24 (2), 766-790.

USACE. 2015. North Atlantic Coast Comprehensive Study: Resilient Adaptation to Increasing Risk, Physical Depth Damage Function, Summary Report. Tech. rep., United States Army Corps of Engineers. https://www.nad.usace.army.mil/Portals/40/docs/NACCS/10A_PhysicalDepthDmgFxSummary _26Jan2015.pdf (accessed on 15 Feb 2019).

USGSA. 2009. DATA.GOV. https://www.data.gov/open-gov/ (accessed on 04 Aug 2021).

Vanicek, Petr. 1991. Vertical datum and NAVD88. *Surveying and Land Information Systems*, 51 (2), 83-86.

Wissman-Weber, Nichole, David L. Levy. 2021. Organizing for climate adaptation: Competing visions in Boston. *Economic Sociology the European Electronic Newsletter*, 22 (2), 24-29.

Zandvoort, Mark, Nora Kooijmans, Paul Kirshen, Adri van den Brink. 2019. Designing with Pathways: A Spatial Design Approach for Adaptive and Sustainable Landscapes. *Sustainability*, 11 (3), 565.

Zobel, Christopher W. 2011. Representing perceived tradeoffs in defining disaster resilience. *Decision Support Systems*, 50 (2), 394-403.

Online Supplemental Sections

EC.1   Proof of Computational Complexity

In this section, we aim to address the computational complexity of the FRM problem. Given a planning horizon $\mathcal{T} = \{1, \ldots, t_{max}\}$, set $\boldsymbol{\Xi} = [\Xi_t : t \in \mathcal{T}]$ containing the sets of sea level states during each period $t \in \mathcal{T}$, sea level state transition probabilities $\boldsymbol{p} = [p_t^{\mathcal{S}\mathcal{S}'} : t \in \{0, \ldots, t_{max} - 1\}, \mathcal{S} \in \Xi_t, \mathcal{S}' \in \Xi_{t+1}]$, a coastal region with the associated set of land grids in the area of interest Φ and the area of relevance Ψ, initial elevations $\boldsymbol{h} = [h_i : i \in \Phi \cup \Psi]$, minimum elevation threshold m, sets $\boldsymbol{R} = [R_t^{\mathcal{S}} : t \in \mathcal{T}, \mathcal{S} \in \Xi_t]$, $\boldsymbol{Q} = [Q_t^{\mathcal{S}} : t \in \mathcal{T}, \mathcal{S} \in \Xi_t]$, $\hat{\boldsymbol{R}} = [\hat{R}_t^{\mathcal{S}} : t \in \mathcal{T}, \mathcal{S} \in \Xi_t]$, and $\hat{\boldsymbol{Q}} = [\hat{Q}_t^{\mathcal{S}} : t \in \mathcal{T}, \mathcal{S} \in \Xi_t]$ containing sets of land grids in Φ or Ψ at risk of permanent or temporary flooding during each period $t \in \mathcal{T}$ and under each sea level state $\mathcal{S} \in \Xi_t$, a neighborhood set $\mathcal{N} = [N_t^{\mathcal{S}}(i) : t \in \mathcal{T}, \mathcal{S} \in \Xi_t, i \in R_t^{\mathcal{S}} \cup Q_t^{\mathcal{S}} \cup \hat{R}_t^{\mathcal{S}} \cup \hat{Q}_t^{\mathcal{S}}]$, cost c of elevating a grid in Φ by one meter at the start of a period, permanent flooding costs $\boldsymbol{g} = [g_i : i \in \Phi]$ and hurricane storm surge related flooding costs $\boldsymbol{f} = [f_i : i \in \Phi]$, a discount rate per-period λ, budgets per-period $\boldsymbol{b} = [b_t : t \in \mathcal{T}]$, minimum elevation threshold m, and a scalar $\mathcal{C}$, the decision version of the FRM problem, denoted by $\langle \mathcal{T}, \boldsymbol{\Xi}, \boldsymbol{p}, \Phi, \Psi, \boldsymbol{h}, \boldsymbol{R}, \boldsymbol{Q}, \hat{\boldsymbol{R}}, \hat{\boldsymbol{Q}}, \mathcal{N}, c, \boldsymbol{g}, \boldsymbol{f}, \lambda, \boldsymbol{b}, m, \mathcal{C} \rangle$, is defined as follows: "Is there an assignment to variables $\boldsymbol{x} = [x_{it\mathcal{S}} : i \in \Phi, t \in \mathcal{T}, \mathcal{S} \in \Xi_{t-1}]$ that satisfies Constraints (4)-(9) and (22)-(23) for which the value of Objective Function (3) (calculated with respect to Constraints (10)-(21) and (24)-(25)) is at most $\mathcal{C}$". We employ a reduction from Knapsack problem to establish the intractability of the decision version of the FRM problem in Theorem 1 below.

THEOREM 1. *The decision version of the FRM problem is NP-complete.*

Proof of Theorem 1   It can be easily verified that given a decision vector $\boldsymbol{x}^0$, verifying whether Constraints (4)-(9) and (22)-(23) are satisfied and the value of Objective Function (3) incorporating Constraints (10)-(21) and (24)-(25) is at most $\mathcal{C}$, can be done in polynomial-time. Therefore, the decision version of the FRM problem belongs to class NP.

Next, we prove that the decision version of the FRM problem is NP-hard by performing a polynomial-time reduction from the well-known NP-complete Knapsack problem (Karp 1972). The decision version of the Knapsack problem, denoted as $\langle \boldsymbol{\alpha} = [\alpha_i : i \in \{1, \ldots, n\}], \boldsymbol{\beta} = [\beta_i : i \in \{1, \ldots, n\}], \sigma, \eta \rangle$, is "Given a finite set of n items each one with the value of α_i and weight of β_i, a desired total value σ, and a knapsack with weight capacity of η, is there a subset $J \subseteq \{1, \ldots, n\}$ such that $\sum_{i \in J} \beta_i \leq \eta$ and $\sum_{i \in J} \alpha_i \geq \sigma$?"

Given an instance of the Knapsack decision problem $\langle \boldsymbol{\alpha}, \boldsymbol{\beta}, \sigma, \eta \rangle$, we transform this instance into a special case of the decision version of the FRM problem in polynomial-time as follows:

1. The length of the planning horizon is set to be equal to one (i.e., $\mathcal{T} = \{1\}$).

2. There is only one sea level state during period 1, which is

$$(s_1, \hat{s}_1) = (\max\{\beta_i : i \in \{1, \ldots, n\}\} + 1, \max\{\beta_i : i \in \{1, \ldots, n\}\} + 1).$$

Therefore, $\boldsymbol{\Xi} = [\Xi_1 = \{(s_1, \hat{s}_1)\}]$.

3. The transition probability $p_0^{(0,0)(s_1,\hat{s}_1)}$ is also set to be equal to one. Therefore, $\boldsymbol{p} = [p_0^{(0,0)(s_1,\hat{s}_1)} = 1]$.

4. The set of land grids in the area of interest is composed of n grids (i.e., $\Phi = \{1, \ldots, n\}$). The set of land grids in the area of relevance is empty (i.e., $\Psi = \emptyset$). Each land grid in Φ is assumed to be surrounded by the sea, and land grids in Φ themselves do not share any border.

5. The initial elevation of each land grid $i \in \Phi$ (i.e., h_i) is set to be equal to $\max\{\beta_i : i \in \{1, \ldots, n\}\} + 1 - \beta_i$. Therefore, $\boldsymbol{h} = [\max\{\beta_i : i \in \{1, \ldots, n\}\} + 1 - \beta_i : i \in \Phi]$.

6. The set of land grids in Φ at risk of permanent flooding during the single period considered and under the single sea level state given (i.e., $R_1^{(s_1,\hat{s}_1)}$) is set to be equal to $\{1, \ldots, n\}$. The set of land grids in Φ only at risk of temporary flooding during the single time period and under the single sea level state (i.e., $\hat{R}_1^{(s_1,\hat{s}_1)}$) is set to be empty. Therefore, $\boldsymbol{R} = [R_1^{(s_1,\hat{s}_1)} = \{1, \ldots, n\}]$ and $\hat{\boldsymbol{R}} = \boldsymbol{Q} = \hat{\boldsymbol{Q}} = [\emptyset]$.

7. The set containing neighbors of each land grid $i \in R_1^{(s_1,\hat{s}_1)}$ within the at-risk network corresponding to the given single period and single sea level state (i.e., $N_1^{(s_1,\hat{s}_1)}(i)$) is set to only contain the sea grid. Therefore, $\mathcal{N} = [\{o\} : i \in \{1, \ldots, n\}]$. The at-risk network for the given single time period and sea level state is illustrated in Figure EC.1 below.

8. The cost of raising a grid $i \in \Phi$ by one meter (i.e., c) is set to be equal to one dollar.

9. The cost of losing a grid $i \in \Phi$ due to inundation (i.e., g_i) is set to be equal to $\alpha_i + \beta_i$, and the cost of hurricane storm surge flood damage to a grid $i \in \Phi$ (i.e., f_i) is set to be equal to zero. Therefore, $\boldsymbol{g} = [\alpha_i + \beta_i : i \in \Phi]$ and $\boldsymbol{f} = [0 : i \in \Phi]$.

10. The discount rate per-period (i.e., λ) is set to be equal to one.

11. The budget for the single considered period (i.e., b_1) is set to be equal to η. Therefore, $\boldsymbol{b} = [\eta]$.

12. The minimum elevation threshold m is set to be equal to $\min\{\beta_i : i \in \Phi\}$.

13. Finally, the upper bound on the total cost in the FRM model (i.e., $\mathcal{C}$) is set to be equal to

$$\sum_{i=1}^{n} (\alpha_i + \beta_i) - \sigma.$$

We now show that the answer to the Knapsack decision problem is a "yes", if and only if the answer to the constructed special case of the FRM decision problem is a "yes". Suppose, there exists a set $J \subseteq \{1, \ldots, n\}$ that satisfies the Knapsack capacity constraint (i.e., $\sum_{i \in J} \beta_i \leq \eta$) and the total value for items in set J is at least σ (i.e., $\sum_{i \in J} \alpha_i \geq \sigma$). Consider the solution corresponding to elevating
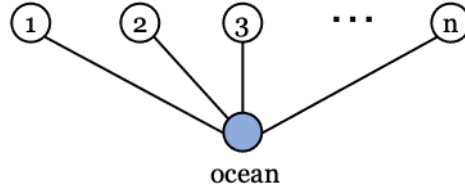
Figure EC.1   Illustration of the at-risk network used in the proof of Thereom 1

the land grids in set J in the constructed FRM problem so that each grid in this set is raised up to the permanent (or storm-related) sea level, and is not permanently flooded. The nodes in set J each cost β_i when elevated, therefore, incurring a total investment cost of $\sum_{i \in J} \beta_i \leq \eta$, meeting the FRM budget limit. So, this solution satisfies Constraints (4)-(9) and (22)-(23). Additionally, as shown in Equation (EC.1) below, the value of Objective Function (3) (calculated with respect to Constraints (10)-(21) and (24)-(25)) is also at most $\mathcal{C}$.

$$EIC + EFC =$$
$$\sum_{i \in J} \beta_i + \sum_{i \in \{1,\dots,n\} \setminus J} (\alpha_i + \beta_i) = \sum_{i=1}^{n} (\alpha_i + \beta_i) - \sum_{i \in J} \alpha_i \leq \sum_{i=1}^{n} (\alpha_i + \beta_i) - \sigma = \mathcal{C}. \quad \text{(EC.1)}$$

Conversely, suppose there exists a set of land grids that are built up to protect against permanent (and temporary) flooding in a way that the investment cost is bounded above by the FRM budget η (i.e., Constraints (4)-(9) and (22)-(23) are satisfied) and the value of Objective Function (3) (calculated with respect to Constraints (10)-(21) and (24)-(25) is at most $\mathcal{C} = \sum_{i=1}^{n} (\alpha_i + \beta_i) - \sigma$. Let $J \subseteq \{1,\dots,n\}$ denote the set of land grids in the FRM model that are not permanently flooded. Consider a solution to the Knapsack problem is which we select the items in set J. Since the grids in J are not permanently flooded, then they should have been elevated to a level higher than or equal to the permanent (or storm-related) water level. Therefore,

$$\sum_{i \in J} \beta_i \leq EIC \leq \eta, \quad \text{(EC.2)}$$

which means that the items in set J satisfy the Knapsack capacity constraint. Additionally, we know that

$$EIC + EFC \leq \mathcal{C} = \sum_{i=1}^{n} (\alpha_i + \beta_i) - \sigma.$$

Since

$$EFC = \sum_{i \in \{1,\dots,n\} \setminus J} (\alpha_i + \beta_i),$$

then, by Inequality (EC.2), we have

$$\sum_{i \in J} \beta_i + \sum_{i \in \{1,\dots,n\} \setminus J} (\alpha_i + \beta_i) \leq \sum_{i=1}^{n} (\alpha_i + \beta_i) - \sigma.$$

This means

$$\sum_{i \in J} \alpha_i \geq \sigma,$$

which indicates that the total value for items in set J is at least σ.

Therefore, the decision version of the FRM problem is NP-hard. Combined with the earlier mentioned fact that this decision problem belongs in class NP, we also conclude that the decision version of the FRM problem is NP-complete. $\square$

EC.2   Data Collection and Transformation for Case Study

Given that Boston is the location of interest in our case study, we need to compile the necessary data to create the actual model parameter values for this region. As we aim to create a useful model for any coastal area, we only use available open-source datasets. Figure EC.2 shows the breakdown of the data references used for compiling the input parameters, with three main categories: sea level, network, and financial data. Given the model's inherent spatial nature, the network-related data are captured and transformed from Geographical Information System (GIS) open-source data. All elevations are referenced to the North American Vertical Datum of 1988 (NAVD88) (Vanicek 1991) to ensure consistency in the spatial data used. Figure EC.2 highlights the three main elements of the data preparation, including identifying the data sources, interactions, and transformations to model parameters. In the following subsections, we will detail the data sources, assumptions made to apply the data accordingly, and the transformation methods needed to produce the model parameters.

EC.2.1   Sea level data

To capture the full range of sea level states (parameters s and $\hat{s}$) over time, we need to incorporate three important factors. These three factors include the climate-induced sea level rise heights and probabilities, tidal range captured by tidal data, and hurricane storm surge heights and probabilities. We will discuss each of these factors in the next four sections.

EC.2.1.1   Climate-induced sea level rise

Before discussing the actual data source for the potential sea level rise scenarios, it is important to briefly mention the Representative Concentration Pathway (RCP) carbon emission trajectories adopted by the Intergovernmental Panel on Climate Change (IPCC 2014). The pathways describe different possible climate futures. All of them are possible and depend on the volume of greenhouse gases emitted now and in the future. Most sea level rise analyses align with these RCP trajectories; therefore, we will segment our data into the four original RCP trajectories of RCP2.6, RCP4.5, RCP6.0, and RCP8.5. Given the non-deterministic future of greenhouse gas emissions reductions, we will treat each of the four RCPs as independent and equally likely.

There are many sources of potential sea level rise within the literature. Looking back over the last few decades (Garner et al. 2018), the one common theme in all the predictions is substantial uncertainty in the best to worst-case sea level rise predictions. One can follow the flow of sea level rise predictions from both plausible or probabilistic perspectives (Ruckert et al. 2019). Given these ever-evolving sea level rise predictions, the model we propose leaves open the ability to incorporate a range of sea level rise predictions. This ability will allow us to be flexible in capturing the expected costs of the inundation and hurricane storm surge flood damages as sea level rise understanding

Data Source **Transformation** **Model Parameter**

Sea Level Data

Representative Concentration Pathways
(IPCC 2014)

Probabilistic Sea Level Rise Curves
(Kopp et al. 2017)

Extreme Water Levels
(NOAA 2018)

Tidal Information
(NOAA 2018)

Boston Sea Level Curves
through 2070

Storm Surge
Scenario Levels

Number of Scenarios (N)

Number of Time Periods (t_{max})

Inundation Flood Levels (s_{jt})

Scenario Probabilities (P_j)

Temporary Flood Levels ($\hat{s}_{jt}$)

Network Data

Geographic Information System
(GIS) Hex Grid overlay

Light Detection and Ranging
(LIDAR) Elevation Data
(MassGIS 2017)

Depth Damage Functions
(United States Army Corps of
Engineers 2015)

Boston Tax Parcel Data
(BostonGIS 2016, and
City of Boston 2020)

Mean of LIDAR point heights
within hex grids

Linear approximation of Depth
Damage Curves

Weighted aggregate building
types within hex grids

Weighted aggregate building
values within hex grids

Weighted aggregate total parcel
values within hex grids

Number of Land Grids (i_{max})

Initial Grid Elevation (h_i)

Grid Depth Damage Coefficient
(f_i)

Value of Grid (g_i)

Financial Data

Discount Rates
(Aerts et al. 2014)

Estimated Build Costs
(Hecht and Kirshen 2019,
Jonkman et al. (2013))

Budget Estimates

Transform annual discount rate
(d) into period rate

Linear approximation of cost to
build levee on hex grid

Discount Rate (λ)

Grid Investment Cost (c)
Minimum Levee Height (m)
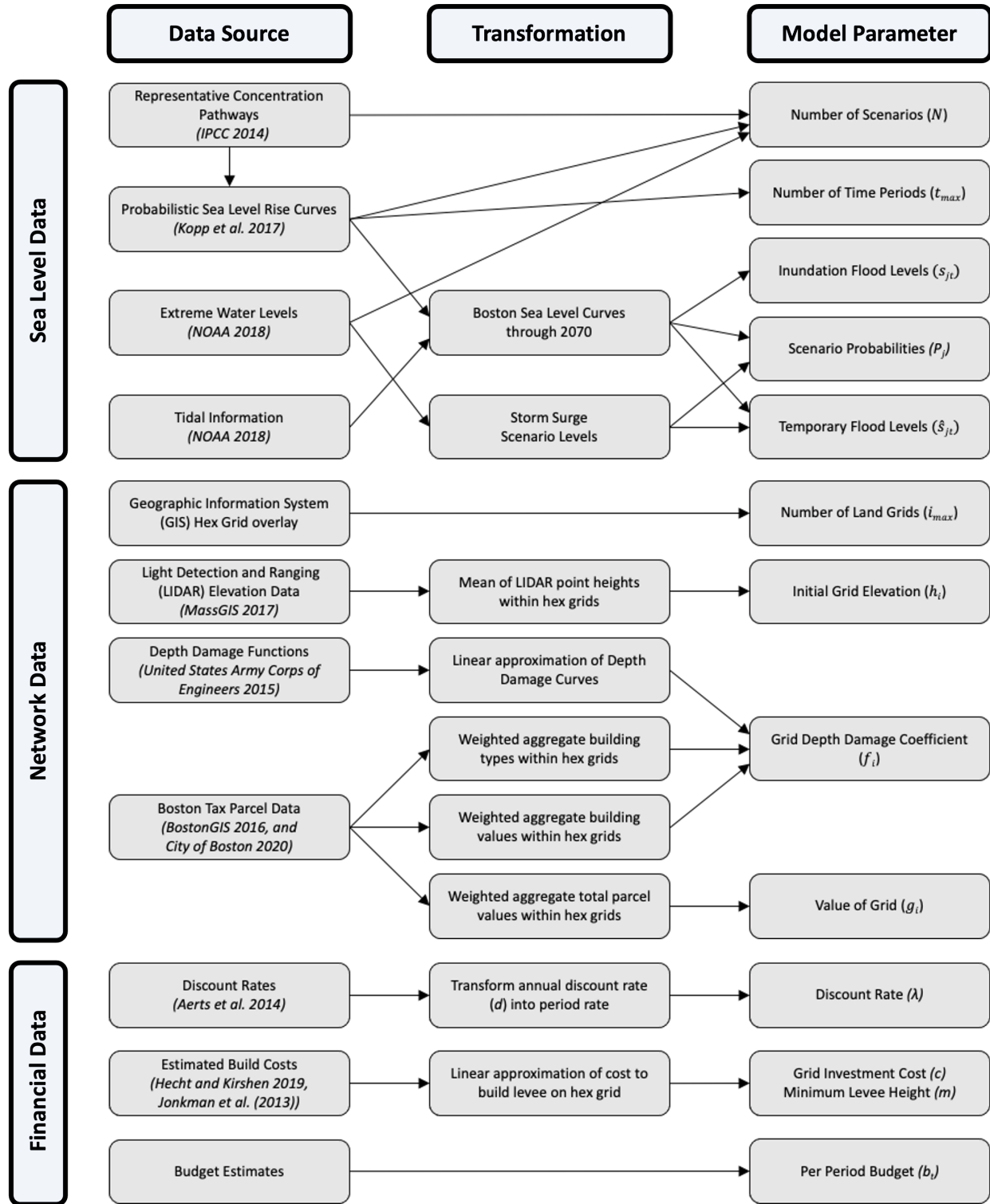
Per Period Budget (b_t)

Figure EC.2   Outline of data sources and their incorporation into model's parameters.

evolves. For parameters s in the sea level states of our model, we utilize the sea level rise predictions captured in Kopp et al. (2017) as the authors provide nine sets of probabilistic sea level curves for each of the four RCPs. These curves predict sea level rise each decade through the year 2100, with further 50-year predictions out to the year 2300. Here we will only be using the period data up to 2070 starting from 2020, which results in five decade-long periods in our model. The data from (Kopp et al. 2017) incorporate applicable sea level rise causes from multiple sources, including ice sheet melt, glacier and ice cap melt, land water storage, oceanographic processes, glacial isostatic adjustments, tectonics, and other non-climate local effects. The authors made their model calculations publicly available for many coastal areas associated with local tidal gauges, including the Boston tidal gauge.

In Kopp et al. (2017), there are nine probabilistic curves associated with each RCP, with the example for RCP8.5 shown in Figure EC.3. For explanation, the curves in Figure EC.3 represent the probability that the sea level rise will be less than or equal to that sea level associated with that curve at that point in time. For instance, in the year 2100, one can see that the sea level for the 50% curve will be 90 cm. That is interpreted to mean that the sea level is 50% likely to be at or below that level in the year 2100. Similarly, when looking at the 99.9% curve in the year 2100, we would expect the sea level is 99.9% likely to be at or below 316 cm in the year 2100. This data provides us with the required sea level curves, the periods t we will need, and a basis for assigning their probabilities, as discussed in Section EC.2.1.4 below.
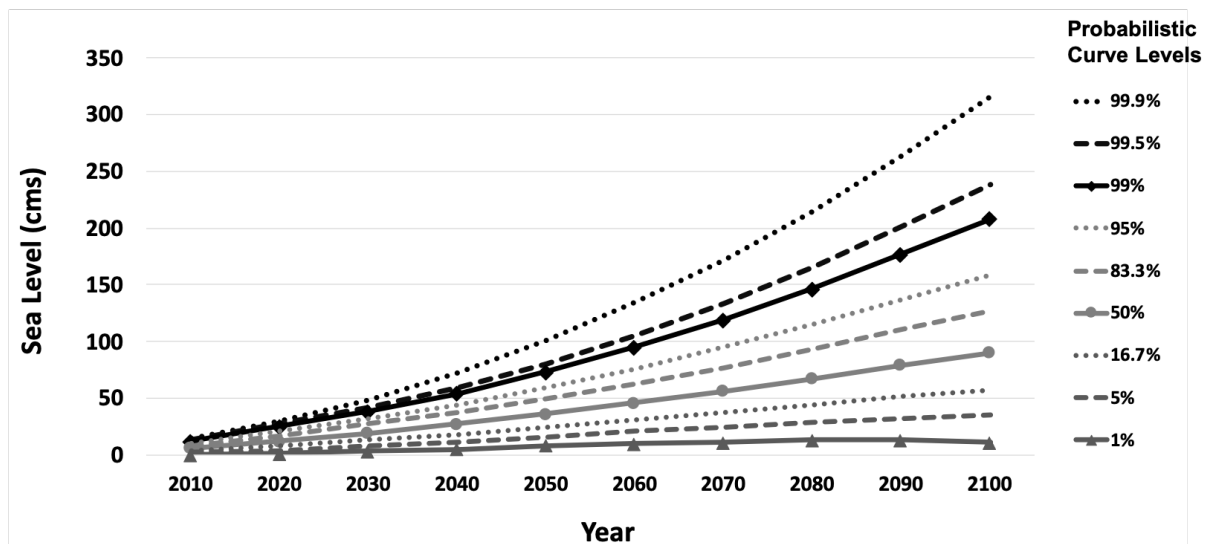

Figure EC.3   Boston sea level rise curves for Representative Concentration Pathway 8.5 (RCP8.5) (Kopp et al. 2017)

EC.2.1.2 Tidal range

To obtain the tidal value used in the model, we reference the National Oceanic and Atmospheric Administration (NOAA) tide gauge based in Boston harbor (NOAA 2018). In using the tidal data, we assume the sea level rise data will account for any changes over time discussed in Section EC.2.1.1. The data we use is relative to North American Vertical Datum of 1988 (NAVD88) (Vanicek 1991), providing us with the Mean Higher High Water level of 1.52 meters as the highest elevation caused by high tides in our sea level data. We add this high tide value to the values reported in Kopp et al. (2017) to obtain the parameters s used in the sea level states of our model.

EC.2.1.3 Hurricane storm surge levels

To determine our storm surge levels, we use the hurricane storm surge data from the National Oceanic and Atmospheric Administration (NOAA) tide gauge based in Boston harbor (NOAA 2018). We assume that storm surge heights over time will remain constant based on the hurricane storm surges and any change in absolute height are captured by factors discussed in Section EC.2.1.1. Table EC.1 shows the surge levels and associated exceedance probability levels for the four hurricane storm surge levels we use in our model. The exceedance storm surge levels represent the likelihood of a storm surge height above the Mean Higher High Water high tide level captured in Section EC.2.1.2. For instance, on average, the 1% level will be exceeded in only one year per century, while the 10% level will be exceeded in ten years per century. As shown in Table EC.1, we use the median value for the four exceedance probabilities for the Boston tidal gauge published by NOAA (NOAA 2018) to simplify the model development and to reduce the risk of overly long model runtimes. We add these values to the parameters s, as determined above, to obtain parameters $\hat{s}$ in the sea level states of our model.

Table EC.1 National Oceanic and Atmospheric Administration (NOAA) storm surge levels

Storm Surge	Exceedance Probability	Water Level above Mean Higher High Water
100-year	0.01	1.41 m
10-year	0.10	1.07 m
2-year	0.50	0.81 m
1-year	0.99	0.56 m

EC.2.1.4 Sea level states paths and their probabilities

To calculate the associated probabilities for each curve under a given RCP, we first transform the RCP's probabilistic curves into time-dependent exceedance curves. Figure EC.4 shows an example of
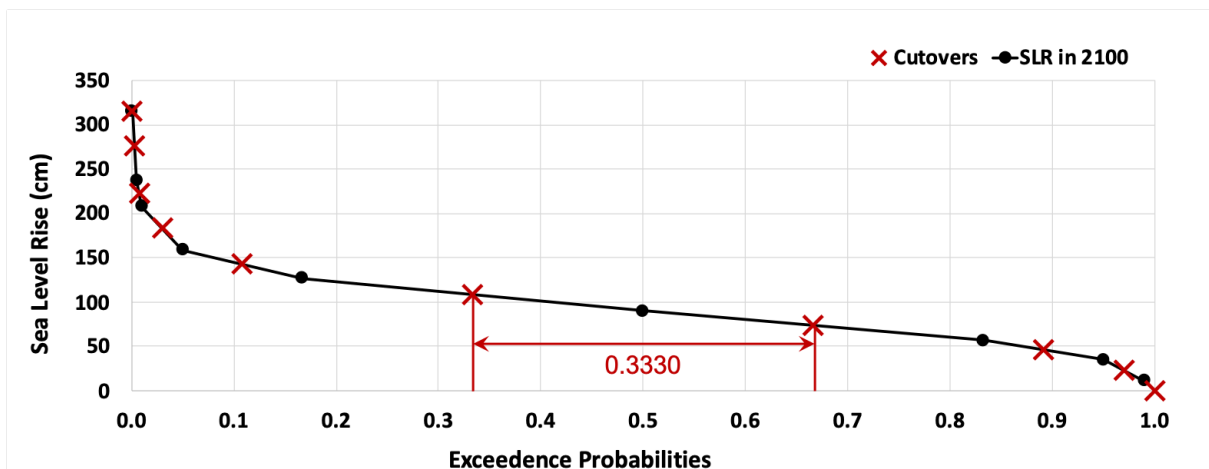
Figure EC.4   Representative Concentration Pathway 8.5 (RCP8.5) sea level rise exceedance curves for year 2100 adapted for Boston from (Kopp et al. 2017)

an exceedance curve for RCP8.5 in the year 2100. Using a linear interpolation methodology (Kirshen et al. 2012), we calculate an estimated probability for each probabilistic curve for a given RCP at a given time. For explanation, considering the exceedance curve in Figure EC.4, we estimate the probability for the 50%-probabilistic curve by taking the halfway points between the 50%- and 83.3%-curves and the 50%- and the 16.7%- curves, and then measure the distance between those two midway points as shown in Figure EC.4. It is important to note that for a given p%-curve in a given RCPα, the actual sea level increases over time, while the estimated probability for the curve (denoted by $P_{curve}^{\alpha,p}$) does not change as the distance between the two midway points remains constant over time. We show the estimated probabilities for each of the nine p%-curves in Table EC.2. We apply the same technique to each β-year storm surge exceedance curve to determine estimated probabilities P_{surge}^{β} as shown in Table EC.3. As mentioned, the probability distribution for the hurricane storm surge levels is assumed to be fixed over time.

Now that we have estimates for the probabilities of each RCP's probabilistic curves and the probabilities of hurricane storm surge instances, we can determine the complete set of possible sea level states paths and their probabilities by bringing this information together. Given an RCP α, to calculate the probability for each of the associated sea level states paths, we treat the probabilities for sea level rise curves $P_{curve}^{\alpha,p}$ and hurricane storm surge levels P_{surge}^{β} as independent. By doing so, we can calculate the estimated probability for a path composed of a p%-curve sea level rise in a given RCP α and a β-year storm surge (denoted by $P_{\alpha,p,\beta}$) as shown in Equation (EC.3). When combining the four RCPs with equal probabilities, we produce a total of $N = 144$ unique sea level states paths, each with the probability of $0.25 * P_{\alpha,p,\beta}$. These will be the paths we use in our simulation-based and scenario-based solution approaches discussed in Sections 4.2 and 4.3. In Table EC.4, we show the

Table EC.2   Estimated probabilities for sea level rise curves for a given Representative Concentration Pathway α

SLR Curve (p)	$P^{\alpha,p}_{curve}$
99.9%	0.0030
99.5%	0.0045
99.0%	0.0225
95.0%	0.0785
83.3%	0.2250
50.0%	0.3330
16.7%	0.2250
5.0%	0.0785
1.0%	0.0300

Table EC.3   Estimated probabilities for four storm surge curves

Storm	Surge curve	P^{β}_{surge}
100 year	1%	0.055
10 year	10%	0.245
2 year	50%	0.445
1 year	99%	0.255

probabilities for each of the 144 sea level states path and the associated values of s and $\hat{s}$ for each path in each period.

$$P_{\alpha,p,\beta} = P^{\alpha,p}_{curve} * P^{\beta}_{surge} \tag{EC.3}$$

Table EC.4: Sea level states paths, probabilities, and sea level values for each period

Path	RCP	SLR Curve	Surge Curve	Path Probability	2030 $(s, \hat{s})$	2040 $(s, \hat{s})$	2050 $(s, \hat{s})$	2060 $(s, \hat{s})$	2070 $(s, \hat{s})$
1	rcp85	1.0%	99%	0.001912500	(154, 210)	(156, 212)	(159, 215)	(161, 217)	(162, 218)
2	rcp85	5.0%	99%	0.005004375	(156, 212)	(159, 215)	(164, 220)	(169, 225)	(172, 228)
3	rcp85	16.7%	99%	0.014343750	(157, 213)	(162, 218)	(168, 224)	(175, 231)	(181, 237)
4	rcp85	50.0%	99%	0.021228750	(159, 215)	(167, 223)	(176, 232)	(186, 242)	(196, 252)
5	rcp85	83.3%	99%	0.014343750	(162, 218)	(172, 228)	(184, 240)	(197, 253)	(212, 268)
6	rcp85	95.0%	99%	0.005004375	(163, 219)	(175, 231)	(190, 246)	(207, 263)	(226, 282)
7	rcp85	99.0%	99%	0.001434375	(165, 221)	(181, 237)	(200, 256)	(222, 278)	(246, 302)
8	rcp85	99.5%	99%	0.000286875	(167, 223)	(184, 240)	(205, 261)	(230, 286)	(258, 314)
9	rcp85	99.9%	99%	0.000191250	(170, 226)	(194, 250)	(223, 279)	(256, 312)	(294, 350)
10	rcp60	1.0%	99%	0.001912500	(152, 208)	(154, 210)	(154, 210)	(156, 212)	(157, 213)

Table EC.4: Sea level states paths, probabilities, and sea level values for each period (Continued)

Path	RCP	SLR Curve	Surge Curve	Path Probability	2030 $(s, \hat{s})$	2040 $(s, \hat{s})$	2050 $(s, \hat{s})$	2060 $(s, \hat{s})$	2070 $(s, \hat{s})$
11	rcp60	5.0%	99%	0.005004375	(154, 210)	(156, 212)	(158, 214)	(163, 219)	(166, 222)
12	rcp60	16.7%	99%	0.014343750	(156, 212)	(160, 216)	(164, 220)	(169, 225)	(175, 231)
13	rcp60	50.0%	99%	0.021228750	(158, 214)	(163, 219)	(170, 226)	(179, 235)	(187, 243)
14	rcp60	83.3%	99%	0.014343750	(160, 216)	(168, 224)	(178, 234)	(189, 245)	(202, 258)
15	rcp60	95.0%	99%	0.005004375	(163, 219)	(172, 228)	(185, 241)	(199, 255)	(215, 271)
16	rcp60	99.0%	99%	0.001434375	(166, 222)	(178, 234)	(195, 251)	(212, 268)	(235, 291)
17	rcp60	99.5%	99%	0.000286875	(168, 224)	(181, 237)	(200, 256)	(220, 276)	(246, 302)
18	rcp60	99.9%	99%	0.000191250	(171, 227)	(190, 246)	(214, 270)	(245, 301)	(281, 337)
19	rcp45	1.0%	99%	0.001912500	(154, 210)	(155, 211)	(156, 212)	(157, 213)	(156, 212)
20	rcp45	5.0%	99%	0.005004375	(156, 212)	(159, 215)	(161, 217)	(165, 221)	(167, 223)
21	rcp45	16.7%	99%	0.014343750	(157, 213)	(161, 217)	(166, 222)	(171, 227)	(175, 231)
22	rcp45	50.0%	99%	0.021228750	(158, 214)	(165, 221)	(173, 229)	(181, 237)	(188, 244)
23	rcp45	83.3%	99%	0.014343750	(160, 216)	(170, 226)	(181, 237)	(192, 248)	(203, 259)
24	rcp45	95.0%	99%	0.005004375	(162, 218)	(174, 230)	(187, 243)	(202, 258)	(216, 272)
25	rcp45	99.0%	99%	0.001434375	(164, 220)	(179, 235)	(197, 253)	(216, 272)	(236, 292)
26	rcp45	99.5%	99%	0.000286875	(166, 222)	(183, 239)	(203, 259)	(224, 280)	(249, 305)
27	rcp45	99.9%	99%	0.000191250	(169, 225)	(192, 248)	(219, 275)	(248, 304)	(281, 337)
28	rcp26	1.0%	99%	0.001912500	(152, 208)	(152, 208)	(151, 207)	(149, 205)	(150, 206)
29	rcp26	5.0%	99%	0.005004375	(154, 210)	(155, 211)	(156, 212)	(158, 214)	(160, 216)
30	rcp26	16.7%	99%	0.014343750	(155, 211)	(159, 215)	(162, 218)	(165, 221)	(168, 224)
31	rcp26	50.0%	99%	0.021228750	(158, 214)	(164, 220)	(170, 226)	(176, 232)	(182, 238)
32	rcp26	83.3%	99%	0.014343750	(161, 217)	(170, 226)	(180, 236)	(189, 245)	(197, 253)
33	rcp26	95.0%	99%	0.005004375	(163, 219)	(175, 231)	(188, 244)	(200, 256)	(210, 266)
34	rcp26	99.0%	99%	0.001434375	(166, 222)	(181, 237)	(198, 254)	(215, 271)	(231, 287)
35	rcp26	99.5%	99%	0.000286875	(167, 223)	(185, 241)	(204, 260)	(223, 279)	(243, 299)
36	rcp26	99.9%	99%	0.000191250	(170, 226)	(193, 249)	(221, 277)	(250, 306)	(278, 334)
37	rcp85	1.0%	50%	0.003337500	(154, 235)	(156, 237)	(159, 240)	(161, 242)	(162, 243)
38	rcp85	5.0%	50%	0.008733125	(156, 237)	(159, 240)	(164, 245)	(169, 250)	(172, 253)
39	rcp85	16.7%	50%	0.025031250	(157, 238)	(162, 243)	(168, 249)	(175, 256)	(181, 262)
40	rcp85	50.0%	50%	0.037046250	(159, 240)	(167, 248)	(176, 257)	(186, 267)	(196, 277)
41	rcp85	83.3%	50%	0.025031250	(162, 243)	(172, 253)	(184, 265)	(197, 278)	(212, 293)
42	rcp85	95.0%	50%	0.008733125	(163, 244)	(175, 256)	(190, 271)	(207, 288)	(226, 307)
43	rcp85	99.0%	50%	0.002503125	(165, 246)	(181, 262)	(200, 281)	(222, 303)	(246, 327)
44	rcp85	99.5%	50%	0.000500625	(167, 248)	(184, 265)	(205, 286)	(230, 311)	(258, 339)
45	rcp85	99.9%	50%	0.000333750	(170, 251)	(194, 275)	(223, 304)	(256, 337)	(294, 375)
46	rcp60	1.0%	50%	0.003337500	(152, 233)	(154, 235)	(154, 235)	(156, 237)	(157, 238)
47	rcp60	5.0%	50%	0.008733125	(154, 235)	(156, 237)	(158, 239)	(163, 244)	(166, 247)
48	rcp60	16.7%	50%	0.025031250	(156, 237)	(160, 241)	(164, 245)	(169, 250)	(175, 256)

Table EC.4: Sea level states paths, probabilities, and sea level values for each period (Continued)

Path	RCP	SLR Curve	Surge Curve	Path Probability	2030 $(s, \hat{s})$	2040 $(s, \hat{s})$	2050 $(s, \hat{s})$	2060 $(s, \hat{s})$	2070 $(s, \hat{s})$
49	rcp60	50.0%	50%	0.037046250	(158, 239)	(163, 244)	(170, 251)	(179, 260)	(187, 268)
50	rcp60	83.3%	50%	0.025031250	(160, 241)	(168, 249)	(178, 259)	(189, 270)	(202, 283)
51	rcp60	95.0%	50%	0.008733125	(163, 244)	(172, 253)	(185, 266)	(199, 280)	(215, 296)
52	rcp60	99.0%	50%	0.002503125	(166, 247)	(178, 259)	(195, 276)	(212, 293)	(235, 316)
53	rcp60	99.5%	50%	0.000500625	(168, 249)	(181, 262)	(200, 281)	(220, 301)	(246, 327)
54	rcp60	99.9%	50%	0.000333750	(171, 252)	(190, 271)	(214, 295)	(245, 326)	(281, 362)
55	rcp45	1.0%	50%	0.003337500	(154, 235)	(155, 236)	(156, 237)	(157, 238)	(156, 237)
56	rcp45	5.0%	50%	0.008733125	(156, 237)	(159, 240)	(161, 242)	(165, 246)	(167, 248)
57	rcp45	16.7%	50%	0.025031250	(157, 238)	(161, 242)	(166, 247)	(171, 252)	(175, 256)
58	rcp45	50.0%	50%	0.037046250	(158, 239)	(165, 246)	(173, 254)	(181, 262)	(188, 269)
59	rcp45	83.3%	50%	0.025031250	(160, 241)	(170, 251)	(181, 262)	(192, 273)	(203, 284)
60	rcp45	95.0%	50%	0.008733125	(162, 243)	(174, 255)	(187, 268)	(202, 283)	(216, 297)
61	rcp45	99.0%	50%	0.002503125	(164, 245)	(179, 260)	(197, 278)	(216, 297)	(236, 317)
62	rcp45	99.5%	50%	0.000500625	(166, 247)	(183, 264)	(203, 284)	(224, 305)	(249, 330)
63	rcp45	99.9%	50%	0.000333750	(169, 250)	(192, 273)	(219, 300)	(248, 329)	(281, 362)
64	rcp26	1.0%	50%	0.003337500	(152, 233)	(152, 233)	(151, 232)	(149, 230)	(150, 231)
65	rcp26	5.0%	50%	0.008733125	(154, 235)	(155, 236)	(156, 237)	(158, 239)	(160, 241)
66	rcp26	16.7%	50%	0.025031250	(155, 236)	(159, 240)	(162, 243)	(165, 246)	(168, 249)
67	rcp26	50.0%	50%	0.037046250	(158, 239)	(164, 245)	(170, 251)	(176, 257)	(182, 263)
68	rcp26	83.3%	50%	0.025031250	(161, 242)	(170, 251)	(180, 261)	(189, 270)	(197, 278)
69	rcp26	95.0%	50%	0.008733125	(163, 244)	(175, 256)	(188, 269)	(200, 281)	(210, 291)
70	rcp26	99.0%	50%	0.002503125	(166, 247)	(181, 262)	(198, 279)	(215, 296)	(231, 312)
71	rcp26	99.5%	50%	0.000500625	(167, 248)	(185, 266)	(204, 285)	(223, 304)	(243, 324)
72	rcp26	99.9%	50%	0.000333750	(170, 251)	(193, 274)	(221, 302)	(250, 331)	(278, 359)
73	rcp85	1.0%	10%	0.001837500	(154, 261)	(156, 263)	(159, 266)	(161, 268)	(162, 269)
74	rcp85	5.0%	10%	0.004808125	(156, 263)	(159, 266)	(164, 271)	(169, 276)	(172, 279)
75	rcp85	16.7%	10%	0.013781250	(157, 264)	(162, 269)	(168, 275)	(175, 282)	(181, 288)
76	rcp85	50.0%	10%	0.020396250	(159, 266)	(167, 274)	(176, 283)	(186, 293)	(196, 303)
77	rcp85	83.3%	10%	0.013781250	(162, 269)	(172, 279)	(184, 291)	(197, 304)	(212, 319)
78	rcp85	95.0%	10%	0.004808125	(163, 270)	(175, 282)	(190, 297)	(207, 314)	(226, 333)
79	rcp85	99.0%	10%	0.001378125	(165, 272)	(181, 288)	(200, 307)	(222, 329)	(246, 353)
80	rcp85	99.5%	10%	0.000275625	(167, 274)	(184, 291)	(205, 312)	(230, 337)	(258, 365)
81	rcp85	99.9%	10%	0.000183750	(170, 277)	(194, 301)	(223, 330)	(256, 363)	(294, 401)
82	rcp60	1.0%	10%	0.001837500	(152, 259)	(154, 261)	(154, 261)	(156, 263)	(157, 264)
83	rcp60	5.0%	10%	0.004808125	(154, 261)	(156, 263)	(158, 265)	(163, 270)	(166, 273)
84	rcp60	16.7%	10%	0.013781250	(156, 263)	(160, 267)	(164, 271)	(169, 276)	(175, 282)
85	rcp60	50.0%	10%	0.020396250	(158, 265)	(163, 270)	(170, 277)	(179, 286)	(187, 294)
86	rcp60	83.3%	10%	0.013781250	(160, 267)	(168, 275)	(178, 285)	(189, 296)	(202, 309)

Table EC.4: Sea level states paths, probabilities, and sea level values for each period (Continued)

Path	RCP	SLR Curve	Surge Curve	Path Probability	2030 $(s, \hat{s})$	2040 $(s, \hat{s})$	2050 $(s, \hat{s})$	2060 $(s, \hat{s})$	2070 $(s, \hat{s})$
87	rcp60	95.0%	10%	0.004808125	(163, 270)	(172, 279)	(185, 292)	(199, 306)	(215, 322)
88	rcp60	99.0%	10%	0.001378125	(166, 273)	(178, 285)	(195, 302)	(212, 319)	(235, 342)
89	rcp60	99.5%	10%	0.000275625	(168, 275)	(181, 288)	(200, 307)	(220, 327)	(246, 353)
90	rcp60	99.9%	10%	0.000183750	(171, 278)	(190, 297)	(214, 321)	(245, 352)	(281, 388)
91	rcp45	1.0%	10%	0.001837500	(154, 261)	(155, 262)	(156, 263)	(157, 264)	(156, 263)
92	rcp45	5.0%	10%	0.004808125	(156, 263)	(159, 266)	(161, 268)	(165, 272)	(167, 274)
93	rcp45	16.7%	10%	0.013781250	(157, 264)	(161, 268)	(166, 273)	(171, 278)	(175, 282)
94	rcp45	50.0%	10%	0.020396250	(158, 265)	(165, 272)	(173, 280)	(181, 288)	(188, 295)
95	rcp45	83.3%	10%	0.013781250	(160, 267)	(170, 277)	(181, 288)	(192, 299)	(203, 310)
96	rcp45	95.0%	10%	0.004808125	(162, 269)	(174, 281)	(187, 294)	(202, 309)	(216, 323)
97	rcp45	99.0%	10%	0.001378125	(164, 271)	(179, 286)	(197, 304)	(216, 323)	(236, 343)
98	rcp45	99.5%	10%	0.000275625	(166, 273)	(183, 290)	(203, 310)	(224, 331)	(249, 356)
99	rcp45	99.9%	10%	0.000183750	(169, 276)	(192, 299)	(219, 326)	(248, 355)	(281, 388)
100	rcp26	1.0%	10%	0.001837500	(152, 259)	(152, 259)	(151, 258)	(149, 256)	(150, 257)
101	rcp26	5.0%	10%	0.004808125	(154, 261)	(155, 262)	(156, 263)	(158, 265)	(160, 267)
102	rcp26	16.7%	10%	0.013781250	(155, 262)	(159, 266)	(162, 269)	(165, 272)	(168, 275)
103	rcp26	50.0%	10%	0.020396250	(158, 265)	(164, 271)	(170, 277)	(176, 283)	(182, 289)
104	rcp26	83.3%	10%	0.013781250	(161, 268)	(170, 277)	(180, 287)	(189, 296)	(197, 304)
105	rcp26	95.0%	10%	0.004808125	(163, 270)	(175, 282)	(188, 295)	(200, 307)	(210, 317)
106	rcp26	99.0%	10%	0.001378125	(166, 273)	(181, 288)	(198, 305)	(215, 322)	(231, 338)
107	rcp26	99.5%	10%	0.000275625	(167, 274)	(185, 292)	(204, 311)	(223, 330)	(243, 350)
108	rcp26	99.9%	10%	0.000183750	(170, 277)	(193, 300)	(221, 328)	(250, 357)	(278, 385)
109	rcp85	1.0%	1%	0.000412500	(154, 295)	(156, 297)	(159, 300)	(161, 302)	(162, 303)
110	rcp85	5.0%	1%	0.001079375	(156, 297)	(159, 300)	(164, 305)	(169, 310)	(172, 313)
111	rcp85	16.7%	1%	0.003093750	(157, 298)	(162, 303)	(168, 309)	(175, 316)	(181, 322)
112	rcp85	50.0%	1%	0.004578750	(159, 300)	(167, 308)	(176, 317)	(186, 327)	(196, 337)
113	rcp85	83.3%	1%	0.003093750	(162, 303)	(172, 313)	(184, 325)	(197, 338)	(212, 353)
114	rcp85	95.0%	1%	0.001079375	(163, 304)	(175, 316)	(190, 331)	(207, 348)	(226, 367)
115	rcp85	99.0%	1%	0.000309375	(165, 306)	(181, 322)	(200, 341)	(222, 363)	(246, 387)
116	rcp85	99.5%	1%	0.000061875	(167, 308)	(184, 325)	(205, 346)	(230, 371)	(258, 399)
117	rcp85	99.9%	1%	0.000041250	(170, 311)	(194, 335)	(223, 364)	(256, 397)	(294, 435)
118	rcp60	1.0%	1%	0.000412500	(152, 293)	(154, 295)	(154, 295)	(156, 297)	(157, 298)
119	rcp60	5.0%	1%	0.001079375	(154, 295)	(156, 297)	(158, 299)	(163, 304)	(166, 307)
120	rcp60	16.7%	1%	0.003093750	(156, 297)	(160, 301)	(164, 305)	(169, 310)	(175, 316)
121	rcp60	50.0%	1%	0.004578750	(158, 299)	(163, 304)	(170, 311)	(179, 320)	(187, 328)
122	rcp60	83.3%	1%	0.003093750	(160, 301)	(168, 309)	(178, 319)	(189, 330)	(202, 343)
123	rcp60	95.0%	1%	0.001079375	(163, 304)	(172, 313)	(185, 326)	(199, 340)	(215, 356)
124	rcp60	99.0%	1%	0.000309375	(166, 307)	(178, 319)	(195, 336)	(212, 353)	(235, 376)

Table EC.4: Sea level states paths, probabilities, and sea level values for each period (Continued)

Path	RCP	SLR Curve	Surge Curve	Path Probability	2030 $(s, \hat{s})$	2040 $(s, \hat{s})$	2050 $(s, \hat{s})$	2060 $(s, \hat{s})$	2070 $(s, \hat{s})$
125	rcp60	99.5%	1%	0.000061875	(168, 309)	(181, 322)	(200, 341)	(220, 361)	(246, 387)
126	rcp60	99.9%	1%	0.000041250	(171, 312)	(190, 331)	(214, 355)	(245, 386)	(281, 422)
127	rcp45	1.0%	1%	0.000412500	(154, 295)	(155, 296)	(156, 297)	(157, 298)	(156, 297)
128	rcp45	5.0%	1%	0.001079375	(156, 297)	(159, 300)	(161, 302)	(165, 306)	(167, 308)
129	rcp45	16.7%	1%	0.003093750	(157, 298)	(161, 302)	(166, 307)	(171, 312)	(175, 316)
130	rcp45	50.0%	1%	0.004578750	(158, 299)	(165, 306)	(173, 314)	(181, 322)	(188, 329)
131	rcp45	83.3%	1%	0.003093750	(160, 301)	(170, 311)	(181, 322)	(192, 333)	(203, 344)
132	rcp45	95.0%	1%	0.001079375	(162, 303)	(174, 315)	(187, 328)	(202, 343)	(216, 357)
133	rcp45	99.0%	1%	0.000309375	(164, 305)	(179, 320)	(197, 338)	(216, 357)	(236, 377)
134	rcp45	99.5%	1%	0.000061875	(166, 307)	(183, 324)	(203, 344)	(224, 365)	(249, 390)
135	rcp45	99.9%	1%	0.000041250	(169, 310)	(192, 333)	(219, 360)	(248, 389)	(281, 422)
136	rcp26	1.0%	1%	0.000412500	(152, 293)	(152, 293)	(151, 292)	(149, 290)	(150, 291)
137	rcp26	5.0%	1%	0.001079375	(154, 295)	(155, 296)	(156, 297)	(158, 299)	(160, 301)
138	rcp26	16.7%	1%	0.003093750	(155, 296)	(159, 300)	(162, 303)	(165, 306)	(168, 309)
139	rcp26	50.0%	1%	0.004578750	(158, 299)	(164, 305)	(170, 311)	(176, 317)	(182, 323)
140	rcp26	83.3%	1%	0.003093750	(161, 302)	(170, 311)	(180, 321)	(189, 330)	(197, 338)
141	rcp26	95.0%	1%	0.001079375	(163, 304)	(175, 316)	(188, 329)	(200, 341)	(210, 351)
142	rcp26	99.0%	1%	0.000309375	(166, 307)	(181, 322)	(198, 339)	(215, 356)	(231, 372)
143	rcp26	99.5%	1%	0.000061875	(167, 308)	(185, 326)	(204, 345)	(223, 364)	(243, 384)
144	rcp26	99.9%	1%	0.000041250	(170, 311)	(193, 334)	(221, 362)	(250, 391)	(278, 419)

EC.2.2 Network data

To create our network, we start by overlaying a grid in the geographic region of interest, which is a neighborhood in Boston and the surrounding region in our case study. We chose to create our grid overlay using hexagonal grids. Although many flood studies use square grids, we use hex grids for two main reasons. First, hex grids provide a tessellated grid structure with equidistant grids between their centers. Second, hex grids have distinct boundary lines with limited ambiguity. The reduced boundary ambiguity overcomes the challenge of determining water flow with square cells as to whether it is just across the four shared sides (four neighbors) or also across the corners (eight neighbors). Using hex grids, the network nodes' neighbors are just the six neighbors sharing same-length borders, which are very straightforward to define and account for flow between nodes. These are the two main reasons we use hex grids to develop our network, but the interested reader can find more background on the pros and cons of hex grids in geospatial analysis applications (Birch et al. 2007, De Sousa et al. 2017).

We conduct all geographical data inputs and transformations for modeling purposes using the Quantum Geographic Information Software (QGIS) application, specifically version 3.10. To create our grid overlays, we use the MMQGIS Python library that allows creating a grid overlay by providing information covering the geographic region of interest and individual grid size. In determining the hex grids' size, we have to trade off between hex grid area size and expected model runtime. On the one hand, the smaller we make the hex grids, the larger the number of overall grids there will be, which will result in a more complex model and longer runtimes to reach suitable solutions. Conversely, the grids should be sufficiently small to keep the model relevant for protecting discrete areas that can be built up over time to provide potential protection for the network. In evaluating the model, we evaluated various size grid overlays to get a sense of model runtime compared to realistic grid sizes for planning. In the end, we have used a grid overlay with hex grids with a side-to-side length of 100 meters and an area of 8660 m^2, resulting in 404 at-risk land grids in the region of interest. We will create our network within this grid structure and conduct the necessary transformations to create grid attributes. In the following sections, we will discuss the assumptions and transformations needed to calculate the grid attributes for elevation (h_i), depth damage coefficient (f_i), and value (g_i) used in the model.

EC.2.2.1 Grid elevation data

To determine each grid's elevation, we start with available Light Detection and Ranging (LIDAR) data for Massachusetts. This dataset is open-source and available online from the MassGIS repository (MassGIS 2017). MassGIS terrain data comes in varying degrees of granularity. The raster file data used in this analysis had elevation data by one square-meter of land coverage. The surveys that captured this data were conducted in 2013-2014 to assist in evaluating hurricane storm damage and erosion of the local environment as part of the United States Geologic Survey (USGS) response to Hurricane Sandy. For the bathtub-type flood analysis used in this study, LIDAR data with this level of accuracy are considered to be of sufficient quality (Gesch 2018). To capture each hex grid's elevation, using the QGIS software, we sampled the elevation from the LIDAR raster values within a given hex grid and then assigned the mean as the elevation of the hex grid. Given the overall exploratory nature of the model, we must accept some limitations to the ability to capture the grid elevations perfectly.

EC.2.2.2 Tax appraisal data

We use the open-source Geographic Information System (GIS) tax appraisal data available from the City of Boston to obtain the value and types of buildings located within the study area. Specifically, we use the tax appraisal data from the 2016 tax year because it was the fullest dataset available at

the beginning of this study. The tax appraisal dataset is available from the City of Boston at their GIS data repository (BostonGIS 2016). Supporting information and metadata were also needed and available from the Analyze Boston website (Boston 2020), including the tax parcel data key and associated property occupancy codes.

It was necessary to profile the data to ensure its quality and applicability due to it being an open-source dataset. There were several elements of the data that required subsequent validation. For example, to properly determine the building structure, we needed to know how many floors were in a given building. Unfortunately, for multi-unit buildings with multiple taxpayers, the dataset's records only had the number of floors associated with a taxable unit (e.g., condo or apartment). To correctly classify the number of floors in a building, we used secondary validation to visually inspect the buildings using Google Streetview (Anguelov et al. 2010) to assess the total number of floors for multi-tenant buildings. The number of floors is essential in determining the classification to assign each building for assigning the appropriate depth damage function. We also used Google Streetview for additional validation when a building in the tax database no longer existed or a building did exist but was not in the tax database. Finally, a subset of buildings and lots in the tax database was categorized as "exempt" for taxation purposes, and had zero appraised value. Examples of such buildings included churches, government buildings, hospitals, and state transportation nodes. Because these tax-exempt parcels have a value of zero, exempt parcels in the model understate the potential total damages. That said, in the overall dataset, only 2% of the tax parcels were exempt, so we leave their value as zero for purposes of this model evaluation.

EC.2.2.3 Depth damage curve estimation

To determine the flood damage associated with temporary related flooding from hurricane storm surges, we need to use the tax parcel data to capture the type of building within each tax parcel. We also need a method of determining flood damage based on the level of flooding. Depth damage functions are typically defined by interpolating flooding depth and damage data through systematic procedures that analyze historical flood events or insurance claims data, or even from synthetic damage data from simulation models (Armal et al. 2020). The resulting function can be used to estimate how much damage a building may experience based on a given depth of flooding.

For purposes of this study, we adapt the hurricane storm surge-related depth damage curves captured following Hurricane Sandy-related flooding in 2012. In the aftermath of Hurricane Sandy, the US Army Corps of Engineers worked with a group of experts to elicit depth damage functions for the building types common in the area affected by Hurricane Sandy. The result was a listing of 14 building types and the associated depth damage function for these buildings when experiencing inundation, erosion, and wave impacts (USACE 2015). For our model with the bathtub-type

flooding methodology, we only use the inundation-related damage curves from USACE (2015) to develop our associated depth damage functions. More specifically, of the 14 building types identified within the study, there are five that we apply to the buildings in our model. Specifically, we used the depth damage curves for one-story commercial, one-story residential, two-story residential, three-story apartment, and high-rise buildings. Not every building in Boston fits perfectly into these categories, so we had to apply a judgment call in some instances. For instance, there are many three- and four-story residential buildings in Boston with very similar characteristics. Given these similarities, we put all of these buildings into the three-story apartment category. Table EC.5 shows the breakdown of buildings and their type classification. Due to our model's linear nature, we applied a linear approximation of the depth damage curves in USACE (2015), with all costs starting at zero. This linearization method introduces potential errors into the model, so we check its sensitivity in the model by running three potential values at 125%, 100%, and 75% of the estimated values captured using our method. Using the linear approximation for each curve, we arrive at the coefficient of the depth damage function for each building in a tax parcel as shown in Table EC.5.

Table EC.5   Breakdown of building types in Boston and associated depth damage coefficients

Building Type	Count	Depth Damage Coefficient per meter
Three Story Apartment	3290	0.203
Two Story Residential	2040	0.203
One Story Commercial	206	0.233
One Story Residential	155	0.246
High Rise	6	0.108

EC.2.2.4   Calculating flood loss values f_i and g_i

With each building's values and types now captured in the tax parcel dataset, it is necessary to transform the applicable tax parcel data within each hex grid into the flood loss coefficients that are the attributes for each hex grid. We next derive the flood cost parameters f_i and g_i by weighting and aggregating the previously described tax appraisal data. Below, we describe the steps necessary to calculate these two grid monetary-related attributes as discussed in Molenaar (1998).

Within the tax dataset, tax entities represent units that are taxable within a tax parcel. There can be more than one tax entity in a tax parcel, but a tax entity can only reside in one and only one tax parcel. We represent the tax entity by index k, where there are K = 7,979 tax entities in the dataset (i.e., $k \in \{1, \ldots, K\}$). Tax parcels are the geographic areas within the data that contain one or more tax entities. Tax parcels will be represented by index l, where there are L = 6,467 tax parcels in the dataset (i.e., $l \in \{1, \ldots, L\}$).

Tax entities have three appraised value fields in the tax dataset: *building value*, *lot value*, and *total value* consisting of the sum of building and lot values. In this analysis, for a given tax entity k, we use the appraised building value (denoted by BV_k) to determine the flood damage costs from temporary flooding, and use the appraised total value (denoted by TV_k) to determine the loss caused due to inundation. We used the appraised values available via the Boston 2016 tax parcel data (Boston 2020, BostonGIS 2016).

Using the information we have for each tax entity, the tax entity values can then be aggregated into the applicable geographic-based tax parcels as described next.

- Appraised Building Value for Tax Parcel l is

$$PBV_l = \sum_{k \in l} BV_k \quad \forall l \in \{1,..,L\}$$

- Appraised Total Value for Tax Parcel l is

$$PTV_l = \sum_{k \in l} TV_k \quad \forall l \in \{1,..,L\}$$

Each tax parcel represents an area of land on the map where the tax entities are located. To allow for aggregating portions of the tax parcels that intersect with the hex grids, we need to determine a unit measure of value within each tax parcel. In this case, we can determine that unit measure by dividing the tax parcel's appraised values by the tax parcel area. Area of the Tax Parcel l is designated as A_l as measured in square meters and is determined by using QGIS software. Using this tax parcel area, we can determine the unit values for both building and total appraised values per square meter within each tax parcel as follows.

- Unit Building Value in parcel l is

$$pbv_l = \frac{PBV_l}{A_l} \quad \forall l \in \{1,..,L\}$$

- Unit Total Value in parcel l is

$$ptv_l = \frac{PTV_l}{A_l} \quad \forall l \in \{1,..,L\}$$

The aggregation's next step is to determine the depth damage value for a square meter of tax parcel l. We can do this by using the information in the data set that indicates the property type along with the applicable depth damage coefficient from Table EC.5. The depth damage coefficient is a linear approximation used to determine the dollars of property damage as a percentage of value per depth of one meter flood. We designate this by D_l, then multiply it with the unit building value pbv_l to attain the per meter squared depth damage per meter of flood level. In other words, the damage value in a meter squared of tax parcel $l \in \{1, \ldots, L\}$ per meter of flooding is $pdv_l = D_l \, pbv_l$

Now that we have our values for parcel depth damage and total value, we need to aggregate those values into the hex grids i to develop the per grid estimated depth damage values $\bar{f}_i$ and the inundation flood loss value g_i. To this aim we will merge the two map layers and evaluate the overlapping areas of the tax parcels captured within each hex grid. The overlapping area between a

hex grid $i \in \{1, \ldots, i_{max}\}$ and a tax parcel $l \in \{1, \ldots, L\}$ is denoted by OA_{il}, and is calculated using the QGIS software. Using these overlapping areas, we can determine the aggregated depth damage and total values associated with each hex grid as described next.

- Hex grid i depth damage value (dollars/meter) is

$$\bar{f}_i = \sum_{\{l \in \{1, \ldots, L\}: i \cap l \neq \emptyset\}} pdv_l OA_{il} \quad \forall i \in \{1, .., i_{max}\}$$

- Hex grid i total value (dollars) is

$$g_i = \sum_{\{l \in \{1, \ldots, L\}: i \cap l \neq \emptyset\}} ptv_l OA_{il} \quad \forall i \in \{1, .., i_{max}\}$$

EC.2.3   Financial data

As discussed in Section 4.1, there are three financial components that we need to incorporate into our model. The first is the cost of investment to elevate a grid (i.e., parameter c). We treat the investment cost as the cost of building a levee on the grid. Typically a levee would have a range of values per meter of height build-up based on the levee height. To determine the cost in our model, we started with a linear estimate of \$450 per foot build-up per linear foot of wall (Hecht and Kirshen 2019) (or \$4,841.28 per meter per linear meter). Given the expected importance of this parameter to the model solutions, and based on values from previous projects (Jonkman et al. 2013), we check the model's cost sensitivity using three values of \$5M, \$15M, and \$25M per kilometer of length for one meter of elevation (\$M/km per m). Converting these costs for the model to use per grid, the values we used were \$0.866M, \$2.598M, and \$4.33M per meter of elevation change for one grid. We do this by using the linear distance measurement of half the perimeter of our hex grids for the length to build.

The next financial parameter we include is a discount rate (d). Wide ranges of discount rates can be used for this type of cost-benefit analysis (Aerts et al. 2014). The value used often depends upon the decision-maker's financial risk tolerance. To account for a range of sensitivity, we incorporate three annual discount rate values of 3%, 5%, and 7%. Given that the time duration of each period in our model is ten years, we end up with an adjusted discount rate parameter in the model of $\lambda = (1+d)^{10}$.

The final financial parameter needed for our model is the budget spent to build up grid elevations for each period (i.e., b_t for all $t \in \{1, \ldots, t_{max}\}$). Given this study's exploratory nature, we use this financial value primarily as a per-period constraint to assess the model under various budget limitations. In reality, if running this model for a government agency, we would need to work with the agency to understand their current budget plans, constraints, and limits on what they would spend for the area under investigation. A simple way to arrive at an acceptable budget range is to look at the city's current budget for its infrastructure development and use that as a constant value

throughout the study period. In the end, we use a band of budgets determined by initially running the model without the budget constraint and picking representative values based on the breakpoints for the initial period spends across all scenarios. This results in the case study budgets ranging from $0 to $600M per period as shown in Table 1 for the case study of Boston. These values span a wide range, with the lower to mid-ranges being within a reasonable range of what we would expect the city to spend to avoid flood damages. The final factor we need to address in the financial data is that the model periods are a decade long, while the flood damages are based on annual factors. Thus, we increase the expected damages by a factor of 10 in calculating all expected flood damages that the model determines.

EC.3 Sets, parameters and variables used in the Flood Risk Mitigation (FRM) model

- t_{max}: Number of periods within the planning horizon.

- $\mathcal{T}$: The set containing all time periods within the planning horizon, i.e., $\mathcal{T} = \{1, \ldots, t_{max}\}$.

- s: The sea level during a period solely due to the climate change effects.

- $\hat{s}$: The sea level during a period due to both climate change effects and hurricane storm surge factors.

- $\mathcal{S} = (s, \hat{s})$: The sea level state during a period.

- Ξ_t: The set containing all possible sea level states during a period t.

- $p_t^{\mathcal{S}\mathcal{S}'}$: The probability that the sea level state during period t is $\mathcal{S}$ and during period $t+1$ is $\mathcal{S}'$ for a given $t \in \{0, \ldots, t_{max} - 1\}$, $\mathcal{S} \in \Xi_t$ and $\mathcal{S}' \in \Xi_{t+1}$.

- $\hat{s}_{max}$: The highest sea level across all sea level states, i.e., $\hat{s}_{max} = \max\{\hat{s} : (s, \hat{s}) \in \Xi_{t_{max}}\}$.

- Φ: The set containing the land grids forming the "area of interest", which are the flooded land grids in the region of interest under sea level $\hat{s}_{max}$.

- Ψ: The set containing the land grids forming the "area of relevance", which are the flooded land grids in the surrounding region with a water path to some flooded land grid in the region of interest without going through the sea under sea level $\hat{s}_{max}$.

- h_i: The initial elevation for a land grid $i \in \Phi \cup \Psi$.

- O: The set containing the hexagonal grids formed on the sea at time zero.

- $R_t^{\mathcal{S}}$: The subset of land grids in Φ at risk of permanent inundation flooding during period t and under sea level state $\mathcal{S} \in \Xi_t$.

- $Q_t^{\mathcal{S}}$: The subset of land grids in Ψ at risk of permanent inundation flooding during period t and under sea level state $\mathcal{S} \in \Xi_t$.

- $\hat{R}_t^{\mathcal{S}}$: The subset of land grids in Φ only at risk of temporary flooding during period t and under sea level state $\mathcal{S} \in \Xi_t$.

- $\hat{Q}_t^{\mathcal{S}}$: The subset of land grids in Ψ only at risk of temporary flooding during period t and under sea level state $\mathcal{S} \in \Xi_t$.

- o: The vertex representing all sea-based grids within a given at-risk network.

- $N_t^{\mathcal{S}}(i)$: The set containing vertices that are adjacent to a vertex $i \in R_t^{\mathcal{S}} \cup \hat{R}_t^{\mathcal{S}} \cup Q_t^{\mathcal{S}} \cup \hat{Q}_t^{\mathcal{S}}$ within the at-risk network during a period t and under a sea level state $\mathcal{S} \in \Xi_t$. This set is also referred to as the neighbors of i within the aforementioned at-risk network.

- c: The cost to elevate a grid in Φ by one meter at the start of a given a period.

- g_i: The cost of losing a grid $i \in \Phi$ due to inundation if the grid is in $R_t^{\mathcal{S}}$ during a period t and under a sea level state $\mathcal{S} \in \Xi_t$, and is permanently flooded.

- f_i: The cost of hurricane storm surge flood damage to a grid i in $R_t^{\mathcal{S}} \cup \hat{R}_t^{\mathcal{S}}$ during a period t and under a sea level state $\mathcal{S} \in \Xi_t$ when the grid is temporarily flooded.

- $\bar{f}_i$: The estimated value for f_i based on tax parcel data and is basis for sensitivity analysis of f_i.

- λ: The discount rate per period to incorporate realistic costs over time.

- d: The standard annual discount rate.

- b_t: The fixed construction and maintenance budget for a period $t \in \mathcal{T}$ that does not carry over into other periods.

- $x_{it\mathcal{S}}$: The decision variable associated with the height of a grid $i \in \Phi$ during a period $t \in \mathcal{T}$ if the sea level state during period $t-1$ is $\mathcal{S} \in \Xi_{t-1}$.

- m: The minimum threshold of elevation increase in any grid in Φ during a period.

- M: A valid upper bound on the elevation increase in any grid in Φ during a period. We use $M = \max\{\hat{s}_{max} - \min\{h_i : i \in \Phi \cup \Psi\}, m\}$ in our FRM model.

- $w_{it\mathcal{SS}'}$: A binary variable that captures if a grid $i \in R_t^{\mathcal{S}'} \cup Q_t^{\mathcal{S}'}$ is inundated during a period $t \in \mathcal{T}$ and under sea level states $\mathcal{S} \in \Xi_{t-1}$ and $\mathcal{S}' \in \Xi_t$ for which $p_{t-1}^{\mathcal{SS}'} > 0$. $w_{it\mathcal{SS}'} = 0$ if the grid is not inundated, and $w_{it\mathcal{SS}'} = 1$ otherwise.

- $z_{it\mathcal{SS}'}$: A continuous variable to capture the water depth used to calculate the temporary flood cost if a grid $i \in R_t^{\mathcal{S}'} \cup Q_t^{\mathcal{S}'} \cup \hat{R}_t^{\mathcal{S}'} \cup \hat{Q}_t^{\mathcal{S}'}$ is not inundated but faces hurricane storm surge related flooding during period t and under sea level states $\mathcal{S} \in \Xi_{t-1}$ and $\mathcal{S}' \in \Xi_t$ for which $p_{t-1}^{\mathcal{SS}'} > 0$.

- $v_{it\mathcal{SS}'}$: A binary variable indicating whether a grid $i \in \Phi$ is elevated at the start of a period $t \in \{2, \ldots, t_{max}\}$ under sea level states $\mathcal{S} \in \Xi_{t-2}$ and $\mathcal{S}' \in \Xi_{t-1}$ for which $p_{t-2}^{\mathcal{SS}'} > 0$.

- $v_{i1(0,0)}$: A binary variable indicating whether a grid $i \in \Phi$ is elevated at the start of the first period.

- $y_{it\mathcal{SS}'}$: A binary variable that indicates whether a grid $i \in R_t^{\mathcal{S}'} \cup Q_t^{\mathcal{S}'}$ is a neighbor of the sea grid or has an adjacent grid $i' \in N_t^{\mathcal{S}'}(i) \cap (R_t^{\mathcal{S}'} \cup Q_t^{\mathcal{S}'})$ that is inundated during period t and under sea level states $\mathcal{S} \in \Xi_{t-1}$ and $\mathcal{S}' \in \Xi_t$ for which $p_{t-1}^{\mathcal{SS}'} > 0$. If grid i is not a neighbor of the sea grid and also does not have an inundated neighbor, then $y_{it\mathcal{SS}'}$ is zero, and one otherwise.

- $\hat{y}_{it\mathcal{SS}'}$: A binary variable that indicates whether a grid $i \in R_t^{\mathcal{S}'} \cup Q_t^{\mathcal{S}'} \cup \hat{R}_t^{\mathcal{S}'} \cup \hat{Q}_t^{\mathcal{S}'}$ is a neighbor of the sea grid or has a hydraulic path to the sea during period t and under sea level states $\mathcal{S} \in \Xi_{t-1}$ and $\mathcal{S}' \in \Xi_t$ for which $p_{t-1}^{\mathcal{SS}'} > 0$. $\hat{y}_{it\mathcal{SS}'}$ is equal to one if grid i is a neighbor of the sea or if such a path exists, and zero otherwise.

EC.4 Full results for simulation and scenario runs

In this electronic companion, we present the full results for the sensitivity analysis in our simulation-based approach discussed in Section 4.2 and the scenario-based approach discussed in Section 4.3. The 81 plots in the following six figures represent results across all 81 parameter combinations, with an overall cost shown with stacked bar charts of the three cost types. Figure EC.5 shows the full results for the simulation runs discussed in Section 4.2. The remaining Figures show the full results for the scenarios discussed in Section 4.3. We omit the zero budget cost curves because the large magnitude of these curves overwhelms the curves for the other budgets, and prevents an effective visualization of the budget effect in each cost benefit curve. At the top of each chart is the combination of parameters for that chart, with the values shown in Table EC.6.

Parameter	High	Mid	Low
Discount rate (d) [%]	7	5	3
Minimum elevation increase (m) [meters]	5	3	1
Grid elevation cost (c) [$M/km per m]	25	15	5
Storm flood damage curve (f_i) [$M/m]	$1.25\bar{f}_i$	$\bar{f}_i$	$0.75\bar{f}_i$

Table EC.6 Parameter values used in sensitivity analysis for charts shown in Section EC.4
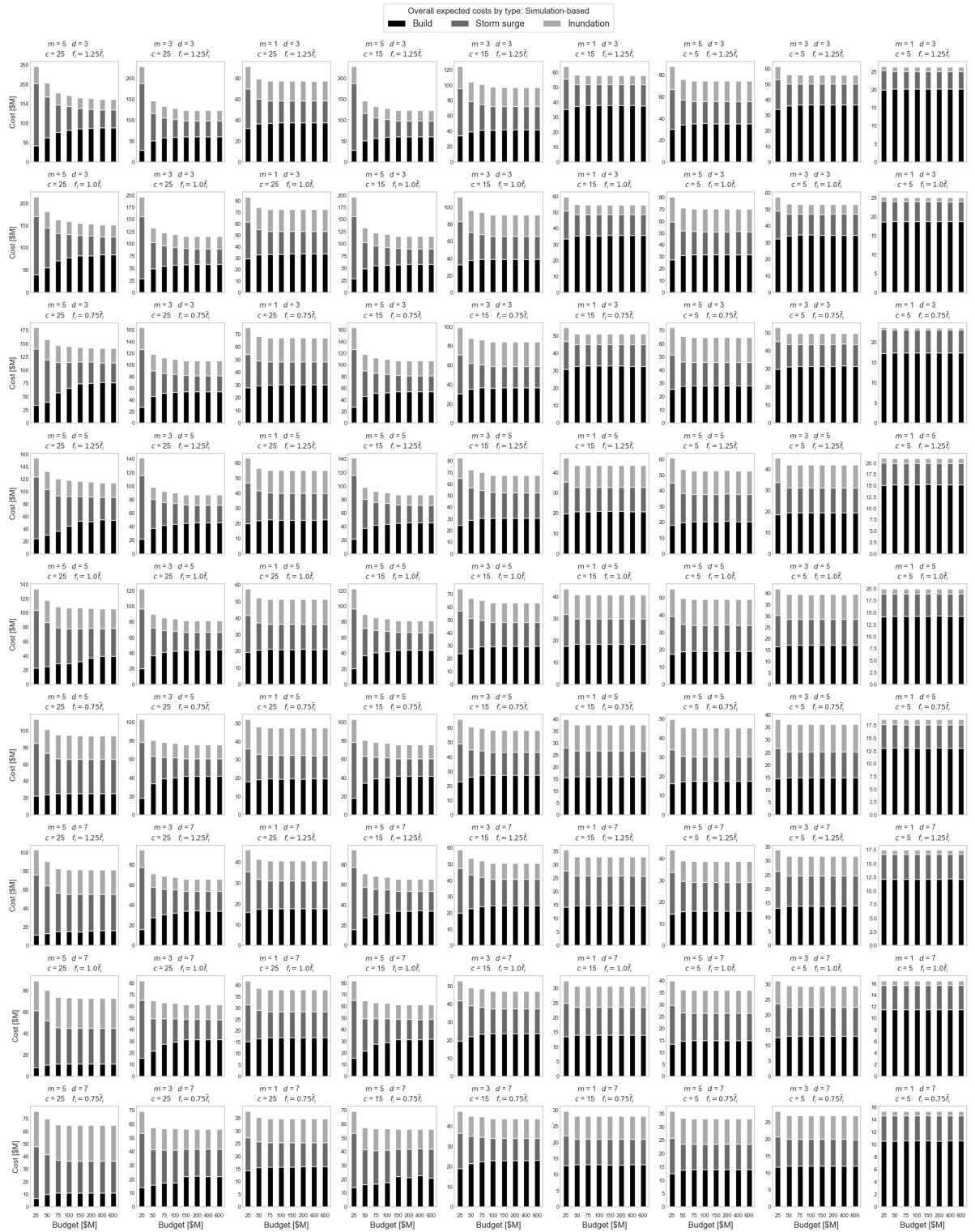
Figure EC.5 Boston simulation expected cost benefit curves by per-period budget with expected costs averaged across full 144 simulated sea level states paths for each of the 81 parameter combinations.
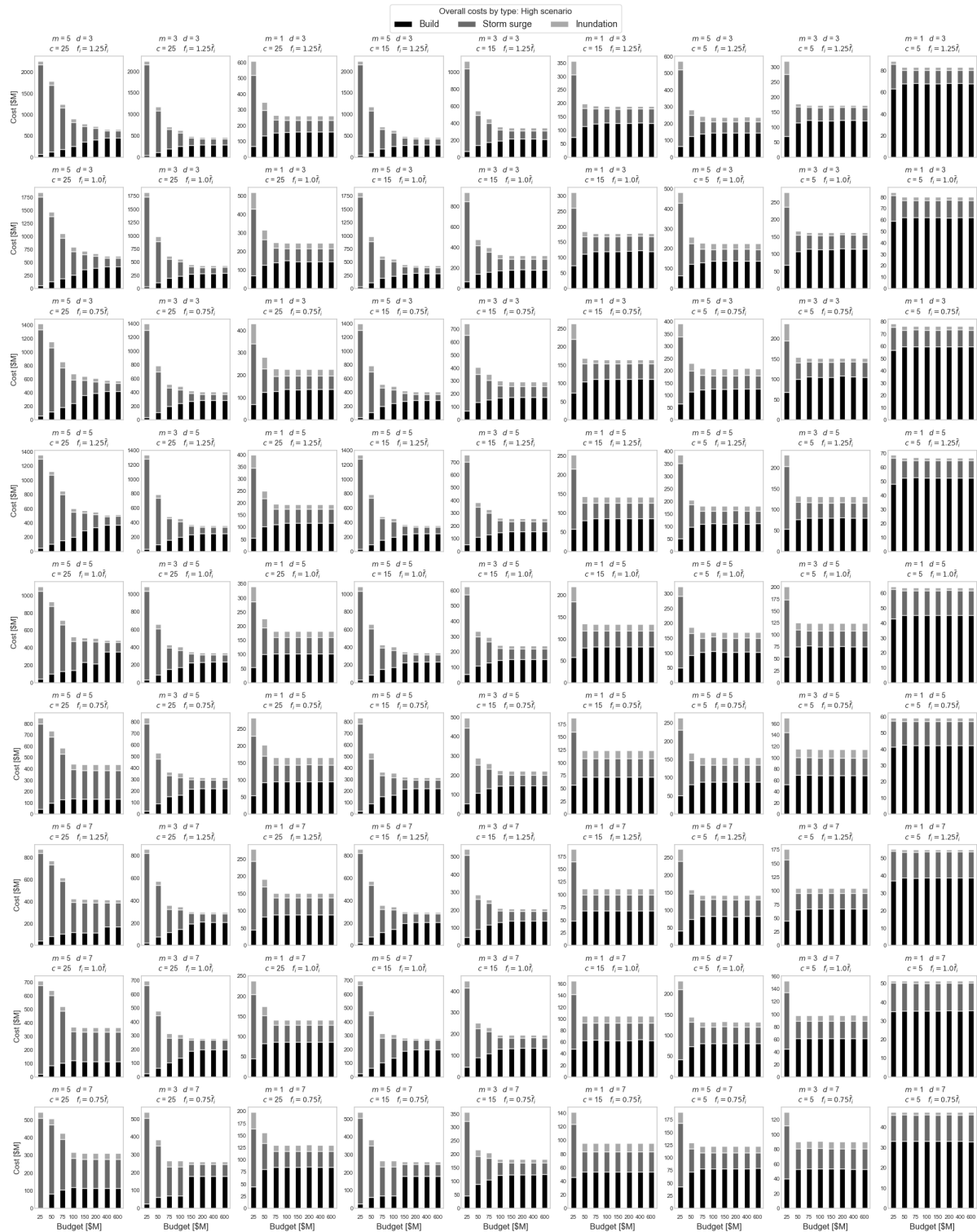
Figure EC.6 Boston High scenario cost benefit curves by per-period budget for each of the 81 parameter combinations.
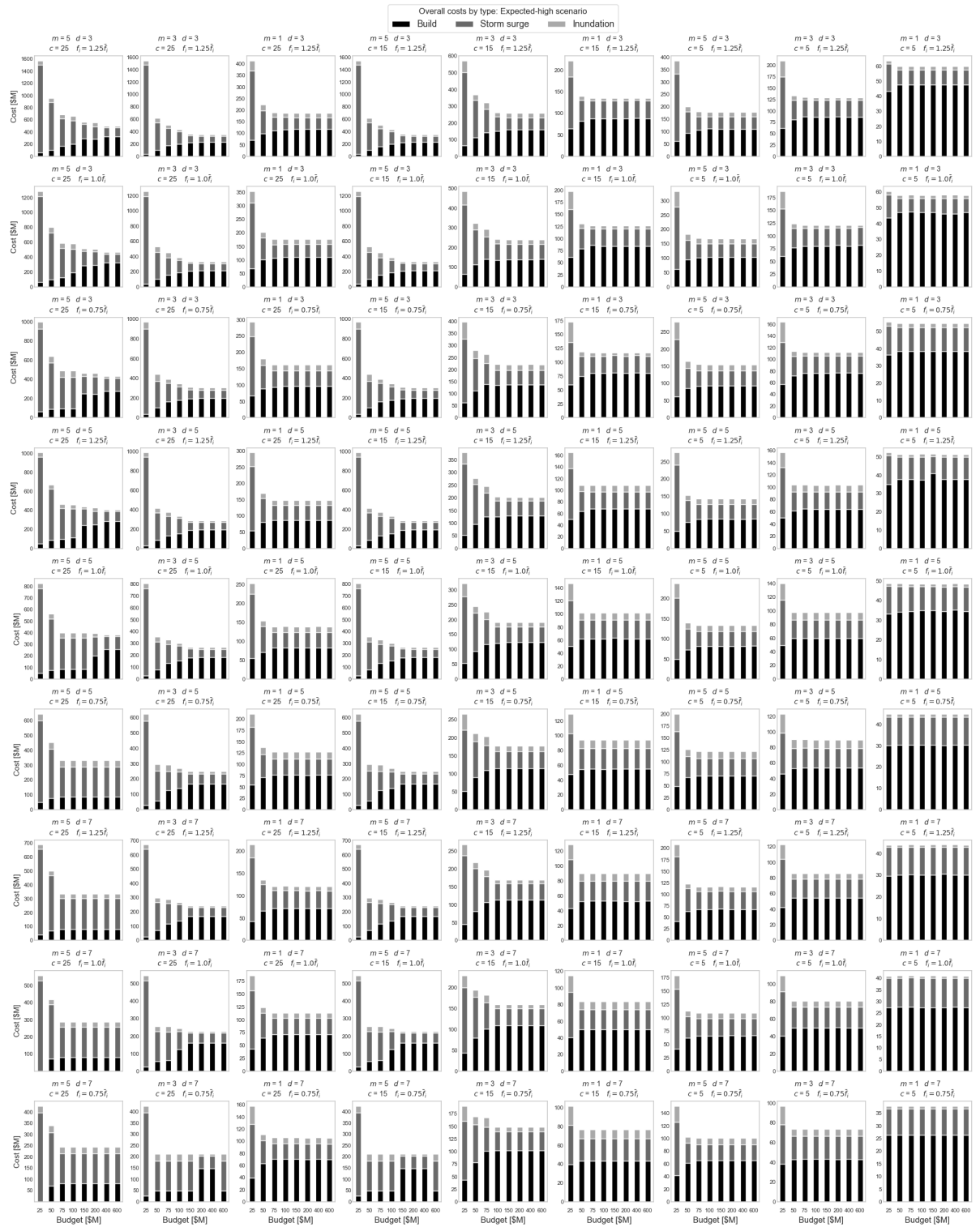
Figure EC.7 Boston Expected-high scenario cost benefit curves by per-period budget for each of the 81 parameter combinations.
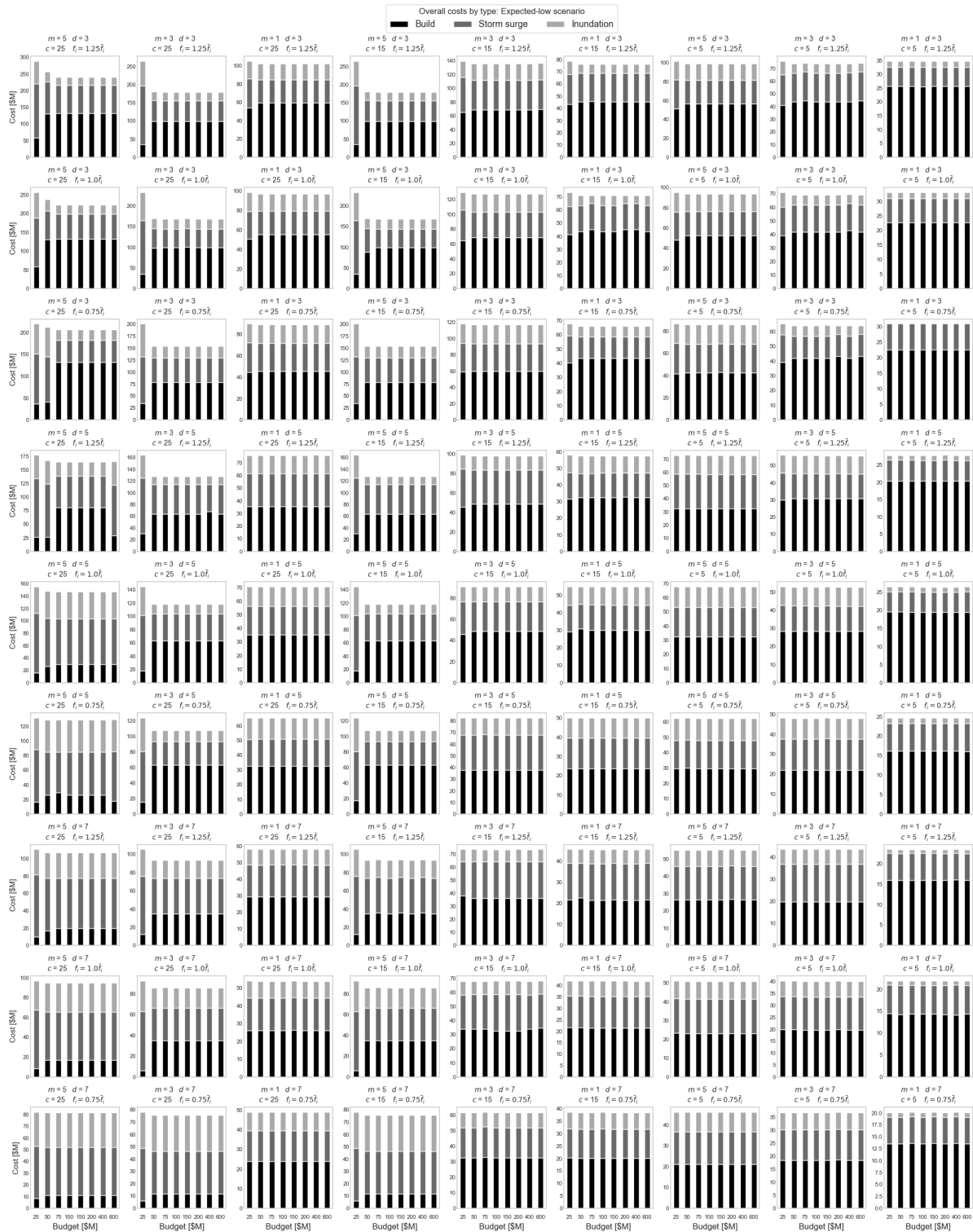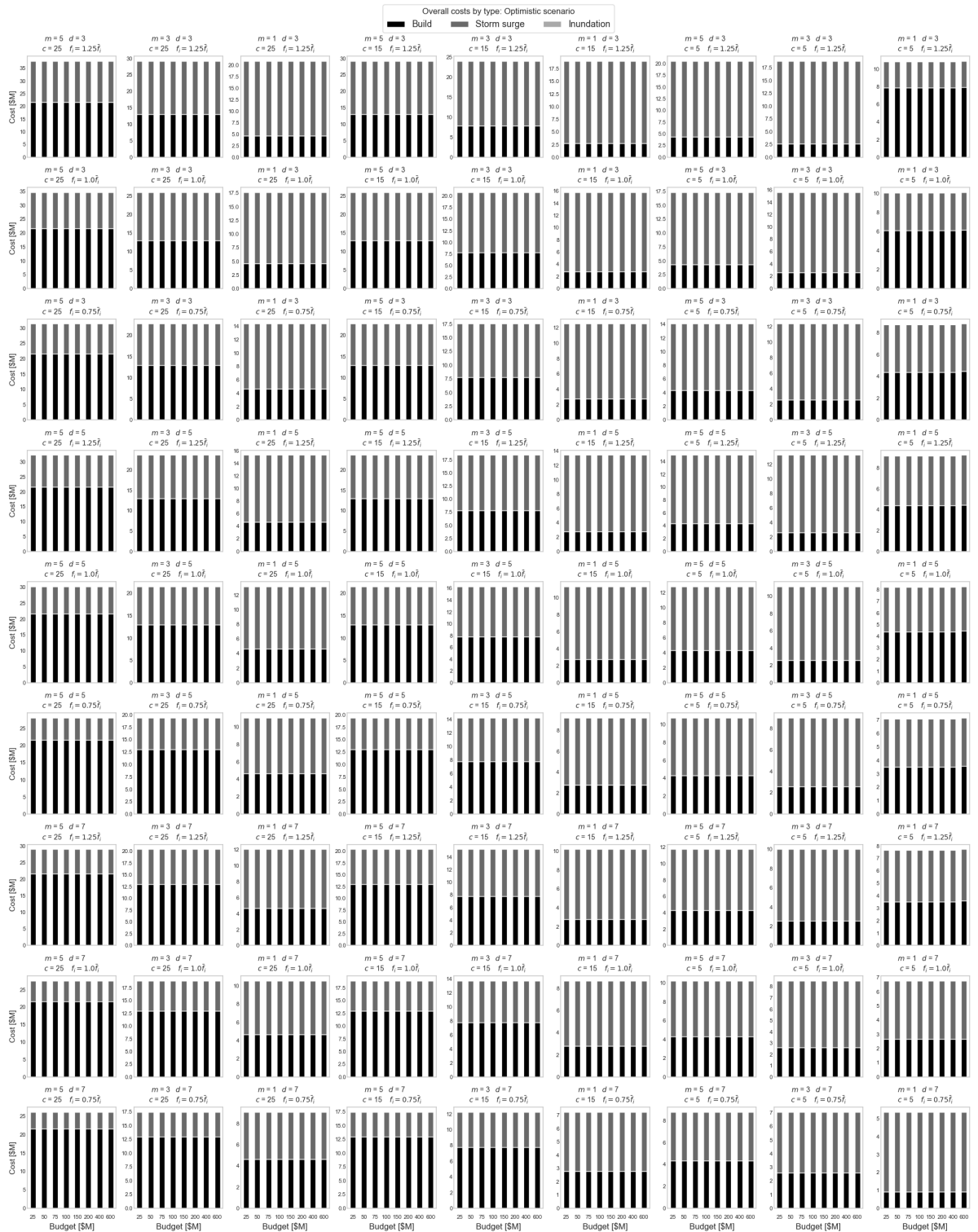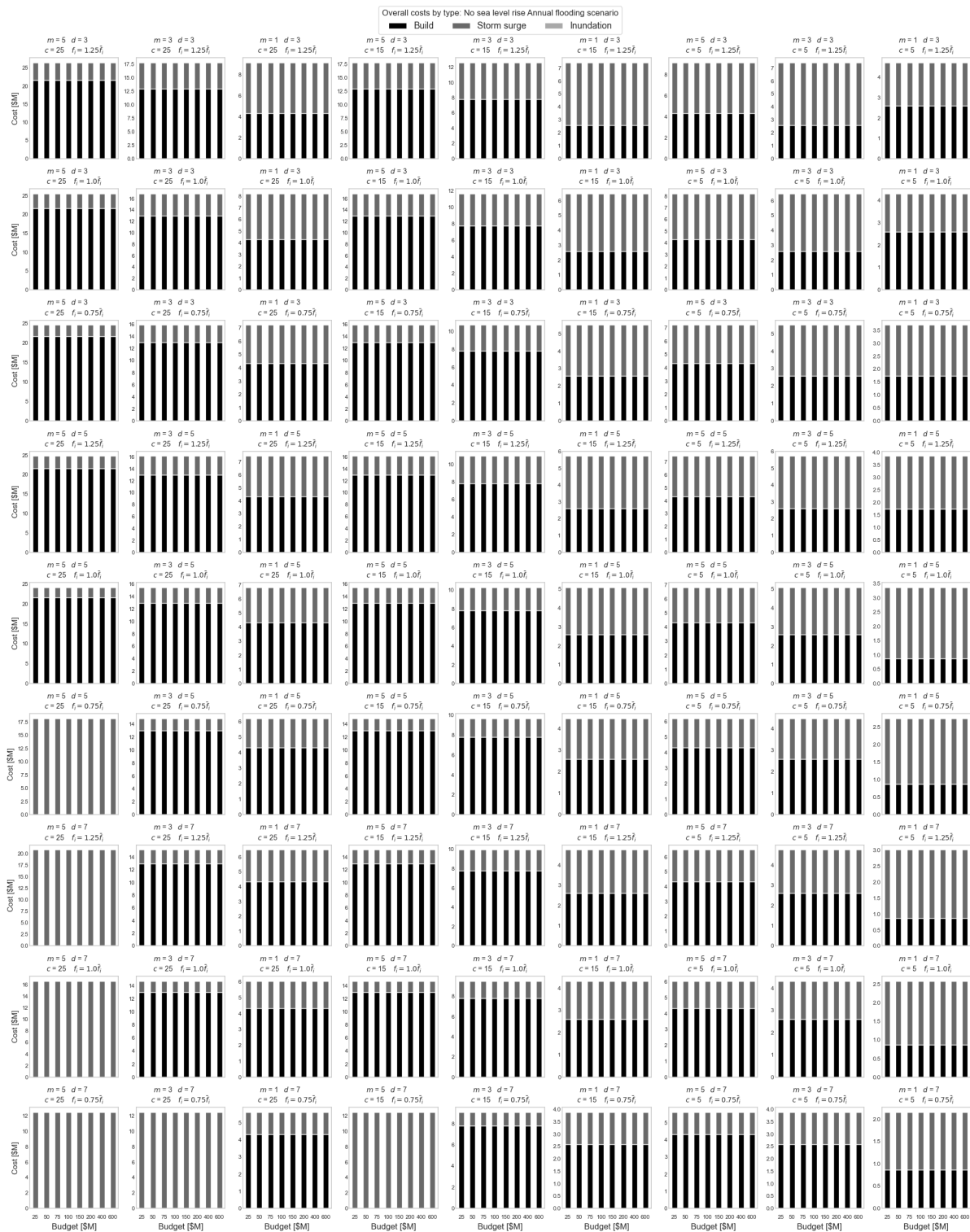
Figure EC.8 Boston Expected-low scenario cost benefit curves by per-period budget for each of the 81 parameter combinations.

Figure EC.9 Boston Optimistic scenario cost benefit curves by per-period budget for each of the 81 parameter combinations.

Figure EC.10   Boston No-sea-level-rise scenario cost benefit curves by per-period budget for each of the 81 parameter combinations.

EC.5 Random network creation and experiment discussion

We created random networks consisting of 402 hexagonal nodes with random selections of approximately 100 sea nodes, 200 surrounding region nodes, and 100 contiguous region of interest nodes that have at least one border grid with the sea. Values for h_i, f_i, and g_i for each grid were selected by randomly sampling the attribute data from Boston. These random network experiments resulted in more than 3M optimization runs across the full range of parameters and sea level states paths.

The pseudocode used to create the random networks for the analysis is presented in Algorithm 1. We start with a square grid made up of 402 hex grids, randomly select sea nodes and Region of Interest (ROI) nodes, randomly assign land elevations h_i to ROI and the Surrounding Region (SR) nodes, and then randomly assign g_i and f_i to the ROI nodes. The result is a network used to run the same experiments as in the Boston case study.

Algorithm 1 Random Network Generation

1: Initialize $baseNetwork$ of 402 hex-grid nodes ($i.e., (23 \times 17)$+11 extra nodes for the last row)

2: **repeat** 50 times

3:     $randomNetwork \leftarrow baseNetwork$

4:     Randomly select up to 3 nodes at the boundary of the $baseNetwork$ as sea nodes

5:     **while** Number of sea nodes < 100 **do**

6:         Randomly select a non-sea node from the $baseNetwork$ that is adjacent to some sea node

7:         Add the selected node to the set of sea nodes

8:     **end while**

9:                    ▷ A *Sea subcomponent* is a connected component composed of sea nodes.

10:     **for each** *Sea subcomponent* **do**

11:         **if** $|Sea\ subcomponent| < 4$ **then**

12:             **while** $|Sea\ subcomponent| < 4$ **do**

13:                 Randomly select a non-sea node from $baseNetwork$ adjacent to *Sea subcomponent*

14:                 Add the selected node to the set of sea nodes and the *Sea subcomponent*

15:             **end while**

16:         **end if**

17:     **end for**

Algorithm 1 Random Network Generation - Continued

18: Randomly select one non-sea node bordering the set of sea nodes

19: Add the selected node to the Region of Interest (ROI) set

20: **while** $|ROI| < 100$ **do**

21:      Randomly select a non-sea node from the *baseNetwork* that is adjacent to *ROI*

22:      Add the selected node to *ROI*

23: **end while**

24:      ▷ A *SR subcomponent* is a connected component composed of Surrounding Region nodes

25: **for each** *SR subcomponent* **do**

26:      **if** $|SR\ subcomponent| < 4$ **then**

27:          **if** all *SR subcomponent* nodes are adjacent to some *ROI* node **then**

28:              Re-label the *SR subcomponent* nodes as *ROI* nodes

29:          **else**

30:              Re-label the *SR subcomponent* nodes as sea nodes

31:          **end if**

32:      **end if**

33: **end for**

34: **for all** non-sea nodes **do**

35:      Randomly sample one h_i elevation from Boston population of h_i

36:      Assign sampled h_i to the chosen node

37: **end for**

38: **for all** *ROI* nodes **do**

39:      randomly sample one f_i and g_i pair from Boston population of f_i and g_i

40:      Assign sampled f_i and g_i pair to the chosen node

41: **end for**

42: save *randomNetwork*

43: **until**

Below, we present the cost benefit curves for the experiments on the 50 random networks. Figure EC.11 shows the combined average of all 50 networks with a cost benefit curve looking at the costs for each budgeted run for one of the 81 parameter combinations. We omit the zero budget cost curves to provide better visualization of the budget effect in each cost benefit curve. To better understand where the model starts being constrained by the budget, we added lower budgets for some model runs. These added per-period budget runs include \$5M and \$12.5M per period budgets for all instances of runs with m at 1m, and \$12.5M where m is at 3m, and c is at \$5M/km per m

or \$15M/km per m. Similar to Figure EC.11, we show the cost benefit curves averaged across all 50 networks for each of the four scenarios discussed in Section 4.3 across the 81 parameter combinations and for each budget. At the top of each chart is the combination of parameters for that chart, with the values shown in Table EC.7. One note of interest in the random network scenario charts, the inundation costs are a fraction of the overall costs, so in many of the bar charts below the reader will notice that the costs are mostly made up of build and storm surge costs, with very small inundation contribution in the stacked bar charts.

Parameter	High	Mid	Low
Discount rate (d) [%]	7	5	3
Minimum elevation increase (m) [meters]	5	3	1
Grid elevation cost (c) [\$M/km per m]	25	15	5
Storm flood damage curve (f_i) [\$M/m]	$1.25\bar{f_i}$	$\bar{f_i}$	$0.75\bar{f_i}$

Table EC.7   Parameter values used in sensitivity analysis for charts shown in Section EC.5

Based on the results observed for the 50 random networks, we conclude that the key takeaways highlighted in Sections 4.2 and 4.3 for Boston case are generalizable to any other coastal area as discussed below.

• We still observe meaningful cost reductions with investments that are a small portion of the "do nothing" flood-related damages.

• Some grids still incur storm-surge flooding and inundation costs even when a surplus budget is available. However, the Boston case study incurs more inundation damage than most random networks. The features of Boston contributing to this effect are its extensive border with the sea where sea level incursion can occur, and multiple areas within Boston connected through groupings of low-lying grids.

• Levee build cost (c) and minimum levee heights (m) still meaningfully affect how much budget is needed to reach minimum overall expected costs before no further spending occurs.

• Overall discounted costs behave consistently with the Boston case, and we see similar effects when delving into the specific costs as discussed in Figure 6. We still observe that the discount rate (d) has the largest effect on overall expected costs, and changes to the storm depth damage function (f_i) has the smallest effect.

• When evaluating the costs from optimistic to high scenarios for sea level states paths, there is still a substantial range of differences in investment required and total overall costs. The same patterns emerge across parameter sensitivity and sea level states paths. Similar to the Boston case, the overall costs are more sensitive to errors in parameter estimations as the decision-maker becomes more risk-averse.
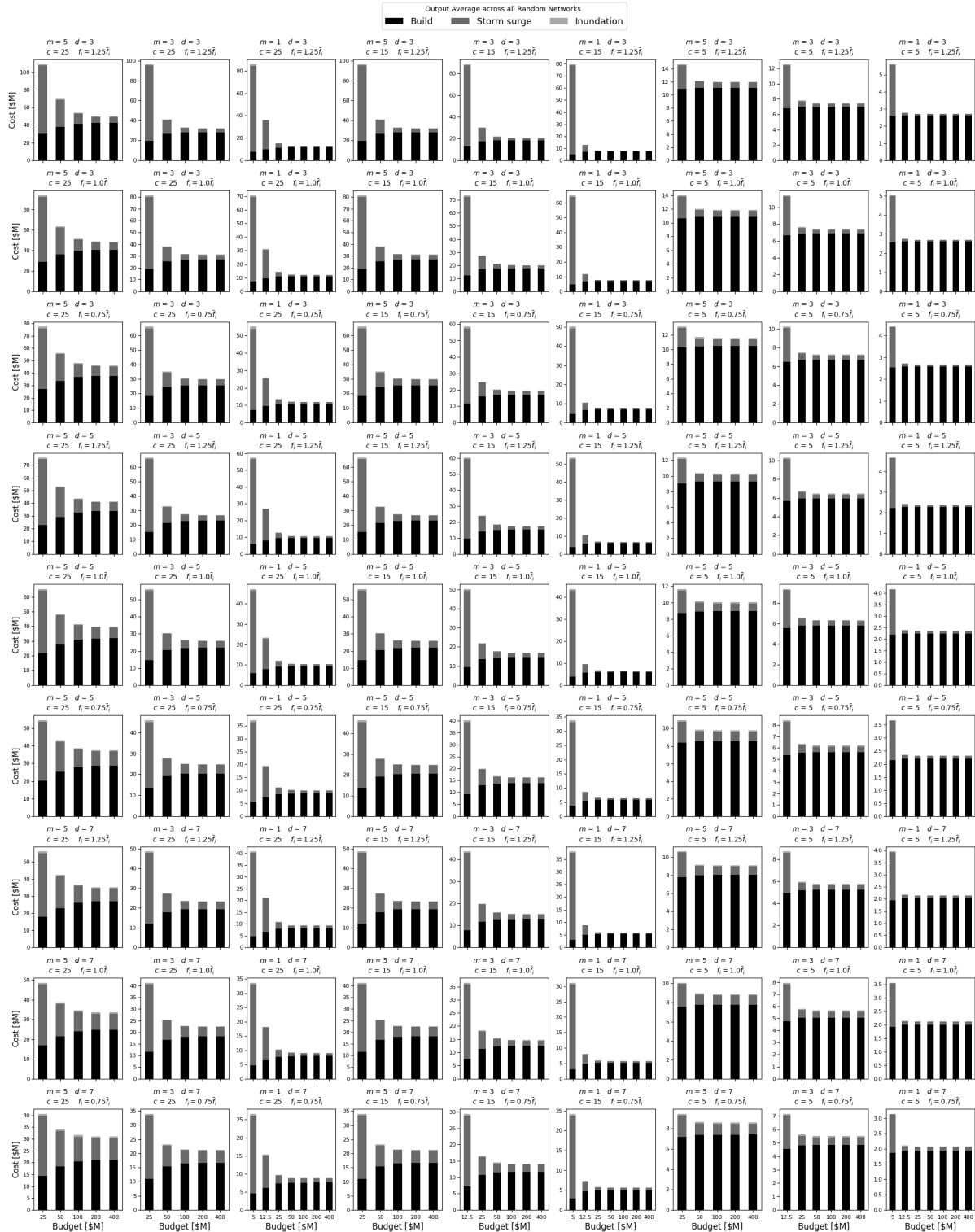
Figure EC.11 Random network simulation expected cost benefit curves by per-period budget with expected costs averaged across all 50 networks for each of the 81 parameter combinations.
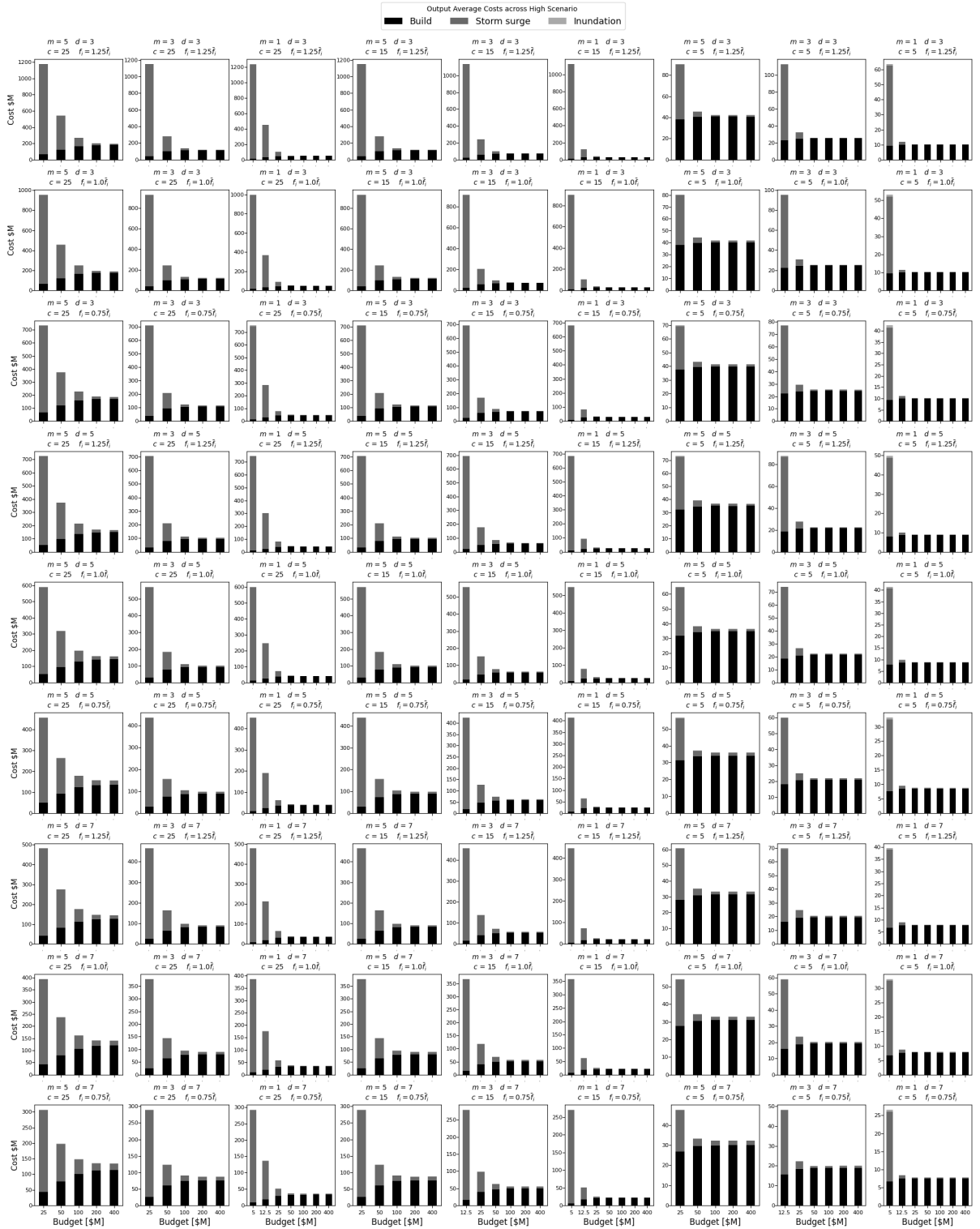
Figure EC.12   Random network High scenario cost benefit curves by per-period budget with scenario costs averaged across all 50 networks for each of the 81 parameter combinations.
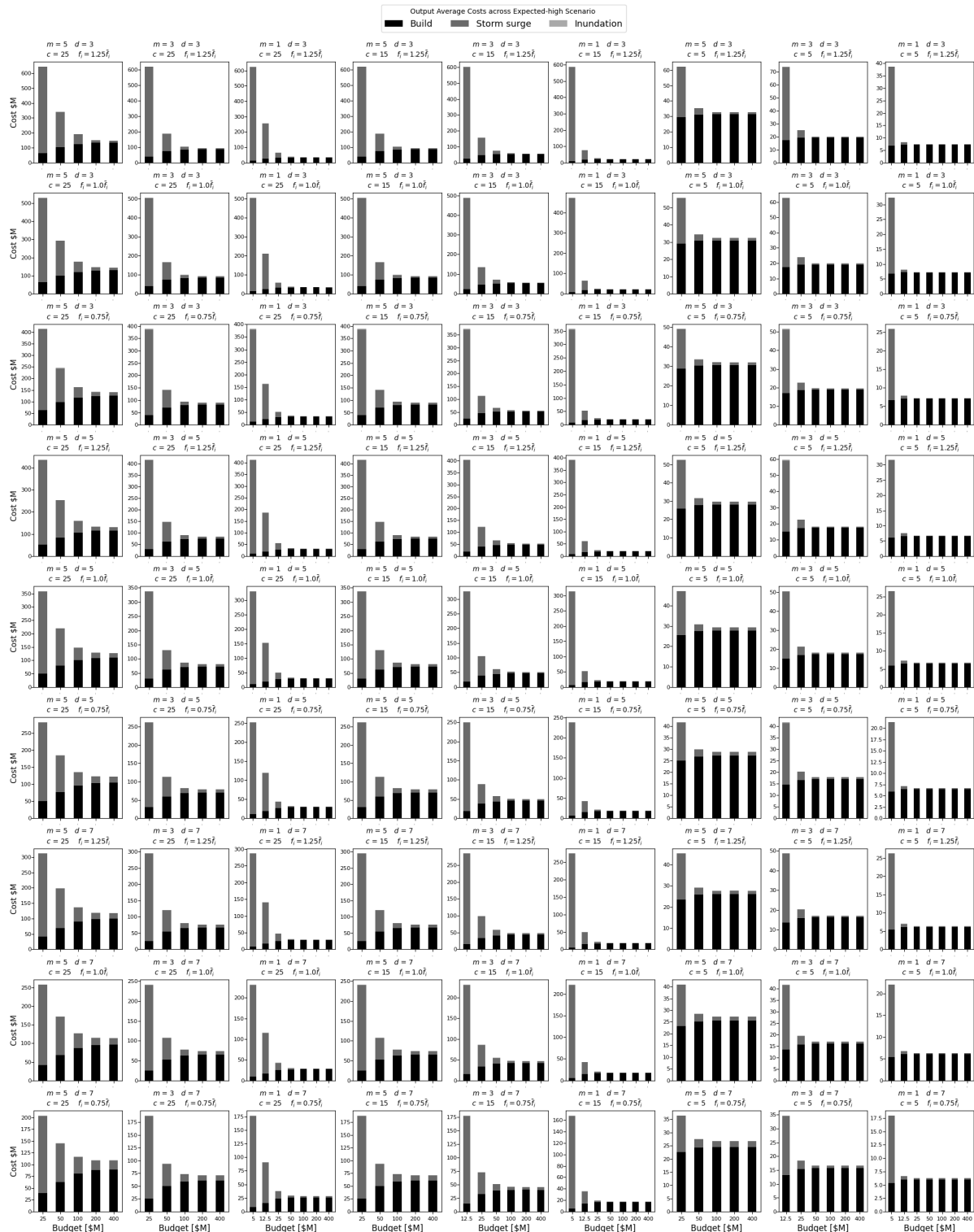
Figure EC.13   Random network Expected-high scenario cost benefit curves by per-period budget with scenario costs averaged across all 50 networks for each of the 81 parameter combinations.
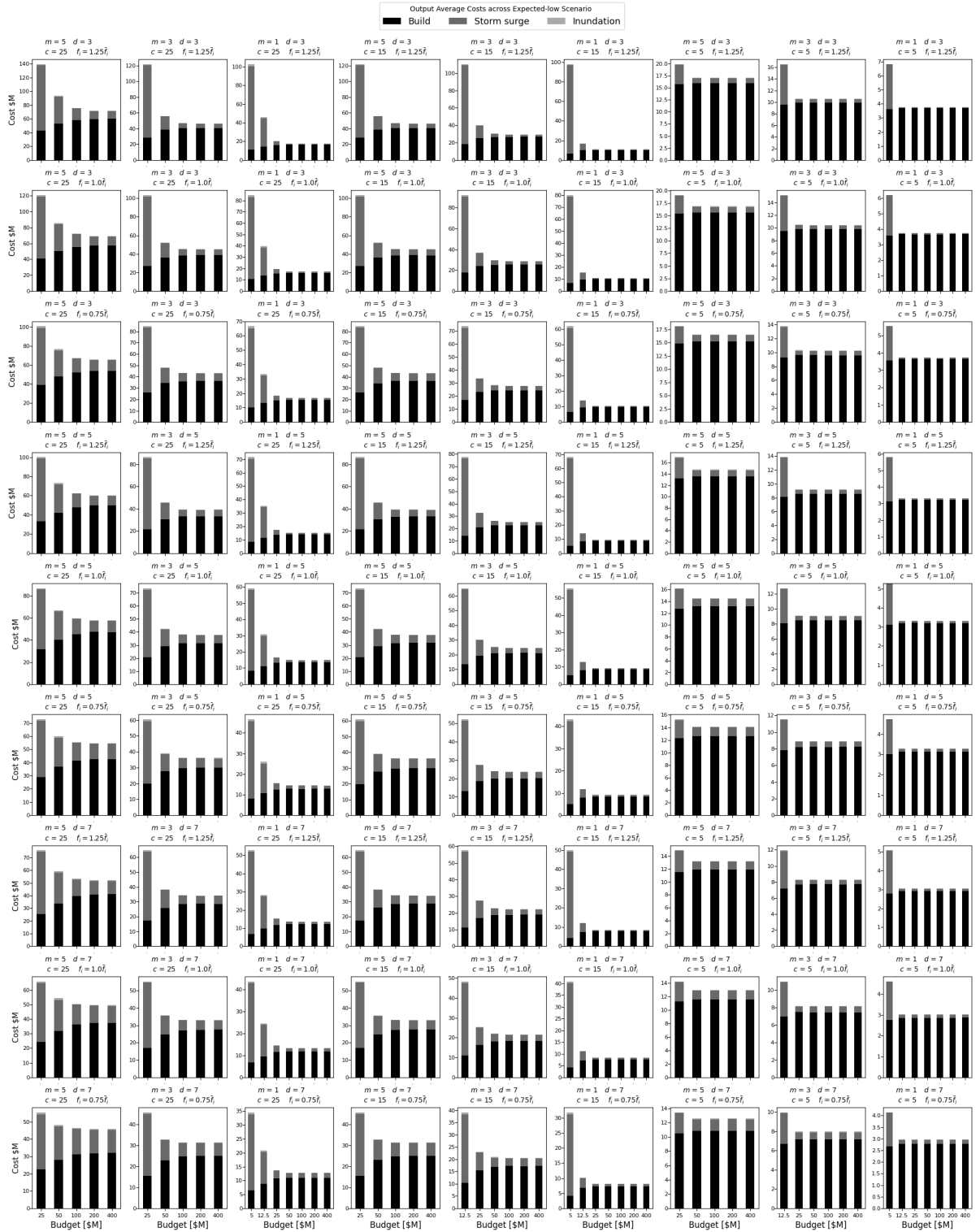
Figure EC.14 Random network Expected-low scenario cost benefit curves by per-period budget with scenario costs averaged across all 50 networks for each of the 81 parameter combinations.
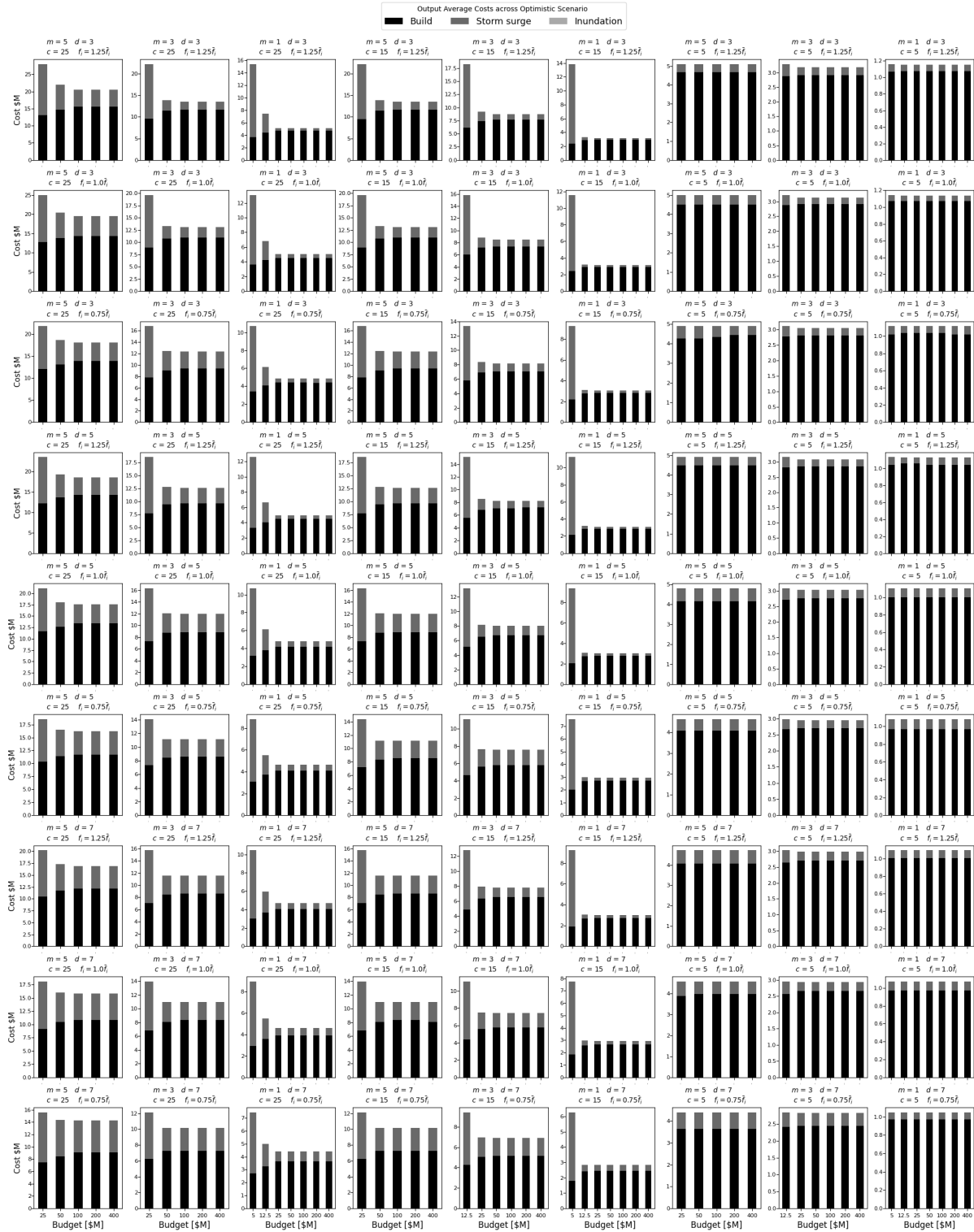
Figure EC.15 Random network Optimistic scenario cost benefit curves by per-period budget with scenario costs averaged across all 50 networks for each of the 81 parameter combinations.